

The effect of humidity and surface functionalisation on the dielectric properties of nanocomposites

Thesis Submitted for the degree of

Doctor of Philosophy

at the University of Leicester

By

Chen Zou

Department of Engineering

University of Leicester

July 2007

The effect of humidity and surface functionalisation on the dielectric properties of nanocomposites

By

Chen Zou

DECLARATION OF ORIGINALITY

This thesis is submitted in fulfilment of the requirements of Doctor of Philosophy in the Department of Engineering, University of Leicester, United Kingdom. All work recorded in this thesis is original unless otherwise is acknowledged in the text reference. No part of this thesis has been submitted for any other degree either to the University of Leicester or to any other University.

Signed

Chen Zou

July 2007

ACKNOWLEDGEMENT

I would like to sincerely thank the following people. You have made the time at University of Leicester well spent.

First and foremost, I must thank Professor John C. Fothergill for being such a wonderful supervisor. Thank him for all his encouragements, guidance, support, and supervision throughout the years and giving me the opportunity to obtain a Ph.D. He shows patience when a student struggles, shows forgiveness when one makes mistakes, shows diligence when meetings fill up his appointment schedule everyday. I could not ask for a better advisor to guide my graduate research.

I wish to thank Professor Leonard A. Dissado for his much helpful advice. His penetrating insight can quickly locate any tiny flaw in my calculation; his profound knowledge pushes me to read more and more scientific books and technical papers to follow his advices.

Dr.Mingli Fu, thank you for generous guides and help, both in research and personal. Without you, I have no chance to obtain a PhD at University of Leicester.

I am thankful to Dr.Stephen W. Rowe and his colleagues at Schneider Electric (France), for supporting my research and helpful discusses and comments. I really miss the scientific meetings held at Autrans.

I wish to thank Professor J. Keith Nelson, Rensselaer Polytechnic Institute (USA), for his kindly providing those polyethylene specimens and invaluable comments and discussions, and permitting me to visit his lab in 2006.

Thank you, Dr.George Chen, University of Southampton (UK), for lending us the pulse generator for PEA. You have changed my future.

Thanks to Andy Willby, for his experimental tuition, help and management. Thank you, Tzimas Antonios, for your enthusiasm and help. You make the time in the lab more fun. Thanks Dr.Kien Ling, Dr.Le Roy and Tong Liu, you all make our group like a family. Thank Gail Iles and all members in her coffee club. It is a pleasure

experience to discuss with physicists in the coffee shop. I wish to thank all the staff at the Engineering Department for making my time at the Department very enjoyable. Especially, Mrs Jenny Ruane, thank you for taking care me since I left home. Thanks to the gentlemen in the workshop. Thank Graham Clark for SEM and TEM measurements. Thanks to Dr.Sarah Hainsworth for directing TEM measurements. Thank you, Paul Williams, for these “liquid lunches” with us every Friday.

The EPSRC (UK) and Schneider Electric (France) are gratefully acknowledged for providing the necessary funding and resources over the course of this PhD.

I must thank my supervisor for Bachelor and Master Degrees, Professor Shengtao Li, in Xi’an Jiaotong University (China), for having so much moral support to me.

I would like to thank my family. Thank you, my wife, Jinping Liu, for your love, good times, and the son you brought for us. I am coming to your side soon.

Thanks all those who lent me a helping hand. To the many people who have not been mentioned but have contributed in some ways to my research work and life, I hope the lack of acknowledgment will not be taken as lack of gratitude.

Lastly, I dedicate this thesis to myself. Nobody really understands what kind of pressure I burdened during the years.

Good luck to all the new PhD students, both you and I will need it.

Chen Zou

The effect of humidity and surface functionalisation on the dielectric properties of nanocomposites

By

Chen Zou

Abstract

Work is reported on composites comprising either epoxy resin or crosslinked polyethylene (XLPE) filled with silica nanoparticles (surface functionalised and unfunctionalised). Measurements were made of the dielectric spectra, charging and discharging currents under high electric fields, and space charge dynamics using the pulsed electroacoustic (PEA) technique. Considerable studies were made of the effect of humidity on epoxy nanocomposites. It was found that the epoxy composites filled with nanoparticles could absorb up to 60% more water by weight than the unfilled epoxy. For composites filled with microparticles, nearly all the water was absorbed by the resin. The glass transition temperature (T_g) for all epoxy samples, measured by both differential scanning calorimetry (DSC) and dielectric spectroscopy, showed a monotonic reduction with increase of hydration resulting in a 20K decrease for fully hydrated samples. This led to the conclusion that the extra hydration found in the nanocomposites was not in the bulk resin but was likely to be located on the surface of the nanoparticles. This is further supported by measurement of the hydration isotherms at room temperature and the resultant swelling as a function of humidity.

A "water shell" model is developed in which there is an inner layer of approximately 5 – 10 bound water molecules on the surface of the nanoparticles, a further layer, approximately 25nm thick, in which water is in sufficient concentration to allow conduction, and an outer layer, approximately 50nm thick, which cannot support true conduction (i.e. the continuous movement of charge carriers.) This model is used to explain the sub-hertz dielectric results (in terms of percolation limited conduction) as well as those at around 1 – 10Hz that indicate the presence of bound or free water.

Content

| | |
|---------------------------------------------------------------------------|------|
| DECLARATION OF ORIGINALITY | i |
| ACKNOWLEDGEMENT | ii |
| ABSTRACT | iv |
| Chapter 1 Introduction | 1-1 |
| Chapter 2 Literature Review..... | 2-1 |
| 2.1 Fundamental knowledge of polymer science..... | 2-1 |
| 2.1.1 General knowledge of polyethylene and crosslinked polyethylene..... | 2-2 |
| 2.1.2 General properties of epoxy resin | 2-3 |
| 2.2 Introduction to nanocomposites | 2-4 |
| 2.3 Research motivation for nanodielectrics..... | 2-5 |
| 2.4 Principles of dielectric spectroscopy analysis..... | 2-7 |
| 2.4.1 The response of dielectrics to electric fields..... | 2-8 |
| 2.4.2 The dielectric response in the frequency domain | 2-10 |
| 2.4.3 The Debye model of dielectric relaxation..... | 2-11 |
| 2.4.4 Modifications to the Debye theory | 2-12 |
| 2.4.5 Dissado-Hill theory and Quasi-d.c behaviour..... | 2-14 |
| 2.4.6 Equivalent circuit analysis of the dielectric response | 2-17 |
| 2.4.7 Master plot technique..... | 2-20 |
| 2.5 Space charge in solid dielectrics | 2-21 |
| 2.5.1 The origin of space charge in polymer | 2-22 |
| 2.5.2 The transport of space charge | 2-22 |
| 2.5.3 Ageing, breakdown and space charge..... | 2-23 |
| 2.6 Percolation and Effective Media Theory | 2-24 |
| 2.7 Electric conduction mechanisms in polymers..... | 2-26 |
| 2.7.1 Electronic processes..... | 2-27 |
| 2.7.2 Schottky injection | 2-27 |
| 2.7.3 Fowler-Nordheim injection..... | 2-28 |
| 2.7.4 Bulk process..... | 2-28 |
| 2.7.5 Ionic conduction..... | 2-30 |
| 2.7.6 Summary for various conduction mechanisms in insulators | 2-30 |

| | |
|---------------------------------------------------------------------|------|
| Chapter 3 Experimental Techniques..... | 3-1 |
| 3.1 Materials preparation | 3-1 |
| 3.1.1 Polyethylene composites..... | 3-1 |
| 3.1.2 Epoxy composites | 3-3 |
| 3.2 Physical and Chemical characterisation..... | 3-4 |
| 3.3 Measurements under the control of relative humidity | 3-7 |
| 3.3.1 Humidity control..... | 3-7 |
| 3.3.2 Hydration measurement..... | 3-11 |
| 3.3.3 Density change of epoxy materials after water-saturation..... | 3-11 |
| 3.3.4 Water diffusion in epoxy specimens..... | 3-12 |
| 3.4 The measurement methods | 3-12 |
| 3.4.1 Differential scanning calorimetry measurement..... | 3-12 |
| 3.4.2 Conduction current measurement | 3-13 |
| 3.4.3 Dielectric Spectroscopy | 3-15 |
| 3.4.4 Pulsed electro-acoustic (PEA) measurements | 3-17 |
| 3.5 Summary | 3-18 |
| Chapter 4 Results | 4-1 |
| 4.1 Hydration behaviour of epoxy specimens..... | 4-1 |
| 4.1.1 Hydration in epoxy specimens..... | 4-1 |
| 4.1.2 Water diffusion in epoxy specimens..... | 4-4 |
| 4.1.3 Density change of the wetted epoxy specimens | 4-7 |
| 4.2 The glass-transition temperature of epoxy specimens | 4-9 |
| 4.3 Conduction current measurement | 4-12 |
| 4.3.1 XLPE..... | 4-13 |
| 4.3.2 Epoxy materials | 4-18 |
| 4.4 Dielectric spectroscopy of epoxy materials | 4-28 |
| 4.4.1 The overall dielectric properties of n3 epoxy specimens..... | 4-29 |
| 4.4.2 The activation energy at low frequencies | 4-33 |
| 4.4.3 The relaxation process caused by bound water..... | 4-35 |
| 4.5 PEA measurement..... | 4-38 |
| 4.5.1 Space charge behaviours of polyethylene specimens | 4-38 |
| 4.5.2 Space charge accumulation in epoxy specimens | 4-44 |

| | |
|--------------------------------------------------------------------|--------|
| Chapter 5 Interfaces and Nanodielectrics | 5-1 |
| 5.1 Interfaces and space charge behaviour of polyethylene..... | 5-2 |
| 5.2 Interfaces and water sorption in epoxy nanocomposites | 5-4 |
| Chapter 6 Water Shell Model and Percolation Phenomennon | 6-1 |
| 6.1 The water shell surrounding the nanoparticles | 6-1 |
| 6.2 Water shell model | 6-5 |
| 6.3 Percolation phenomenon in nanocomposites..... | 6-8 |
| 6.4 Ageing..... | 6-12 |
| Chapter 7 Conclusions and Future Work..... | 7-1 |
| 7.1 Conclusions..... | 7-1 |
| 7.2 Future work..... | 7-3 |
| Appendix I: LabView program for conduction current measurement . | AI-1 |
| Appendix II: The deduction of the water diffusion equations..... | AII-1 |
| Appendix III: The dielectric spectroscopy of epoxy materials | AIII-1 |
| Appendix IV: Electrode design..... | AIV-1 |
| Chapter 1 References | C1R-1 |
| Chapter 2 References | C2R-1 |
| Chapter 3 References | C3R-1 |
| Chapter 4 References | C4R-1 |
| Chapter 5 References | C5R-1 |
| Chapter 6 References | C6R-1 |
| Appendix II Reference..... | AIIR-1 |
| List of Publications | |

Chapter 1

Introduction

Materials and their development are fundamental to society. Major historical periods of society have been ascribed to materials, The Stone Age, The Bronze Age, and The Iron Age, comprise the “Three Age system” [1] and clearly semiconductors have greatly influenced recent development. Scientists will open the next societal frontiers not by understanding a particular material, but rather by understanding and optimising the relative contributions afforded by material combinations. The most recent of these is nanotechnology. Nanotechnology includes techniques for controlling, modifying and fabricating materials and devices with nanometric dimensions and seems to be expected all the current problems in any scientific from electronic to medicine and biology [2].

The nanoscale and associated nanoscience and technology afford unique opportunities to create revolutionary material combinations. Naturally-occurring biological systems have taken advantage of the properties of the interactions of organic materials at the nanoscale, we are now exploiting combinations with inorganic materials. These new materials circumvent classic material performance trade-offs by accessing some desirable properties and exploiting unique synergisms between materials. This only occurs when the length-scale of morphology and the fundamental physics associated with a property coincide on the nanoscale. The combination of fundamental understanding of materials and the realization of fabrication and processing techniques that provide simultaneous structural control on the nano, micro-, and macro-length scales is the core of the exciting area of nanoengineered materials. Examples of such material technologies are rapidly increasing, impacting many diverse areas of the commercial and military arena.

Polymeric materials are widely used in a variety of industries; they have excellent bulk and physical properties, are easy to process and construct, and, as such, are relatively inexpensive. Fillers and particles are often added to modify stiffness and

strength, thermal conductivity, electric breakdown, endurance and high field stability [3, 4] and to reduce the cost of the material. Polymeric nanocomposites (PNCs) (or polymer nanostructured materials) represent a radical alternative to conventional-filled polymers or polymer blends. In contrast to the conventional systems where the reinforcement is on the order of micrometers, discrete constituents on the order of a few nanometers exemplify PNCs [5]. In this case, nanofillers are the fundamental building blocks in the design and creation of assembled nanograined larger scale structures with excellent compositional and interfacial flexibility. Furthermore, there are good theoretical reasons, i.e., electrical, mechanical, chemical, thermal, etc, why the pursuit of nanocomposites for dielectric applications may have particular promise [6].

Fillers with one dimension less than 100nm are unique because they have an extremely large surface area for their size; a relatively small concentration can therefore lead to a high specific area [6]. This large surface area leads to changes in morphology that significantly impact electrical properties [7]. The surface can also change the trap density and depth. Since interfaces lead to dielectric effects (such as the transition region in the *p-n* junction) or electrochemical effects (such as the Gouy-Chapman layer), one would expect a high specific area to lead to significant dielectric effects [8]. There is increasing evidence from several laboratories that the use of nano-fillers allows the local environment and interface physics to be changed in ways which can have a profound effect on the properties of the resulting composite [9]. For example, the threshold field for space charge accumulation within some polymers can be considerably increased by incorporating nanofillers [10]. Hence, composites with nano-fillers exhibit properties superior to conventional composites. By proper choice of the surface conditions of nanofiller, it is hoped that the properties of the resulting dielectric can be engineered to the desirable characteristics.

Humidity is typically regarded as a key role in the degradation processes of many composites filled with inorganic fillers. Water may plasticize and induce relaxation in the composite, swell the composites, and therefore degrade the mechanical properties of the composite. A weakness caused by water may have a detrimental effect on the improved mechanical [11] and electrical behaviours of nanocomposites and counteract the effort of incorporating nanofillers. If nanofillers are incorporated, the

specific area of the epoxy – particle interface is greatly increased as the particle dimensions decrease, and this is a potential location for water [12]. The situation might become worse. Although a lot of research has been carried out on the mechanical properties, the effect of water on the dielectric properties of nanocomposites has not been well established [13].

This thesis presents both an experimental study and a theoretical analysis of the development and response of nanocomposite dielectric structures systems. The research investigates the effects of water and the surface of nanofillers on the dielectric properties of nanocomposites. After giving a literature review over the research field in Chapter 2, measurements performed of dielectric spectroscopy, space charge measurement and conduction current in nanocomposites, of both crosslinked polyethylene (XLPE) and epoxy resin, are introduced in Chapter 3. Chapter 4 of the thesis presents the experimental results. The following chapters 5 and 6, investigate the causes of the unique dielectric behaviour of nanocomposites. In Chapter 5, it is shown that the interfacial effect of nanofillers and surface functionalisation of nanofillers plays critical roles in determining the dielectric properties of nanocomposites. Chapter 6 uses a “water shell” model to explain the dielectric behaviour of the water-absorbed epoxy materials using the percolation theory. An “alternative scenario” for ageing in composite materials, in which the interfaces between the particles and the host material gradually weaken, is supported. Finally, in Chapter 7, some conclusions obtaining from this research are presented together with suggestions for further work.

Chapter 2

Literature Review

In this chapter, a literature review of the research field is presented, which includes the background knowledge of polymer science, nanocomposites, principles of dielectric spectroscopy, theories of polarization, space charge in polymer, percolation theory and conduction mechanisms in polymer.

2.1 Fundamental knowledge of polymer science

Polymers are very large molecules (macromolecules) that are comprised or built up of smaller units known as monomers. The arrangements of these units, the various types of chains that can be synthesised and the shapes that these chains can bend themselves into, result in a class of materials that are characterised by an enormous and intriguing range of properties [1]. In terms of their chemical structure, they might be usefully classified as condensation or addition polymers. Condensation polymers are produced by the reaction of functional groups on the monomers, resulting in the loss of a small molecule (usually water); hence the chains lack certain groups that were present in the original monomers. Addition polymerisation involves either a free radical or ionic mechanism. In the former case, polymerisation occurs via a chain reaction involving three stages. Firstly, chain initiation, in which free radicals are produced by either heat or ultraviolet light, followed by propagation, whereby unsaturated monomers are added to the chain by reaction with free radicals. After the propagation stage, whereby the chain is built up, chain termination occurs, usually by recombination of free radicals. Certain unsaturated monomers may also polymerise by an ionic addition mechanism, whereby an ionic charge is transferred between reacting monomers. Branching may occur in addition reactions if a free radical forms within the growing chain, rather than simply at the end of that chain. Similarly, cross-linking may occur either as part of the polymerisation process (for example with dienes which contain two unsaturated groups) or by the addition of cross-linking agents to linear chains, examples of such agents being sulphur or peroxides [2].

Several polymers (such as epoxy resin) will not undergo any definite transition from solid to liquid but will instead undergo a thermal transition between a glassy and rubbery state, which temperature defines as the glass transition temperature (T_g). In addition, a number of polymers will crystallise on cooling from the melt, forming spherulites or other structures, which are considered to be semicrystalline, existing in a state intermediate between that of crystalline and amorphous solids. The reason these materials are called "semicrystalline" is that some fraction of the polymer remains uncrystallized, or amorphous when the polymer is cooled to room temperature. The amorphous polymer becomes trapped between the growing crystals. As a result of the highly entangled nature of the polymer chains, the movement of the amorphous polymer becomes restricted [1].

Usually, polymers display an extremely high resistivity and electrical breakdown strength, and have been applied widely as the insulators [3] in power systems.

2.1.1 General knowledge of polyethylene (PE) and crosslinked polyethylene (XLPE) [3]

Polyethylene is a thermoplastic polymer consisting of long chains of the monomer ethylene. The ethylene molecule, C_2H_4 is $CH_2=CH_2$, Two CH_2 groups connected by a double bond, as shown in figure 2.1,

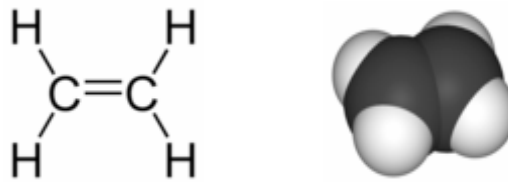


Figure 2.1. The chemical structure of ethylene

Polyethylene is created through polymerisation of ethylene, a long chain structure as shown in figure 2.2.

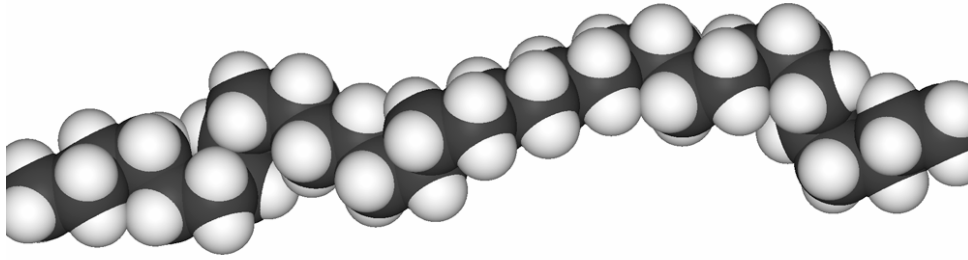


Figure 2.2. The 3D Space-filling model of a polyethylene chain

Polyethylene is classified into several different categories based mostly on its density and branching. The mechanical properties of polyethylene depend significantly on variables such as the extent and type of branching, the crystal structure, and the molecular weight.

Although polyethylene is a thermoplastic polymer, the product (XLPE) becomes thermosetting once it is crosslinked. Crosslinked polyethylene covalent bonds which “crosslink” adjacent polymer chains, changing the thermoplastic into thermoset (since it no longer flows when it melts).

Crosslinked polyethylene has better properties related to mechanical and electrical ageing, than those of polyethylene.

2.1.2 General properties of epoxy resin [3]

Epoxy or polyepoxide is a thermosetting epoxide polymer that cures (polymerizes and crosslinks) when mixed with a catalyzing agent or “hardener”. Most common epoxy resins are produced from a reaction between epichlorohydrin and bisphenol-A, and retain an amorphous structure, which is a thermoset. The structure of epoxy is described in figure 2.3.

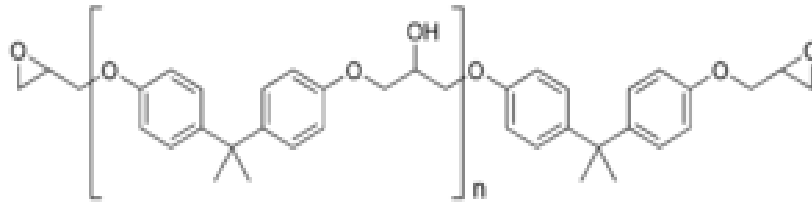


Figure 2.3. Structure of unmodified epoxy prepolymer. n denotes the number of polymerised subunits and is in the range from 1 to about 25

The applications for epoxy based materials are extensive and include coatings, adhesives and they form the matrix for composite materials such as those incorporating carbon fibre, inert particles, and fibreglass reinforcements. The chemistry of epoxies and the range of commercially available variations allow cured polymers to be produced with a very broad range of properties. In general, epoxies are known for their excellent adhesion, chemical and heat resistance. They are good to excellent mechanical properties and very good electrical insulating properties. The properties of the composites can, however, be significantly modified from that of the epoxy itself, for example silver-filled epoxies with good electrical conductivity are available, although the epoxy itself is electrically insulating.

2.2 Introduction to nanocomposites

Lewis has argued that many dielectric processes are controlled by interfaces [4]. The reinforcement of polymers using nanofillers is promising in the production of modern plastics. A short-range highly immobilized layer develops near the surface of the nanofiller. This bound layer, however, influences a much larger region surrounding the particle in which conformational behaviour and chain kinetics are significantly altered. This so-called interaction zone is responsible for material property modifications, especially when the curvatures of the particles approach the chain conformation length of the polymer structure. They are fundamental in controlling the dielectric strength of insulating polymers. The relatively high proportion that the interaction zone occupies in nanofilled polymers with reduced molecular chain mobility provides an opportunity both for a fundamental study of this interaction zone, and for optimising performance [4]. In the simplest situation, the bonding of a polymer to filler can be expected to give a layer of immobilized polymer. This could

change the crystallinity of a semicrystalline material such as XLPE [3]. The size of this layer is critical to the global properties of the composites. Recent activity in the formulation of nanodielectrics using, in particular, both thermosetting resins and polyolefins has shown some significant promise both in terms of the mechanical [5] properties and when used as electrical insulators [6]. Clays and inorganic oxides of nanometric dimensions are the most common particles used to provide the filler material, but there is also, for good reason, interest in functionalising the particle surface to bring about preferred coupling [7]. For example, it is shown in this work, that hydrophobic functionalisation may be particularly useful in this respect.

2.3 Research motivation for nanodielectrics

Nanodielectrics are multi-component dielectrics possessing nanostructures, the presence of which lead to significant changes in one or several of their dielectric properties [8]. From the strictly commercial viewpoint, electrical insulating materials are a huge business, ranging from the large amounts of material used in the high-voltage power industry to thin films for electronics fabrication. It was postulated in the proposal for this work that even a 10% improvement in an electrical property such as dielectric withstand strength would have enormous commercial impact worldwide [9]. To achieve the commercial objectives, a better characterisation of the physical and dielectric properties of materials with nanoscale filler formulations are required. Moreover, scientists have to gain an understanding of the underlying physics, in particular the way in which nanoparticles interact in a polymer matrix and how they affect dielectric ageing and breakdown. However, even though such work has been started in recent years, the underlying physics of the way in which nanoparticles interact in a polymer matrix have not been fully understood. Indeed, nanotechnology has not focused much on the opportunities for dielectric materials; but rather centred on optical and mechanical applications.

Polyethylene has been widely used for cable systems [3]. Polyethylene as one of the typical dielectric materials is composed of crystal regions and amorphous regions, and lamella and spherulites, and intermediate regions between them. Polyethylene is simple in its chemical structure, but its morphology is relatively complicated particularly if crosslinked. In service, temperature strongly influences the morphology

and thus the electro-chemical properties of the insulation. The physical structure characterization constitutes a key topic. The degree of crystallinity has been first invoked to explain changes of insulation characteristics due to modifications under thermal treatment. The evolution of the size and the number of crystallites may be an important factor. Moreover amorphous regions, which are considered as responsible for controlling some of the electrical properties such as the dielectric withstand strength, must be also taken into account due to the high susceptibility to evolution of the mobility of these domains under thermal treatment [10].

The increasing use of thermosets, such as XLPE and epoxy resin, is supported by the following advantages:

- The material remains solid, even at high temperatures and has a high level of thermal dimensional stability
- The moulded parts are characterised by their hardness and feature a smooth, quality surface finish
- Epoxy and its end products offer low extrusion, flame retardancy

However, thermosets are crosslinked, which creates an irreversible 3D-network and cannot be re-moulded. For this reason they are not recyclable and not considered to be environmentally friendly. This is, perhaps, the biggest disadvantage to thermosets, and a significant issue to solve.

It is reasonable to postulate inherent weak regions in polymers, whether they are thermoplastic or thermosetting. These weak regions (crystal and amorphous regions and their interfaces, higher order structures in morphology such as spherulites) are susceptible to generate trees due to local dielectric breakdown. The free volume of an amorphous network region is larger than that of the base part of polyethylene. Regions containing higher-than-average free volume may be electrically (and mechanically) weaker, this is qualitatively consistent with dielectric breakdown starting in the free-volume. Although in the presence of different viewpoints [11], some models based on the conductivity anisotropy where the electrical current flows selectively in narrow amorphous regions in between lamellae, and gives rise to Joule heating to evaporate the amorphous polyethylene and create gaseous channels or charge accumulation. The electric field in a region can exceed its intrinsic strength

due to trapping of injected charge carriers leading to a partial breakdown of the insulation. Further evidence for the importance of morphology may be found in the measurements of space charge.

2.4 Principles of dielectric spectroscopy analysis

Dielectric spectroscopy depends on the polarisation that is induced in a material due to the effect of an external electrical stress. Dielectric spectroscopy can provide useful information on the electrical properties of the specimens. Moreover, this technique can be used as analytical tool whereby the dielectric data is related to other properties such as the polymer molecule structure or morphology [2], or its degradation and ageing.

The interaction of electric field with matter is of fundamental importance in basic and applied science. Many aspects of dielectric response, especially in the presence of non-linear processes, are more easily understood in terms of the response to time-dependent signals [12]. However, there exists a very powerful alternative approach which offers a very considerable theoretical and practical advantage, provided that a linear system is studied, and this is the determination of the response to harmonic excitation, i.e., sinusoidal waves [12].

The mathematical basis for the treatment of the frequency domain response rests on the Fourier transformation of a given function of time $G(t)$, defined by the Fourier transform [12]:

$$F[G(t)] = \psi(\omega) = (2\pi)^{-\frac{1}{2}} \int_{-\infty}^{\infty} G(t) \exp(-i\omega t) dt \quad (2-1)$$

The Fourier transform gives the frequency spectrum $\psi(\omega)$ of the time-dependent function $G(t)$ - the amplitudes and phases and frequencies of the sinusoidal waves which make up the given time signal. The inclusion of i in the above expression means that any transformed term will be complex, i.e., it will possess both real and imaginary components. This therefore indicates that any resulting expressions will take into account the phase behaviour of the response of a specimen [2] as well as the ratio of the amplitudes.

2.4.1 The response of dielectrics to electric fields

2.4.1.1 Electrostatics

The interaction of electromagnetic fields with matter is described by Maxwell's equations

$$\nabla E = -\frac{\partial}{\partial t} B \quad (2-2)$$

$$\nabla H = j + \frac{\partial}{\partial t} D \quad (2-3)$$

$$\text{div} B = 0 \quad (2-4)$$

$$\text{div} D = \rho_e \quad (2-5)$$

In this set of equations E and H describe the electric and magnetic fields, D describes the dielectric displacement, B , the magnetic induction, j the current density and ρ_e the density of charges [13].

For small electric field strengths D can be expressed by

$$D = \varepsilon^* \varepsilon_0 E \quad (2-6)$$

where ε_0 is the dielectric permittivity of vacuum ($\varepsilon_0 = 8.854 \times 10^{-12} \text{ C} \cdot \text{V}^{-1} \cdot \text{m}^{-1}$). ε^* is the complex relative dielectric permittivity [14]. For a periodic electrical field $E(t) = E_0 \exp(-i\omega t)$ (ω is the radial frequency, $i = \sqrt{-1}$) the complex dielectric function ε^* is defined by

$$\varepsilon^*(\omega) = \varepsilon'(\omega) - i\varepsilon''(\omega) \quad (2-7)$$

where $\varepsilon'(\omega)$ is the real part and $\varepsilon''(\omega)$ the imaginary part of the complex dielectric function.

The polarisation P describes the dielectric displacement which originates from the response of a material to an external field only. Hence it is defined as

$$P = D - D_0 = (\varepsilon^* - 1)\varepsilon_0 E = \chi^* \varepsilon_0 E = N_0 \alpha E \quad (2-8)$$

with $\chi^* = (\epsilon^* - 1)$, where χ^* is the dielectric susceptibility of the material under the influence of an external electric field. N_0 is the number of dipoles per volume unit, α is the polarisability of the charge. The equation also connects the dielectric displacement with the contributions from the geometrical and polarisability of the material.

2.4.1.2 Types of polarisation

The polarisation behaviour is directly related to the electronic, atomic, orientational and interfacial polarisation of the material. The first two of these are induced by the applied field, and are caused by displacement of the electrons within the atom (its polarisation time scale is $\sim 10^{-15}$ s), and atoms within the molecule ($\sim 10^{-12} - 10^{-13}$ s), respectively. The orientational polarisation ($\sim 10^{-9} - 10^{-3}$ s) is the classical type of polarisation originally treated by Debye (1945) and only exists in polar materials, i.e., those with molecules having a permanent dipole moment [15]. There are therefore no restoring forces tending to impose a preferred direction, only the randomising influence of thermal agitation. The interfacial polarisation appears in heterogeneous materials in which the relaxation time is longer than that of the orientational polarisation [16]. It comes from the accumulation of charges at the interfaces between the various phases constituting materials when these various phases have different permittivities and conductivities. For very conductive solutions, a layer of ions will form adjacent to the electrodes [17 – 20]. This will alter the charge distribution within the system and results in a marked rise in capacitance as the frequency is lowered [2]. This effect is known as “electrode polarisation” that normally is an unwanted effect and should be removed or corrected for. It is possible that some of the effects observed around nanoparticles in the composites studied here result in similar effects.

Electronic and atomic polarisation are temperature independent, but orientational polarisation, depending on the extent to which the applied field can order the permanent dipoles against the disordering effect of the thermal energy of their environment, varies inversely with absolute temperature. All of these polarisation mechanisms can only operate up to a limiting frequency, after which a further frequency increase will result in their disappearance. Because of the spring-like nature

of the forces involved, it is possible to observe the specific polarisation at a specific frequency region [12].

2.4.2 The dielectric response in the frequency domain

Dielectric analysis usually involves applying a field of fixed or varying frequency to a specimen and measuring the response. As the frequency of the field changes, different mechanisms of polarisation will predominate. It is the analysis of these mechanisms that provides the basis of dielectric spectroscopy [2]. Since some polarisations are temperature dependent, the activation energies and dipolar types of some specific relaxation processes can be obtained by measuring the dielectric responses over a range of temperatures.

When an external field is removed from a charged capacitor, that capacitor will discharge over a period of time, depending on the capacitance itself and the resistance in the discharge circuit. In an alternating system, charge movement will change direction in order to “keep up” with the fluctuations in the field when that field changes direction. As this realignment will inevitably be non-instantaneous, the response will take place over a period of time. According to equation 2-1, the frequency dependent response function can be described in the time dependent response function by Fourier transform.

If the Fourier transform is applied to polarisation phenomena, then

$$P^*(\omega) = \varepsilon_0 i \chi^*(\omega) E^*(\omega) \quad (2-9)$$

where χ is the susceptibility of the specimen, which is complex and may therefore be expressed in terms of its real and imaginary components, i.e.:

$$\chi^*(\omega) = \chi'(\omega) - \chi''(\omega) \quad (2-10)$$

The susceptibility is related to the permittivity, which may also be expressed in terms of the real and imaginary components, i.e. equation 2-7.

The capacitance C^* results can also be used to analyse the dielectric properties of the specimen even if the dimensions of the specimen are unknown. As to the parallel plate specimens,

$$C^*(\omega) = C'(\omega) - iC''(\omega) = \frac{4\pi A}{d} \varepsilon'(\omega) - i \frac{4\pi A}{d} \varepsilon''(\omega) = \frac{4\pi A}{d} [\chi'(\omega) + 1] - i \frac{4\pi A}{d} [\chi''(\omega) + 1] \quad (2-11)$$

where A is the area of the specimen, and d is the thickness of the specimen.

2.4.3 The Debye model of dielectric relaxation

It is convenient to study relaxation process by measuring the real and imaginary components of the permittivity over a range of frequencies. As is well known, these relaxation processes are a function of the structure of the specimen, and may be used as the means of characterising materials. The frequency dependence of the reorientation process was the subject of extensive work by Debye (1945) [21, 22] and is summarised below. The real and imaginary (loss) components of the susceptibility for a reorientation dipole may be derived from equation 2-1 and are given by

$$\chi^* = \chi(0) \cdot \frac{1}{1 + i\omega\tau} \quad (2-12)$$

In terms of permittivity, the equation may be given by

$$\varepsilon^* = n^2 + \frac{(\varepsilon_s - n^2)}{1 + i\omega\tau} \quad (2-13)$$

from which one can show that, $\varepsilon' = n^2 + \frac{(\varepsilon_s - n^2)}{1 + \omega^2\tau^2}$ and $\varepsilon'' = n^2 + \frac{(\varepsilon_s - n^2)\omega\tau}{1 + \omega^2\tau^2}$, where

n is the refractive index (equivalent to $\varepsilon^{\frac{1}{2}}$ at optical frequencies) and ε_s is the static field permittivity (i.e. the permittivity at zero frequency). τ is the relaxation time of the system and a characteristic of the material, as it gives the time constant of the dipolar reorientation process.

2.4.4 Modifications to the Debye theory

However, in practice, the Debye response is seldom seen, as systems invariably contain more than one dipole, hence the behaviour is likely to be complicated by interactions between these components. In general, the Debye relaxation is only observed in some dilute solutions or in ferroelectric materials in which the interaction between dipoles in the condensed system plays an important role. The measured shape of the dielectric loss spectrum, ε'' , is broader and more asymmetric than that reported by Debye, possibly because it comprises several simple relaxations (for example due to a distribution of molecular weights), and is determined by the integration of the distribution function $G(t)$ [20, 23]:

$$\varepsilon^* = \varepsilon_\infty + \int_0^\infty \frac{\varepsilon_s - \varepsilon_\infty}{1 + i\omega\tau} \cdot G(\tau) \cdot d(\tau) \quad (2-14)$$

There exist several proposed models for obtaining the distribution $G(t)$ [24, 25] but the problem has not been properly resolved. Hence, empirical formulae obtained in the frequency domain are based on “non-Debye” types of relaxation that have been developed by Cole, Davidson, Harvriiak and Negami [26 – 28]. The latter is the most general:

$$\varepsilon^* = \varepsilon_\infty + \frac{\varepsilon_s - \varepsilon_\infty}{[1 + (i\omega\tau)^\alpha]^\beta} \quad (2-15)$$

where α and β are the parameters dependent on the form of response

- If $\alpha = \beta = 1$, it is a Debye response;
- For $0 < \alpha < 1$ and $\beta = 1$, it is the Cole-Cole response for amorphous solids and certain polymers [26];
- $\alpha = 1$ and $0 < \beta < 1$ are representative of the dielectric response of liquids and polymer solutions. This model was proposed by Davidson and Cole [27];
- $0 < \alpha < 1$ and $0 < \beta < 1$ corresponds to the Harvriiak-Negami response [28] and in general constitutes a good description for representing the behaviour of polymers [29], which is similar to that obtained by Dissado and Hill (§2.4.5).

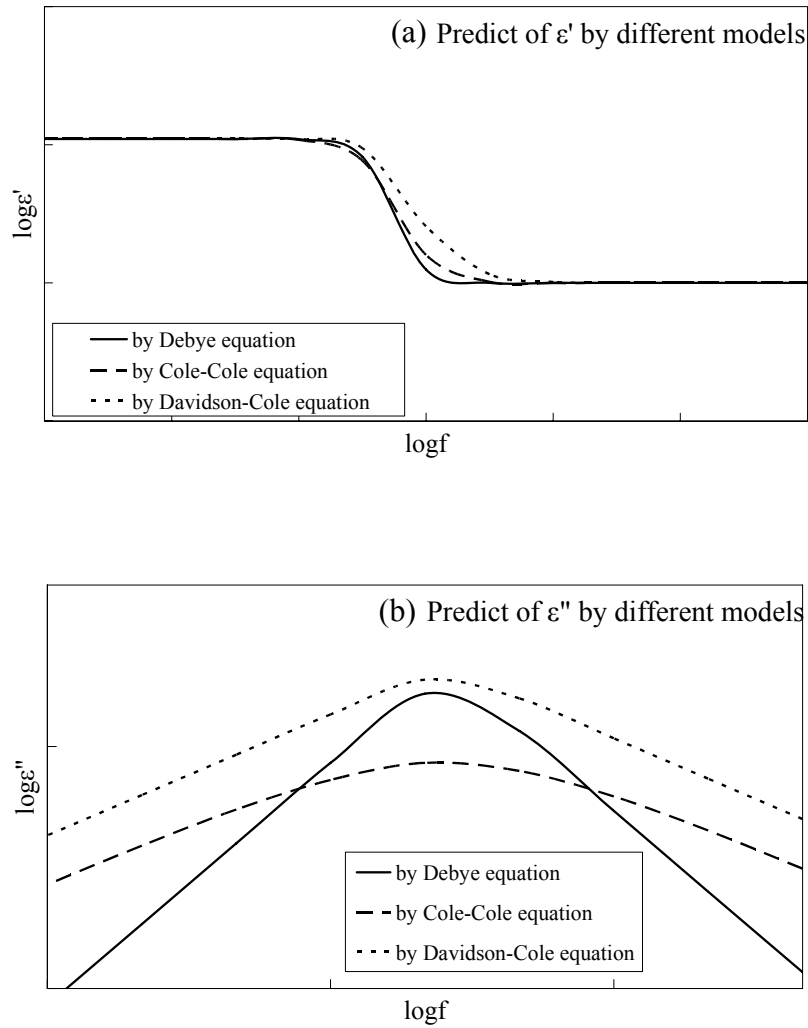


Figure 2.4. The real (a) and imaginary (b) parts of permittivity predicted by different models

In addition, at very low frequencies, a conductivity σ_{dc} may cause a strong increase in loss, which is easily visible in the imaginary part of the $\epsilon^*(\omega)$. The conductivity term can be added, which shows as

$$\epsilon^* = \epsilon_\infty + \frac{\epsilon_s - \epsilon_\infty}{[1 + (i\omega\tau)^\alpha]^\beta} + \frac{\sigma_{dc}}{j\epsilon_0\omega} = \epsilon'(\omega) - j[\epsilon''(\omega) + \frac{\sigma_{dc}}{\epsilon_0\omega}] \quad (2-16)$$

The connection between the real and imaginary parts of expression equation 2-11 corresponds to the dissipation factor $\tan \delta$. This is therefore expressed as

$$\tan \delta = \frac{[\varepsilon''(\omega) + \frac{\sigma_{dc}}{\varepsilon_0 \omega}]}{\varepsilon'(\omega)} \quad (2-17)$$

This measurement is often used in the qualification of dielectric properties of insulators.

2.4.5 Dissado-Hill theory and Quasi-d.c behaviour (QDC)

There are several further modifications that rely on the use of two power indices (as the Harvriiak-Negami does above) as it is arguable that a single susceptibility function is insufficient in most cases. Jonscher [30] has argued that power law behaviour is so common in dielectric behaviour that there must be a universal mechanism involved in all dielectric materials. It is suggested that the presence of many-body interactions, rather than a distribution of relaxation times, was a more likely explanation for the observed behaviour. The early work led Dissado and Hill [31] to develop a quantum mechanical approach (the Dissado-Hill theory) which makes certain predictions of real dielectric behaviour.

The essential features of the Dissado-Hill theory are firstly that materials are assumed to be composed of clusters. There are spatially-separated groups within a specimen that show cooperative behaviour during the relaxation process. The relaxation behaviour of these clusters will affect the overall shape of the response, as well as the absolute values at any particular frequency. The authors suggested that two power law exponents were required to fit a given set of data. These two exponents (n and m) are considered to refer to the degree of cooperation within a cluster and between separate clusters, respectively, with $0 < n < 1$, $0 < m < 1$. The theory further predicts that the Debye plot may be modified such that the loss slope above ω_p will be given by $(n-1)$ and below ω_p will be given by m . The Dissado-Hill equation is included here, which is of the form [31]

$$\chi_\omega = \frac{\chi_0}{\left\{ \frac{\omega_p}{\omega_p + i\omega} \right\}^{n-1}} \left[{}_2F_1(1-n, 1-m; 2-n; \frac{\omega_p}{\omega_p + i\omega}) \right] \quad (2-18)$$

where $0 < n < 1$, $0 < m < 1$, and ${}_2F_1(;;)$ is the Gaussian hypergeometric function, which is essentially an average function. The significance of the Dissado-Hill theory will be explained in conjunction with individual examples of application of the model.

In dielectric spectroscopy, a dielectric loss peak is often observed in the frequency dependence of the imaginary part of the susceptibility, in company with a dielectric increment in the real part [32 – 35].

The shape of the peak is generally given by [12]

$$\chi'(\omega) \propto \chi''(\omega) \propto \omega^{-(1-n)} \quad (\omega > \omega_p) \quad (2-19a)$$

$$\chi''(\omega) \propto \chi(0) - \alpha\chi'(\omega) \propto \omega^{+m} \quad (\omega < \omega_p) \quad (2-19b)$$

where α is a constant, and $\chi(0)$ is the susceptibility at zero frequency. The constants n and m are between zero and one. ω_p is the reciprocal of the relaxation time and it is the peak frequency of the dielectric loss dispersion.

It can also be shown that [36]

$$\chi''(\omega) / \chi'(\omega) = \cot(n\pi/2) \quad (\omega > \omega_p) \quad (2-20)$$

According to equations 2-19 and 2-20, as a QDC polarisation, there are two conditions should be fulfilled. One is the curves of the real and imaginary parts are parallel, their slopes are slightly lower than -1, and the loss tangent is constant in a range of frequencies; the other is the parameter n in equation 2-20 is constant and less than unity.

Jonscher found another form of response in which equation 2-19a is valid for both frequency ranges mentioned in equations 2-19a and 2-19b. No loss peak was observed in any of the frequency ranges. The response goes into a steeply rising branch towards the low frequency end. The susceptibility has been shown to be normalised with respect to its dependent variables in the same way as loss peak [12]. The same behaviour is called as anomalous low frequency dispersion (LFD) by Jonscher, or quasi d.c conductance (QDC) by Dissado and Hill.

Quasi d.c explained by the dynamical possibilities inherent in the material structure and possessing limiting partial diffusion behaviour [32]. Dissado and Hill developed a physical model to explain the mechanism of this process. The model is based on the concept of clusters of quasimobile charges possessing partial structural regularity, which leads to a power law response [31 – 33].

Replacing $l-n$ by p in equation 2-19a yields:

$$\chi'(\omega) \propto \chi''(\omega) \propto \omega^{-p} \quad (0.5 < p < 1) \quad (2-21)$$

This kind of behaviour can be explained by assuming self-similarity in the system or in its relaxation process. If p becomes equal to 1 then the process will be a d.c conductance. Equation 2-21 can be written in terms of capacitance as

$$C'(\omega) \propto C''(\omega) \propto \omega^{-p} \quad (2-22)$$

where C' and C'' are the real and imaginary parts of capacitance. Since $\tan \delta = C''/C'$, it is clear from this equation that $\tan \delta$ is constant.

Hence, QDC is a charge transport process that exhibits a region of constant phase angle behaviour (CPA) [35]. This form of response originates from the presence of partially mobile charge carriers in the material.

The difference of susceptibility response functions at the bottom and upper limits of frequency among the models of dielectric dispersion behaviour are shown in table 2.1.

Table 2.1. Susceptibility Response Functions for Different Models of Dielectric dispersion Behaviour

| Types | α | β | $\omega\tau \ll 1$ | $\omega\tau \gg 1$ |
|-----------------------|------------------|-----------------|--------------------|-------------------------|
| Debye | 1 | 1 | ω^0 | ω^{-1} |
| Cole-Cole | $0 < \alpha < 1$ | 1 | ω^0 | $\omega^{-\alpha}$ |
| Davidson-Cole | 1 | $0 < \beta < 1$ | ω^0 | $\omega^{-\beta}$ |
| Harvriiliak-Negami | $0 < \alpha < 1$ | $0 < \beta < 1$ | ω^α | $\omega^{-\alpha\beta}$ |
| Jonscher-Dissado-Hill | | | | |
| (i) reorientation | | | ω^m | ω^{n-1} |
| (ii) QDC | | | ω^{n_2-1} | ω^{n_1-1} |
| Maxwell-Wagner | | | ω^1 | ω^{-1} |

2.4.6 Equivalent circuit analysis of the dielectric response

A further technique that is often used to characterise the response of dielectric materials is to compare the specimen to a resistor/capacitor circuit which would give an identical response, i.e., an “equivalent circuit”.

(1) DC polarisation

An insulator may be described by a resistor R_s in series with a capacitance C_s , as shown below.

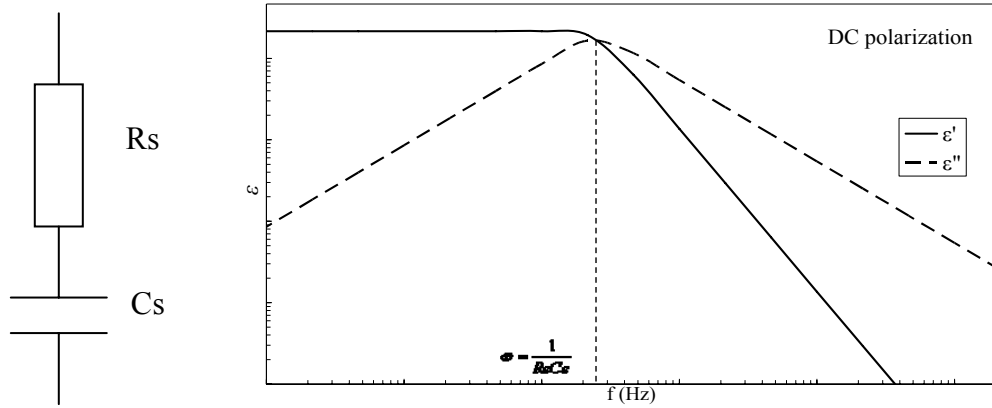


Figure 2.5. Schematic circuit diagram and the real/imaginary components of the complex dielectric permittivity for the DC polarisation

$$Z(\omega) = R_s + \frac{1}{i\omega C_s} = \frac{1}{i\omega C_0 \epsilon(\omega)}, \quad \epsilon^*(\omega) = \epsilon'(\omega) - i\epsilon''(\omega)$$

$$\Rightarrow \epsilon'(\omega) = \frac{C_s}{C_0(1 + R_s^2 \omega^2 C_s^2)}$$

$$\epsilon''(\omega) = \frac{R_s \omega C_s^2}{C_0(1 + R_s^2 \omega^2 C_s^2)}$$

$\Rightarrow \epsilon'(\omega)$ is monotonically decreasing from a constant value with ω increasing

$$\epsilon''(\omega) \text{ has a peak at } \omega = \frac{1}{R_s C_s}$$

$$\Rightarrow \epsilon''(\omega) \propto \omega^{-1} \text{ when } \omega \gg \frac{1}{R_s C_s}$$

(2) Maxwell-Wagner polarisation

In the case of solid protonic conductors such as solid acids, polymers, oxide ceramics, and intercalation compounds [37, 38], the electrodes are usually “blocking”, namely they are able to eliminate free exchange between electronic and protonic charge carriers at the specimen–electrode interfaces. In practice, this configuration can be easily achieved by interposing an extremely thin layer of an insulating material between the metallic electrode and the specimen: no steady-current can then flow, but there is a build-up of space charge within the specimen adjacent to the electrodes, that lead to the formation of electrical double layers. The associated capacitance and complex admittance due to this polarization is so large, particularly at low

frequencies, that the correction for it is one of the major requisites in obtaining meaningful measurements on conductive specimens [39]. This phenomenon is referred as the Maxwell-Wagner (MW) effect. The MW polarisation is expected at the low frequency range. If the permittivity of the additive is reduced, the MW transition band shifts to quite low frequencies. Maxwell-Wagner (MW) polarisation can be described as the below circuit.

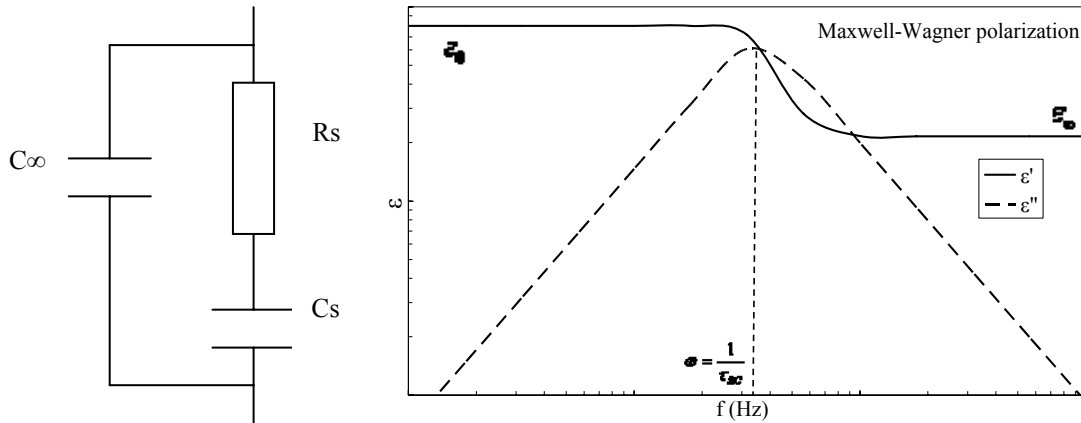


Figure 2.6. Schematic circuit diagram and the real/imaginary components of the complex dielectric permittivity for the Maxwell-Wagner polarisation

$$Y(\omega) = i\omega C_0 \varepsilon(\omega) = i\omega C_\infty + \frac{1}{R_s + \frac{1}{i\omega C_s}}$$

$$\Rightarrow \varepsilon'(\omega) = \varepsilon_\infty + \frac{\varepsilon_0 - \varepsilon_\infty}{1 + \omega^2 \tau_{RC}^2}$$

$$\varepsilon''(\omega) = (\varepsilon_0 - \varepsilon_\infty) \frac{\omega \tau_{RC}}{1 + \omega^2 \tau_{RC}^2}$$

$\Rightarrow \varepsilon'(\omega)$ has the upper onset ε_0 and the bottom onset ε_∞ ,

when $\omega \rightarrow \frac{1}{\tau_{RC}}$, $\varepsilon' \propto \omega^{-2}$

$\varepsilon''(\omega)$ has a peak value at $\omega = \frac{1}{\tau_{RC}}$, when $\omega \gg \frac{1}{\tau_{RC}}$, $\varepsilon'' \propto \omega^{-1}$,

when $\omega \ll \frac{1}{\tau_{RC}}$, $\varepsilon'' \rightarrow 0$

(3) Considering the conduction effect

If the conduction effect is considered, a resistor R_p should be in parallel with the MW model.

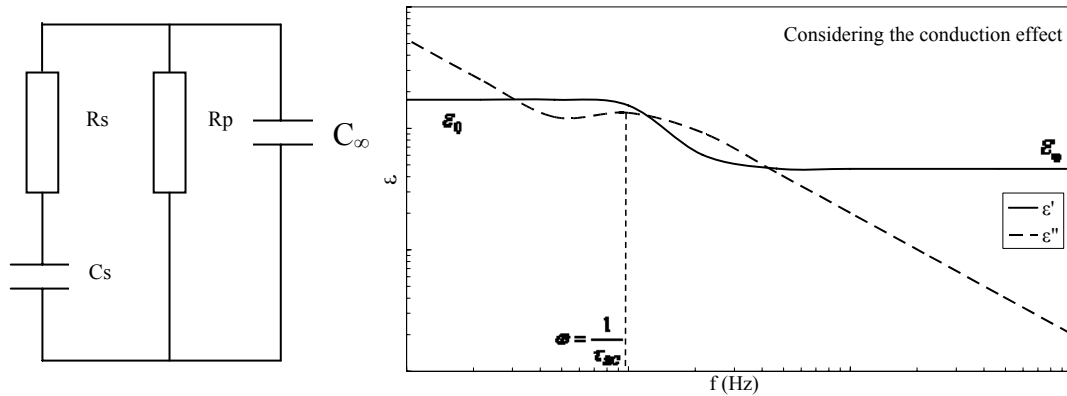


Figure 2.7. Schematic circuit diagram and the real/imaginary components of the complex dielectric permittivity under the consideration of the conduction effect

$$\varepsilon(\omega) = \varepsilon_{\infty} + \frac{\varepsilon_0 - \varepsilon_{\infty}}{1 + i\omega\tau_{RC}} - \frac{i}{\omega C_0 R_p}$$

$$\Rightarrow \varepsilon'(\omega) = \varepsilon_{\infty} + \frac{\varepsilon_0 - \varepsilon_{\infty}}{1 + \omega^2 \tau_{RC}^2}$$

$$\varepsilon''(\omega) = \frac{(\varepsilon_0 - \varepsilon_{\infty})\omega\tau_{RC}}{1 + \omega^2 \tau_{RC}^2} + \frac{1}{\omega C_0 R_p}$$

$\Rightarrow \varepsilon'(\omega)$ has the upper onset ε_0 and the bottom onset ε_{∞} ,

when $\omega \gg \frac{1}{\tau_{RC}}$, $\varepsilon' \propto \omega^{-2}$;

$\varepsilon''(\omega)$ has a peak value at $\omega = \frac{1}{\tau_{RC}}$, when $\omega \ll \frac{1}{\tau_{RC}}$ or $\omega \gg \frac{1}{\tau_{RC}}$, $\varepsilon'' \propto \omega^{-1}$

2.4.7 Master plot technique

It is often found that the frequency dependence does not change very obviously with temperature, at least over temperature ranges over which the material does not alter its structure in any significant way. This means that it is often possible to normalise the data for different temperatures by shifting the frequency spectra laterally (or in some cases both laterally and vertically) into coincidence obtaining sometimes a single “master plot” which gives a complete description of the behaviour when accompanied by the locus of the translation point [12, 40].

This technique consists in taking a family of loss spectra in log-log representation of frequency, with temperature as the usual parameter [12]. Normally, the curve at the lowest (or the highest) temperature will be chosen as the base curve, and the other curves shifted to coincide with this base curve in the log-log figure [12]. The distances which the other curves shift will be recorded and used to calculate the activation energy of the relaxation processes [12]. When the spectral shape of the loss characteristic does not change significantly with changing temperature, the master plot is uniquely determined [12]. Moreover, the density of data points on the master plot is significantly higher than the original temperatures runs, thus increasing the reliability of the information contained in the master plot [12]. Also, the activation energy of the relaxation process can be calculated using the Arrhenius equation [12]:

$$\omega_p(T) = \nu_0 \exp(-E_a / kT) \quad (2-23)$$

2.5 Space charge in solid dielectrics

The behaviour of charge in solid dielectrics has been investigated extensively by many means. Space-charge limited field conduction (SCLC) may result when such charge is trapped [41]. Under a sufficiently strong electric field, the traps may become filled and cause the current to rise by several orders of magnitude to be equivalent to electrical breakdown or ageing. It has been proposed that the presence of persistent space charge can enhance the electrical field locally and is an important factor in determining electrical ageing and breakdown [3]. To obtain a polymeric material with desirable dielectric behaviour, some questions about space charge have to come to mind.

- How does space charge come into being?
- How does space charge accumulate and decay under a high electrical field?
- How does space charge behaviour affect the dielectric properties of polymer?

These questions above are discussed in this section.

2.5.1 The origin of space charge in polymer

Generally, space charge may be supplied from the electrode or be generated within the bulk of the polymer. The supply of charge from the electrode involves a transfer of either electrons or holes across the electrode-polymer interface. These processes are strongly dependant on the conditions at the interfaces, which include electrode materials [42], surface defects [41], impurities [42], oxidation and so on [43, 3, 44]. The generation of space charge within the bulk of the polymer is usually associated with ionisation of chemical species in the polymer. These may be chemical products introduced during the manufacturing of the material, such as residues of a crosslinking reaction, antioxidant and other impurities [44]. In addition, the formation of space charge in polymers subjected to HVDC stress is strongly dependent on applied stress and temperature. Thus, various different distributions of space charge may be observed, even in the same specimen [44, 41].

The combination of a spatially inhomogeneous resistivity and current density can be given by

$$\zeta(x) = J\varepsilon \frac{d\rho(x)}{dx} \quad (2-24)$$

where ζ is the space charge density, J is the current density, ε is the absolute permittivity, and ρ is the electrical resistivity [45].

Moreover, some localised polarisations, for example, water trees, might enhance space charge accumulation in the polymers.

2.5.2 The transport of space charge

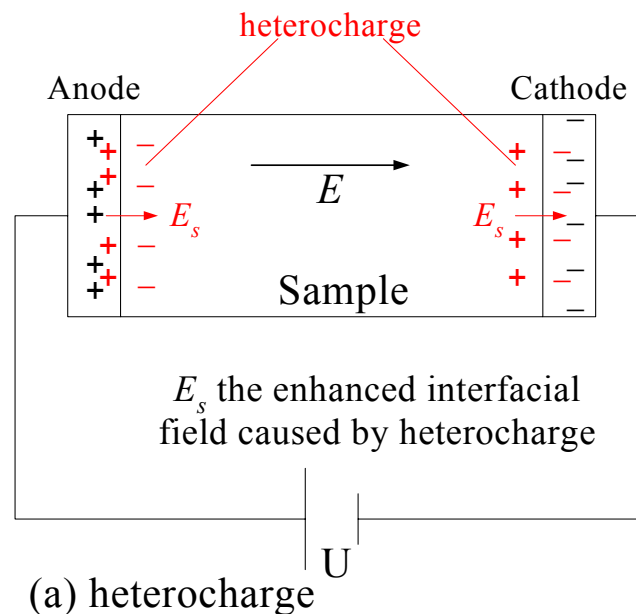
The accumulation of space charge in a solid will require charge to be transported, which is a process, at least at low charge carrier energies, comprising a series of transfers between localised states.

It would be possible to ionise a donor site and the electron so removed to proceed through the solid via a series of acceptor states [41]. However the charges of the ionised donor and acceptor states are Coulombically attracted and likely to be strongly

coupled [41]. Equally there is the possibility of the hole of the ionised donor proceeding through a series of donor states but the same strong coupling to the electron in an acceptor state will limit this [41]. These situations do not give rise to a net overall space charge in the solid. Production of net space charge (the imbalance between amounts of incoming and outgoing charges) will come about either by electron injection into the solid via acceptor states or electron ejection out of the solid from donor states (hole injection) [41].

2.5.3 Ageing, breakdown and space charge

The presence of persistent space charge can distort the electrical field locally and is an important factor in determining electrical ageing and breakdown [41]. Figure 2.8 shows the influence of the heterocharge (figure 2.8a) and homocharge (figure 2.8b) on the interfacial and bulk fields of polymers. If heterocharge is induced at the interfaces near the electrodes, an additional field is formed in this region. This region of heterocharge accumulated has to stand a higher field, figure 2.8a. Contrarily, the local field in the bulk of the matrix is enhanced if homocharge is formed, figure 2.8b.



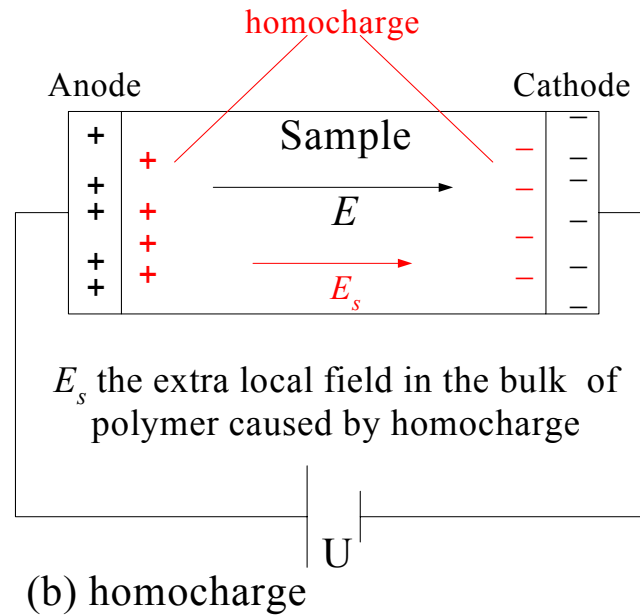


Figure 2.8. The detrimental situations to the polymer specimens caused by heterocharge (a) and homocharge (b)

Equation 2-24 indicates that the space charge density is proportional to the current density in the case of a dielectric with a spatially changing resistivity. It is expected that space charge may increase rapidly above a nonlinear threshold in the current density, and, indeed, this has been observed [46].

Space charge is considered one of the major causes of degradation in polymers. It can, of course simple increase the local electrical field in the bulk of insulation or at the electrode-insulation interfaces (as discussed above). However, space charge may involve the storage of electromechanical energy that may increase the degradation reaction rate. Moreover, this causes ionisation, excitation and recombination phenomena that involve considerable energy exchanges which may lead to thermalisation [47] of potential charge carriers.

2.6 Percolation and Effective Media Theory

Most modelling of electrical properties of composites attempts to predict both the electrical properties and the mechanical properties. By using the electrical properties to determine the microstructure, the mechanical properties can be predicted through the microstructural models.

Many mixing models exist which are able to predict property are based on the dc conductivity/resistivity, and work best for dilute composites. These models include:

$$\text{Parallel Model} \quad \sigma_m = v_i \sigma_i + v_c \sigma_c \quad (2-25)$$

$$\text{Series Model} \quad \frac{1}{\sigma_m} = \frac{v_i}{\sigma_i} + \frac{v_c}{\sigma_c} \quad (2-26)$$

$$\text{Lichteneckers Rule} \quad \log \sigma_m = v_i \log \sigma_i + v_c \log \sigma_c \quad (2-27)$$

where σ_c and σ_i are the conductivities of the conducting and insulating phase respectively, v_c and v_i are the volume fractions of the conducting and insulating phase, respectively, and σ_m is the conductivity of the composite [48].

Another popular method of predicting the properties of composites is percolation theory, which is based on the assumption that the properties will change greatly when the second phase is totally connected from one side of the composite to the other [49]. The volume fraction at which this occurs is called the percolation threshold. It depends on many factors including the connectivity of the phases, the size of each phase, the shape of each phase, and the wetting behaviour of the phases. Percolation models allow for a large (orders of magnitude) change of properties over a very small concentration range [50].

As a mixing system, composites filled with inorganic fillers are ideal objects from the point of view of percolation theory. When the concentration of fillers is low, the composites will behave more like the insulting matrix; once the volume fraction of fillers reaches the certain percolation threshold, for example ~19 vol% in systems containing spherical impurities [51], the electrical properties of composites can be obviously changed by the channels formed in which charges carriers connect inorganic fillers.

Percolation theory can be mixed with the Effective Media theory [52], which models the complex conductivity (dielectric constant) over the entire volume fraction and a limited frequency range, as

$$(v_i) \frac{\sigma_i^{1/s} - \sigma_m^{1/s}}{\sigma_i^{1/s} + (1/f_c - 1)\sigma_m^{1/s}} + (v_c) \frac{\sigma_c^{1/t} - \sigma_m^{1/t}}{\sigma_c^{1/t} + (1/f_c - 1)\sigma_m^{1/t}} = 0 \quad (2-28)$$

where s and t are modelling parameters, which only depend on the concentration of interruptions along the highly conducting direction [52]. f_c is the critical volume fraction, and all other variables are defined as equations 2-25 to 2-27 [49].

In the effective media theory, the composites are considered as a disordered network composed of inorganic fillers, the average effects of the random conductances in such system will be represented by an anisotropic “effective network” in which all the conductances in a certain direction have the same value. These effective conductivities $\bar{\sigma}_v$ are self-consistently determined by the requirement that the fluctuating “local fields” in the random network should be average to zero [52].

2.7 Electric conduction mechanisms in polymers

Normally, at the low electrical fields, it is found or assumed that the conduction of electrical current in polymers and insulators is ohmic. However, the polymers electrical properties change when subjected to higher electric fields and temperatures for a long time. The conduction and storage of charge in polymers depends on lots of material parameters such as crystallinity, crosslinking and additives [53].

The electrical conduction mechanisms in composites are complicated. The classical conduction and transport mechanisms found in conductors and semiconductors are not found in polymers. This is due to the difference of morphology and chemistry of the polymer. Consequently different mechanisms operate. Charge injection from electrodes into polymer, traps and volumetric conduction, tunnelling and hopping conduction were found to play an important role in conduction and charge transport in polymers. Electric conduction may therefore depend on material preparations and their thermal history and it becomes very difficult to determine the conduction mechanism. In general, electric conduction may occur through the movement of either electrons (holes) or ions. The conductivity, σ , varies exponentially with temperature and can be described as

$$\sigma = \sigma_0 \exp\left(-\frac{\phi}{kT}\right) = \sum q_i n_i \mu_i \quad (2-29)$$

where σ_0 is a material constant, ϕ is the activation energy, k is the Boltzmann constant, T is the temperature, q_i , n_i and μ_i is the charge, the density and the mobility of the *i*th species, respectively.

The steady state conduction current in composites is controlled by either electrode or bulk processes. Usually, more than one mechanism may operate at the same time, but only one is dominating.

2.7.1 Electronic processes

Under a high external field, many electrons may be injected into polymers from the cathode. However, the condition of the electrode-insulator interface is very complicated [3]. Electrical, chemical and physical defects are likely to exist at the interface. Such defects include protrusions, imperfect contacts, dangling bonds, and local polarisation, contaminants, and traps. The main two theories that describe the interface phenomenon are Schottky and Fowler Nordheim. Electrons are injected from electrodes into the bulk of material. Electrons need to overcome a potential barrier to cross from electrode into insulator. Crossing the barrier depends on applied electric field and the interface defects [54].

2.7.2 Schottky injection

The Schottky injection mechanism arises from field assisted thermionic injection of electrons from an electrode into the conduction band of the insulator [53]. Schottky injection describes a way in which electrons are transferred from electrodes into a dielectric [54]. At an electrode-insulator interface, electrons overcome the potential barrier, leave the metal electrode and move to the adjacent insulation material. The barrier is assumed to be abrupt between the metal and the insulator. In Schottky injection the barrier is modified by the electrostatic attraction between the positively charged electrodes, since it has lost an electron. This electrostatic attraction leads to a change in the barrier due to the electron potential energy.

The current density, J , can be obtained by the following equation,

$$J = AT^2 \exp\left(-\frac{\phi - \beta_s \sqrt{E}}{kT}\right) \quad \left(\beta_s = \sqrt{\frac{e^3}{4\pi\epsilon_0\epsilon_r}}\right) \quad (2-30)$$

where A is the Richard-Dushman constant ($A = 1.2 \times 10^6 \text{ A} \cdot \text{m}^{-2} \cdot \text{K}^{-1}$), ϵ_0 is the permittivity of free space, ϵ_r is the dielectric permittivity and E is the applied electrical field at the electrode interface.

2.7.3 Fowler-Nordheim injection

At high fields and short distances the potential barrier becomes very thin and non-classical mechanisms come into existence. Classical physics is no longer valid in this situation. Particles exhibit particle-wave duality and the principle of uncertainty comes into play [54]. This will lead to electrons tunnelling through a potential energy barrier despite not having enough energy to hop over them. Also electrons will have a finite probability of existing at two different localised states. When this occurs at the contact barrier it is known as Fowler-Nordheim injection.

It is noted Fowler-Nordheim injection is unlikely to occur through a polymer film. It would probably have to be less than 40 nm thick. It may occur at a film-electrode boundary under high enough fields, or perhaps even at the surface of a nanoparticle [54].

2.7.4 Bulk process

The main two theories of conduction mechanisms in the bulk under the influence of a high electrical field are Space Charge Limited Conduction (SCLC) and the Poole-Frenkel mechanisms.

SCLC occurs when the current becomes limited by space charge injected by the electrodes. The current flowing between the electrodes will then depend on the charge concentration, the type of charge, the injecting properties of the electrodes, the mobility of the charge carriers and the trapping characteristics of the insulation. If the situation is highly injecting electrodes and uniformly distributed space charge exists, the current density can be expressed as

$$J = \theta \frac{9\varepsilon_0\varepsilon_r\mu V^2}{8d^3} \tag{2-31}$$

where θ is the ratio of electrons in the conduction band and in traps, μ is the mobility, V is the applied voltage and d is the thickness of the insulator.

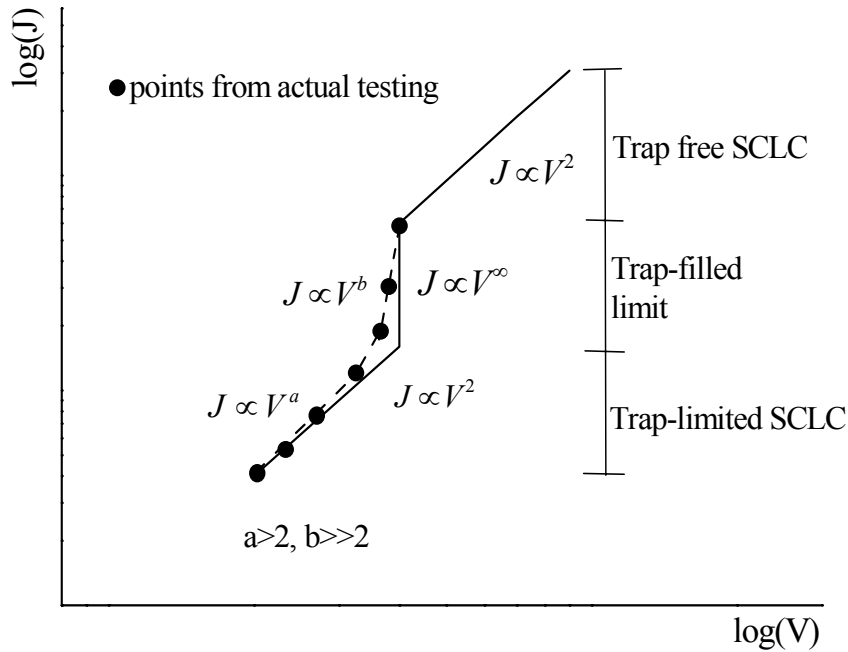


Figure 2.9. Schematic diagram showing current density J versus applied voltage V in the case of space charge limited conduction

As shown in figure 2.9, in practice, the real curve of J versus V exhibits a steep increment of J with a very high slope (3 – 10) rather than $J \propto V^\infty$ during the process of trap-filled limit.

The Poole-Frenkel mechanism is the bulk equivalent to the Schottky effect and arises from field dependent thermionic emission from traps in the bulk of the insulator [55]. An electron trapped in a donor state is normally surrounded by a potential barrier with height ϕ . If a donor state is ionised, the Coulombic force between the electron and the donor will modify this energy barrier. With an applied field, the reduction of the barrier becomes proportional to the square root of the applied field. The conduction current strongly depends on the expression of the energy band of the material, which is

$$\sigma = \sigma_0 \exp\left(\frac{\beta_{PF} \sqrt{E}}{2kT}\right) \quad \left(\beta_{PF} = \sqrt{\frac{e^3}{\pi \epsilon_0 \epsilon_r}}\right) \quad (2-32)$$

where σ_0 is a constant.

Hence, the Poole-Frenkel effect is strongly related with temperature T , at room temperature the probability of creating free electrons and/or free holes is small. Wintle has argued that the Poole-Frenkel mechanism for field dependent conduction is unacceptable, despite the many papers devoted to it, because under typical conditions the maximum of the barrier to escape is -8 nm from the trap, and the putative free carrier will collide with phonons and thermalise before it reaches the escape zone [56].

2.7.5 Ionic conduction

If an ion is trapped in a symmetrical potential well, there is a certain probability of moving from one position to an adjacent for this ion due to thermal oscillations. With the increasing applied field, the probability is increasing in the direction of the field. The expression of current density J at a certain temperature T is given as [57],

$$J \propto \sinh\left(\frac{qdE}{2kT}\right) \quad (2-33)$$

where q is the charge of this ion, and d is the distance between neighbouring positions.

2.7.6 Summary for various conduction mechanisms in insulators

Some basic conduction processes in insulators are expressed in table 2.2 [58].

Table 2.2. Basic conduction processes in insulators [58]

| Processes | Expression | Voltage/temperature dependence |
|-------------------------|-----------------------------------------------------------------------------------|------------------------------------------------------------------------------------------|
| Ionic | $J \propto \frac{E}{T} \exp(-\Delta E_{ai} / kT)$ | $\sim \frac{V}{T} \exp(-d'/T)$ |
| Electron hopping | $J \propto E \exp(-\Delta E_{ae} / kT)$ | $\sim V \exp(-c/T)$ |
| Schottky emission | $J = A^* T^2 \exp\left[-\frac{e(\phi_B - \sqrt{eE / 4\pi\epsilon_i})}{kT}\right]$ | $\sim T^2 \exp\left(\frac{-B + aV^{1/2}}{kT}\right)$ |
| Poole-Frenkel emission | $J \propto E \exp\left[-\frac{e(\phi_B - \sqrt{eE / \pi\epsilon_i})}{kT}\right]$ | $\sim T^2 \exp\left(\frac{-B + 2aV^{1/2}}{kT}\right)$ |
| Space-charge-limited | $J = \frac{8\epsilon_i \mu V^2}{ed^3}$ | $\sim V^2$ |
| Tunnel (field) emission | $J \propto E^2 \exp\left[-\frac{8\pi\sqrt{(2m^*)}(e\phi_B)^{3/2}}{3ehE}\right]$ | $\sim V^2 \exp\left(-\frac{b}{V}\right)$ or $\sim V \exp\left(-\frac{b}{V^{1/2}}\right)$ |

A^* , effective Richardson constant;

ϕ_B , barrier height;

E , electric field;

ϵ_i , insulator dynamic permittivity;

m^* , effective mass;

d , insulator thickness;

ΔE_{ae} , activation energy of electrons;

ΔE_{ai} , activation energy of ions;

$B = e\phi_B$; $a = (e^3 / 4\pi\epsilon_i dk^2)^{1/2}$;

Positive constants independent of V or T are b , c and d' .

Chapter 3

Experimental Techniques

In this chapter the polymeric materials preparation and measurement methods are presented. The aims of each measurement and how to set up each experiment are introduced. An important part of the work is the characterisation of the physical, chemical and dielectric behaviours of nanocomposites at various hydration levels. To study these, a method of controlling the relative humidity during the measurements is also presented in this chapter.

3.1 Materials preparation

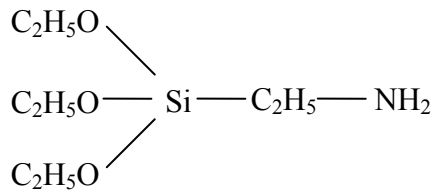
Two types of thermosetting polymers were studied in this research. One is crosslinked polyethylene (XLPE), and the other is an amorphous material: epoxy resin. Both of them are widely used in electrical systems, for example, high voltage power cables, the insulation of power transformers, line posts, rotating machines, etc. Information about the polymers is provided below.

3.1.1 Polyethylene composites

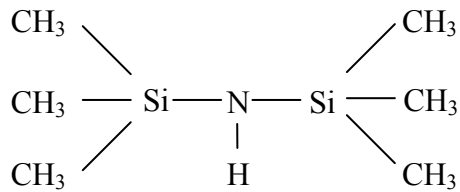
The polyethylene nanocomposites studied were prepared and kindly provided by Prof J Keith Nelson, Rensselaer Polytechnic Institute, USA.

The host matrix used in this study was a cable grade polyethylene (Borealis LS4212). This is a high purity, filtered resin containing antioxidants. These additives are non-ionic and do not contribute to the base polymer conductivity. The polyethylene contains the cross-linking agent dicumyl peroxide (DCP), which reacts at temperatures above the compounding temperature creating a crosslinked matrix. This was studied both unfilled and filled with 5% (by weight) of fumed SiO₂ nanoparticles having a mean diameter of 15 nm. As well as characterising composites containing unfunctionalised particles, some were functionalised using [1]:

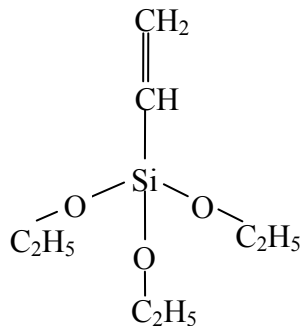
(a) Aminosilane (polar)



(b) Hexamethyldisilazane, [HMDS] (polar)



(c) Triethoxyvinylsilane (non-polar)



For the sake of comparison, polyethylene – SiO₂ composites have also been formulated utilizing microparticles. Specimens were given the following abbreviations:

- base resin specimen: XLPE
- with 5 wt% silica microparticles: MPE
- with untreated nanoparticles: UnnPE
- with aminosilane treated nanoparticle:s AmnPE
- with hexamethyldisilazane treated nanoparticles: HmnPE
- with triethoxyvinylsilane treated nanoparticles: VinPE

Proper dispersion of filler, cross-linking, and elimination of cross-linking byproducts are essential to achieving the optimum properties of the nanocomposite. Since absorbed water will cause particle agglomeration, vacuum drying of all the micro and nano-particles was carried out at 468K for 24 hours immediately prior to compounding (except for the vinylsilane-treated particles which were dried at 433K to prevent damage to the functionalisation). The composite was mixed with a melt mixer above the melting temperature of the polymer [1].

The laminar specimens were used for dielectric spectroscopy, conduction current measurement and pulsed electro-acoustic analysis (PEA). All specimens were created by hot pressing, and allowed to cool slowly to room temperature, keeping the pressure constant. The specimens were post-cured under vacuum. The specimens meant for electrical testing were metallised to a thickness of ~15 nm by sputtering gold.

3.1.2 Epoxy composites

The epoxy specimens were prepared by Schneider Electric, France.

The resin studied was an epoxy based on diglycidyl ether of bisphenol A (Araldite CY 225 from Huntsman) and cured with a hardener (HY 227, Huntsman). The process diagram of epoxy specimens is shown in figure 3.1. Before being mixed, CY 225 and HY 227 were put in a vacuum oven (10^3 Pa, 333K) for two hours to remove water and to preheat them, and the inorganic fillers, both nano- and micro-, were put in another vacuum oven (10^3 Pa, 423K) for over 17 hours to remove water and then cooled to 333K. The epoxy CY 225 was mixed with the same weight of hardener HY 227 in a vacuum agitator tank, i.e., the polymerization tank (10^3 Pa, 333K) and stirred for 15 minutes. Then the inorganic filler was added very slowly, and stirring was maintained for 45 minutes. After that, the accelerator (DY 062, CIBA Speciality Chemicals) was added and stirring for another 15 minutes. The rotation rate was 500 rpm. During the moulding process, the fluid of epoxy resin containing the particles was cast into the plate moulds assisted by a vacuum pump. The condition of cure was in a vacuum oven (10^2 Pa) at 373K for 2 hours and postcured out of the mould at 403K for 16 hours packed in iron plates with a weight on top, then cooled to 333K for 4 hours to protect specimens from the residual stresses.

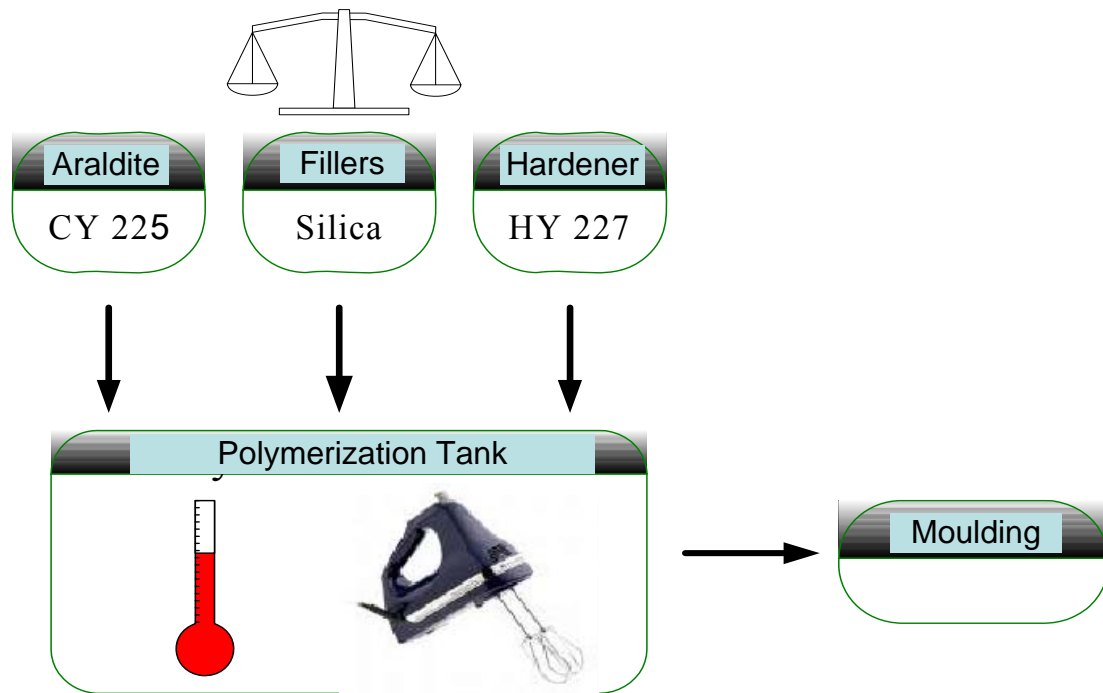


Figure 3.1. Process diagram of Epoxy specimens

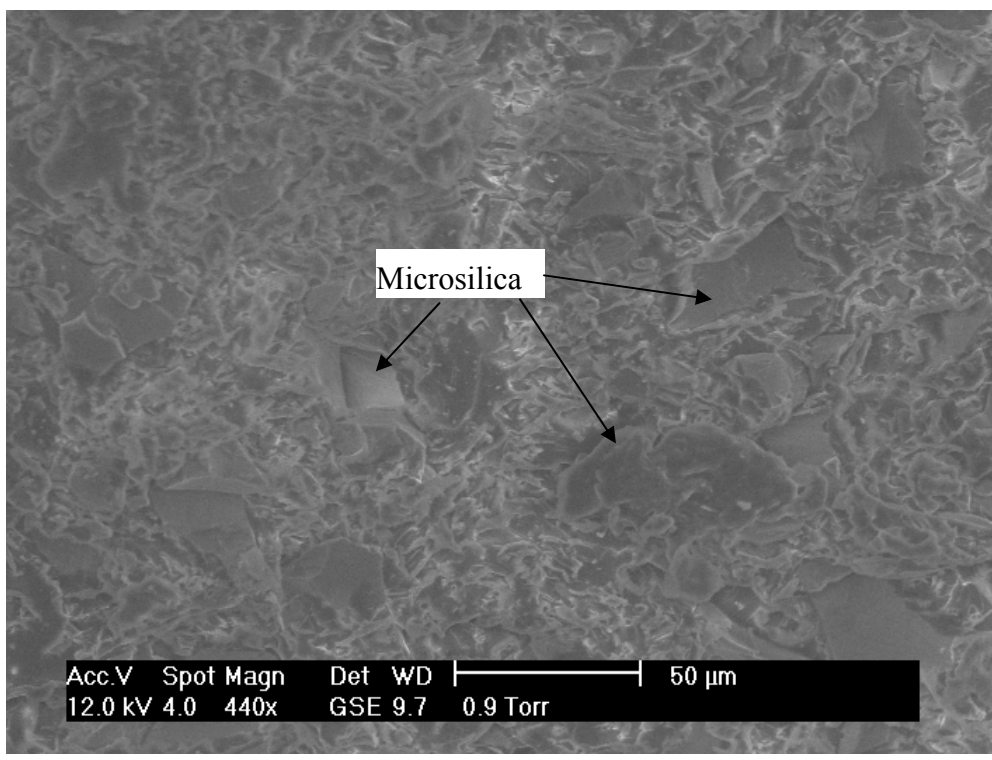
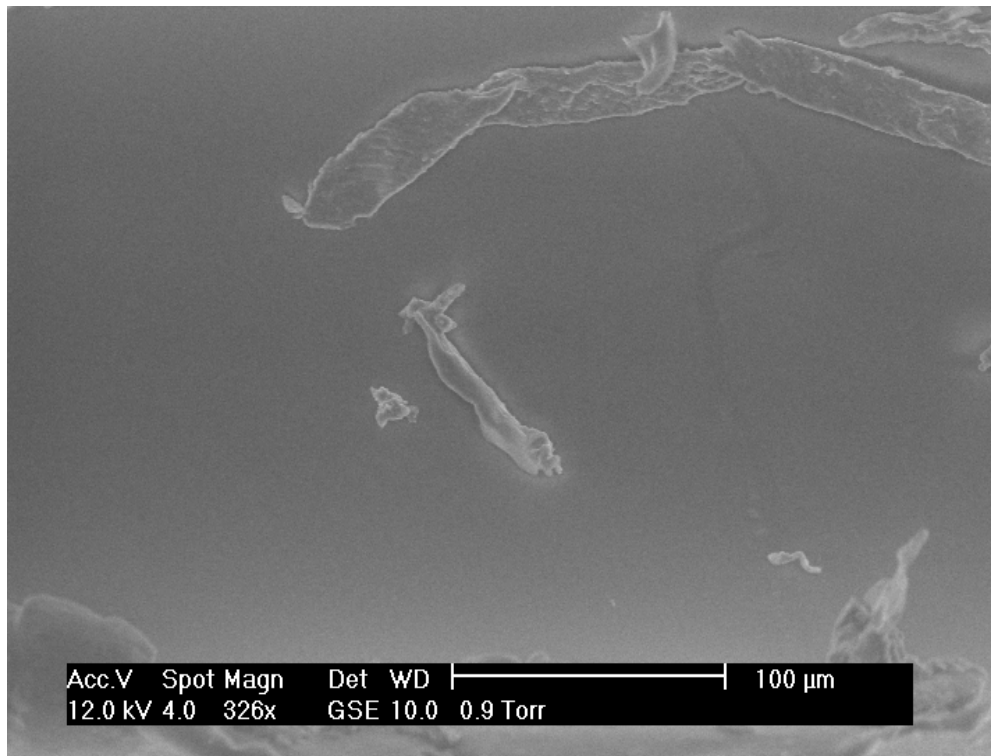
The abbreviations used for the epoxy composites are as follows:

- unfilled epoxy resin: matrix
- with 3 wt% nanofiller: n3
- with 9 wt% nanofiller: n9
- with 60 wt% microfiller: M60

The average size of the nanoparticles was 50 nm, and that of the microparticles was 40 μm . The epoxy specimens were cast into plates with the thickness of 0.5 ± 0.1 mm. The plates of epoxy specimens were cut into the disks with a diameter of 60 ± 2 mm. The weight range of such disks was 1.3 – 3.4 g.

3.2 Physical and Chemical characterisation

The surface conditions and homogeneity of epoxy composites were investigated with a Phillips XL30 ESEM scanning electron microscope (SEM). SEM photographs of epoxy materials are shown in figure 3.2.



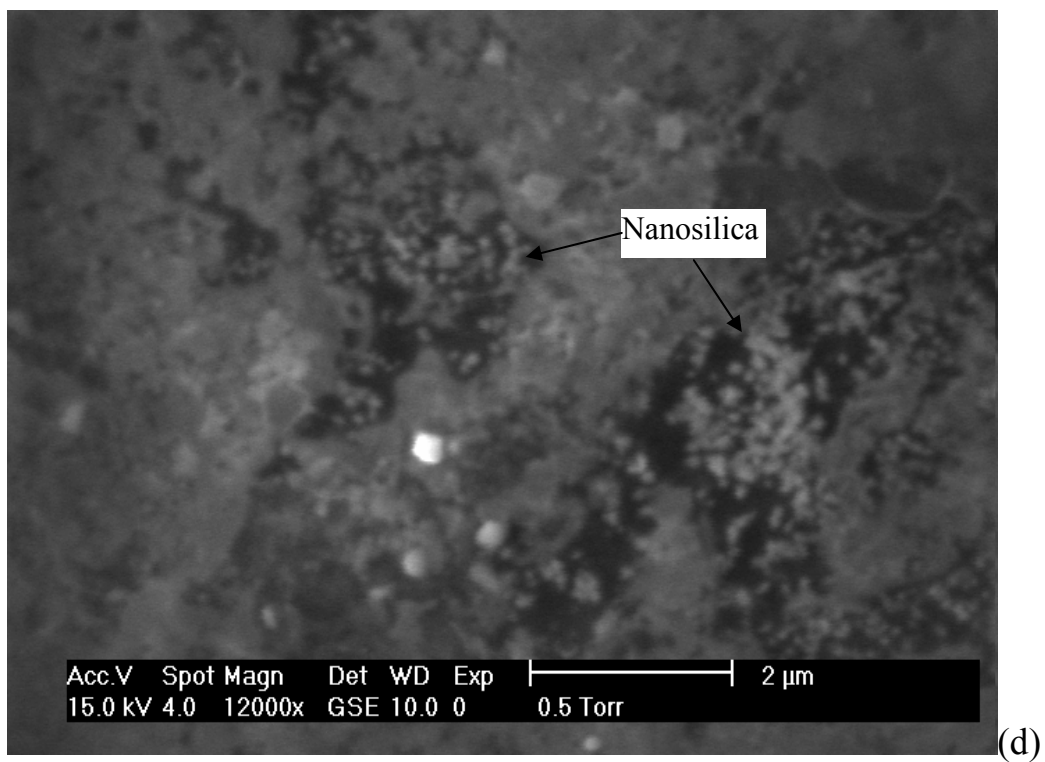
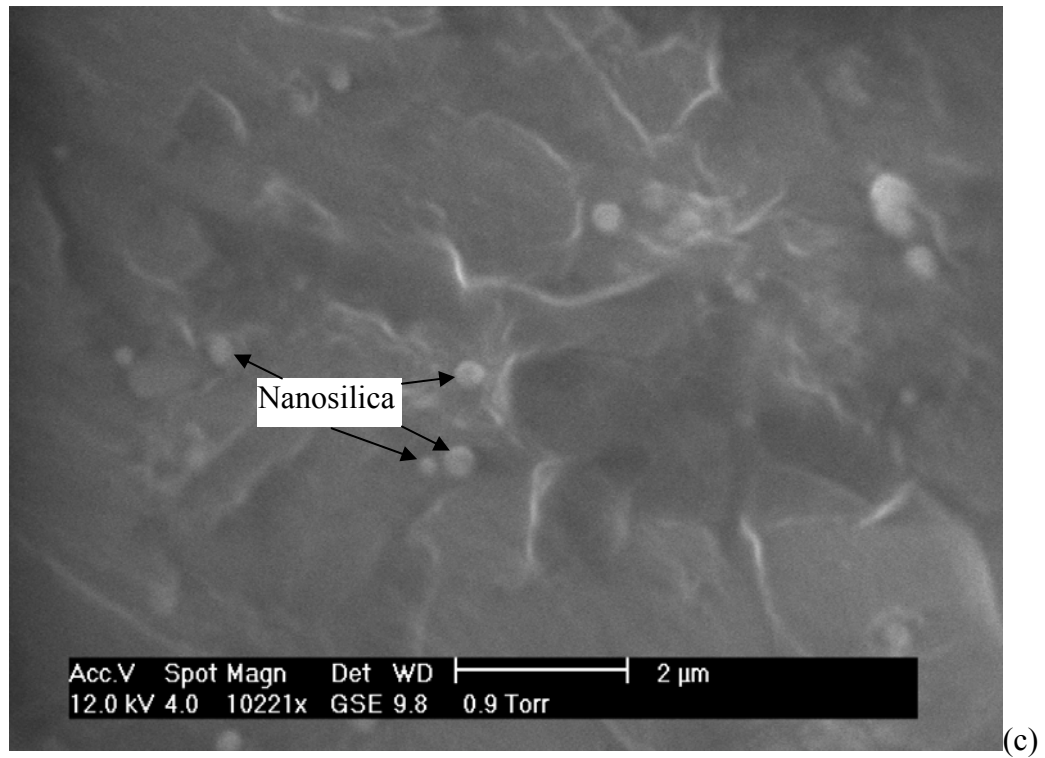


Figure 3.2. SEM photographs of epoxy materials, (a) epoxy matrix; (b) microcomposites (M60); (c) 3 wt% nanocomposites; and (d) 9 wt% nanocomposites

According to figure 3.2, the surface condition of the epoxy matrix was quite smooth and flat. The average size of microparticles in microcomposites, which is observed in figure 3.2(b), is about 40 μm , this coincides with that of microparticles before mixed into epoxy matrix. Figure 3.2 (c) shows a typical micrograph for the n3 system indicating good dispersion. The n9 system was also generally well dispersed, although Figure 3.2 (d) shows a region in which there is more agglomeration than usual.

The average distance between each nanoparticle and its neighbours in nanocomposites 3 wt% (1.5 vol%) filled is about 3 – 10 times bigger than the average size of nanoparticles, which might be beyond the range of an interfacial zone around nanoparticles; however, the average distance in nanocomposites 9 wt% (4.5 vol%) filled is greatly reduced, and in general, some nanoparticles in 9 wt% nanocomposites even are connected with the others. For 60 wt% micro-filled composites, the average distance between each microparticle and its neighbours is quite small compared to the average size of microparticles, only about 10 – 20 μm .

The observation by SEM provided an overall view of the surface condition of epoxy specimens. This confirms the good dispersion of nano-particles into the epoxy matrix, and the average distance between each particle and its neighbour. Such information is important in the further analysis of the dielectric properties of epoxy specimens and the interface region surrounding the nanoparticles.

3.3 Measurements under the control of relative humidity

3.3.1 Humidity control

In this research, the effect of water on the dielectric properties of epoxy materials was investigated carefully. To obtain such results, the relative humidity had to be controlled during the measurements.

The specific points of relative humidity can be obtained by some specific saturated salt solutions. The method to obtain the certain humid environment has been informed by reference [2]. The relative humidity varies as the temperature changes, however, the relative humidity can be determined for a given saturated salt solution at a given temperature. The relationship between the relative humidity and temperature of

various saturated salt solutions is given in figure 3.3. Information on the solubility of salts can be found in literature [3].

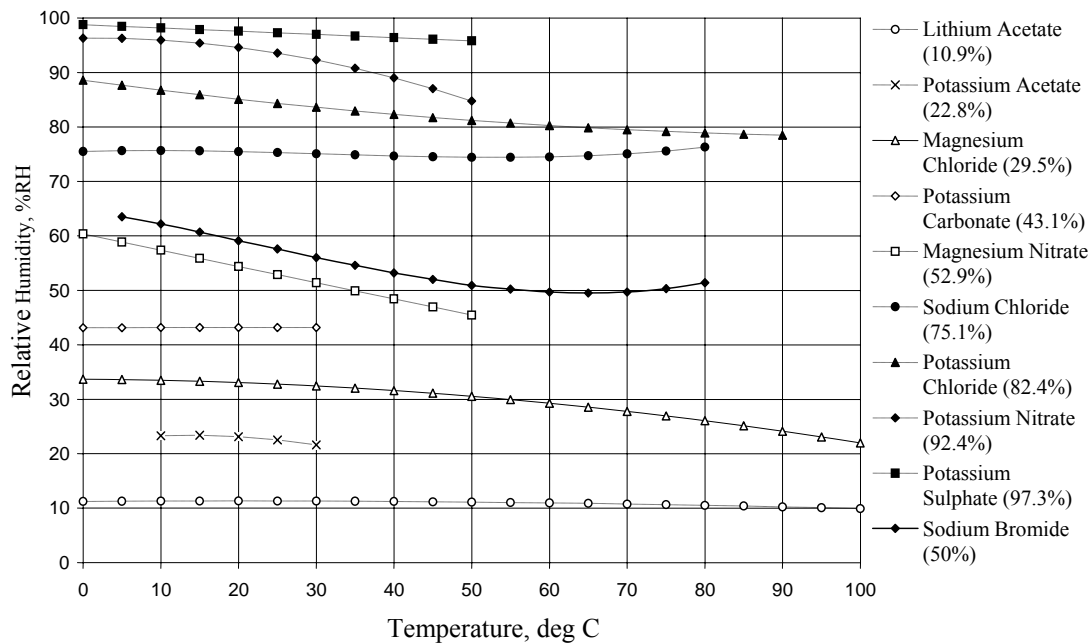


Figure 3.3. Equilibrium relative humidity of various saturated salt solutions versus temperature (drawn from the data in reference [2])

Five different humidity conditions were chosen in the testing:

| Nominal RH% | Conditions | Resultant RH (298 – 353K) |
|-------------|--------------------------------------|------------------------------|
| 0% | controlled by silica gel | <5% |
| 30% | saturated MgCl ₂ solution | 26 – 33% |
| 50% | saturated NaBr solution | 51 – 59% |
| 75% | saturated NaCl solution | 74 – 76% |
| 100% | de-ionised water | >95% |

Between the two extreme conditions, i.e., the dried (0% RH) and water-saturated (100% RH), the other three relative humidities, 30%, 50% and 75% RH, were chosen to fulfil some requirements as below. The first requirement is that the salts should be cheap, easy to buy, and convenient to use, for example, non-toxic. The second is that the conditions they achieve should be close to that of typical environments for running electrical devices, in which relative humidity ranges normally from 20 to 70% RH.

The last and the most important one is that the fluctuation of relative humidities when temperature ranges from 298 to 353K should be as small as possible, i.e., relative humidity keeps as stable as possible when temperature changes (<10%).

The following points need to be noted during the process of humidity control [2],

1. Purity of the salts is above 99%, anhydrous form;
2. The salt crystals shall be added to water at a much higher temperature than required; the solution shall then be cooled down. The solution temperature is set as 353K rather than 298K which is needed;
3. The salt shall be dissolved in water in such a proportion that 30 – 90% of the weight of specimen remains undissolved. Consequently, a weighed specimen for the solution shall be heavier (by 30%) than the one corresponding to the solubility limit at a given temperature. For example, according to reference [3], the solubility of MgCl_2 at 353K is 5.7829 g, then $5.7829 \times 150\% = 8.674\text{g}$. The real situation was that the saturated MgCl_2 solution was prepared by 10 g MgCl_2 salt with 100 g de-ionised water. For saturated NaBr solution (to fulfil 50% RH), the solubility of NaBr is 1.2 g at 353K; the saturated NaBr solution was prepared by 4.7 g NaBr salt with 51 g de-ionised water;
4. It is very important to keep the time long enough to let moisture diffuse into epoxy specimen. By comparing the loss factors between the values after exposing in humid environment some time, when the difference between the value and the next one is smaller than 5%, it is considered as nearly stable. Normally, the hydration comes into equilibrium after a minimum of three days exposing to a humid environment.

A sealed electrode-clamber was designed to maintain the given humid environments during the dielectric spectroscopy and other measurements. It is shown in figure 3.4.

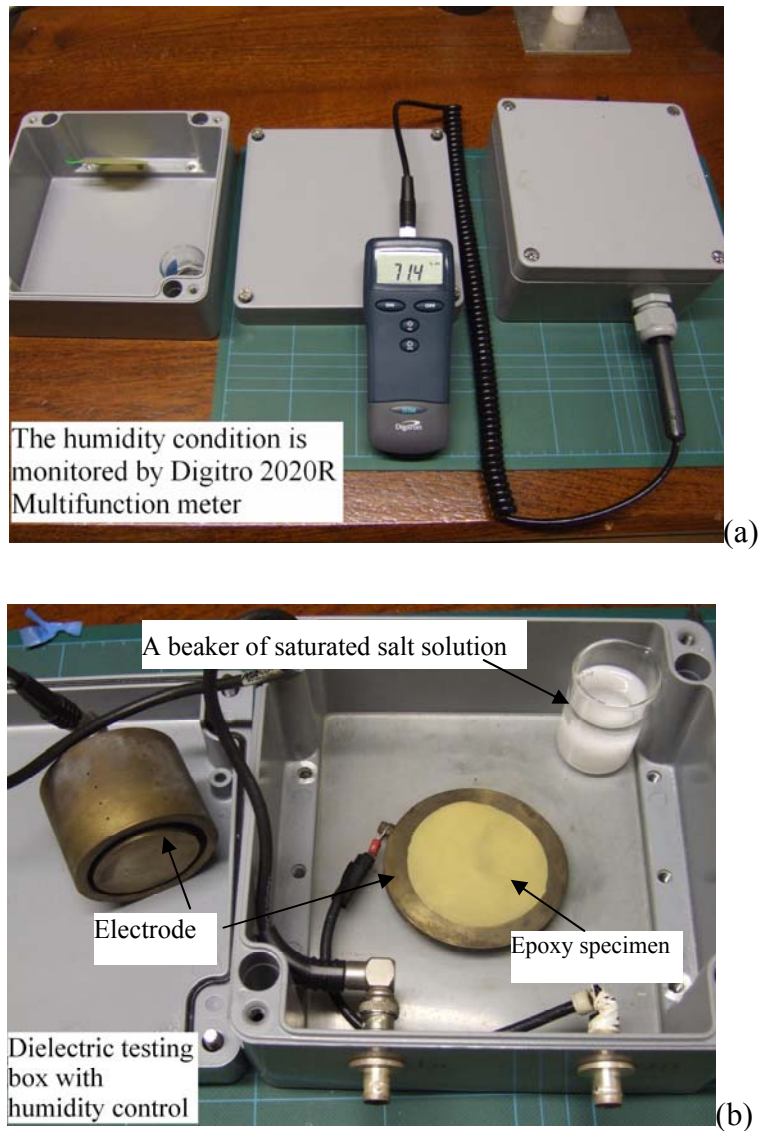


Figure 3.4. (a) The RH monitored by Digitron 2020R;
(b) dielectric spectroscopy electrode chamber with the RH control

Before dielectric spectroscopy measurement, the specimens have been kept under the same humid environment as that of the measurement for one week to stabilise the hydration. The variation of hydration with the time due to the diffusion of water into the specimens is discussed further in § 3.3.4.

The relative humidity was monitored by a Digitron 2020R multifunction meter during this process, shown in figure 3.4. All the specimens were stood-up to permit water diffusion occurring from both sides of specimens during this processing. The weights of the specimens were monitored periodically to confirm the equilibrium of water absorption at room temperature (293K).

To measure dielectric properties under 0% RH environment, the specimens were dried in vacuum oven (10^2 Pa) at 353K for one week before testing. The specimen in 100% RH environment was prepared by immersing the specimen in de-ionised water for one week to reach water-saturated condition.

During the measurements, the silica gel, saturated $MgCl_2$ solution, saturated NaBr solution, saturated NaCl solution and de-ionised water were correspondingly put in the sealed electrode chamber to maintain the given RH environment.

3.3.2 Hydration measurement

Long-term exposure to water can lead to loss of weight by leaching of the by-products of synthesis, unreacted material, or products of degradation [4]. Water sorption in composites can reflect the free volume in the matrix, the mobility of polymer molecule chains, or the tightness of the bonds between inorganic filler and the resin matrix [5]. Normally, if the composite can absorb a lot of water, this suggests there are some weaknesses in the composite, i.e., some cracks, microvoids, a bigger free volume in the resin matrix, or the bonds between inorganic filler and the resin matrix are very weak so that water can break in easily.

To measure the hydration in epoxy materials at various relative humidities, the specimens were put in the sealed aluminium chamber under a given relative humidity for two weeks to reach water equilibrium before they were taken out, surface cleaned, and weighed. A digital scale with resolution to 0.001 g (Sartorius E400D, OHAUS Corp, USA) was used to weigh the specimens.

3.3.3 Density change of epoxy materials after water-saturation

The density change of epoxy materials was measured between the dried and water-saturated specimens. The plate specimens with thickness ~ 0.5 mm were dried in a vacuum oven (10^2 Pa) at 353K for two days. Before being subjected to humidity, the mass and dimensions (using a digital micrometer with an accuracy of 0.0001 mm) of the specimens were measured at the dried condition. After drying, those specimens were immersed into de-ionised water for two weeks. To achieve the maximum of water absorption, the water containing the specimens was heated to 373K for 6 hrs at

the beginning of this test and slowly cooled to the room temperature, i.e., 298K. The thickness data of nine different places on each plate were recorded and compared before and after water saturation.

Measuring the changes in mass and volume of polymer helps to understand the location of the water within the composites. If the specimens swell greatly, this means most water might exist in the resin matrix. However, if the volume of the specimens changed slightly though a lot of water was absorbed, this suggests water might be located at the interfacial zone between inorganic filler and the resin matrix, or microvoids. The real situation might be deduced by observing the density change. This is explained in more detail in § 5.2.

3.3.4 Water diffusion in epoxy specimens

Water diffusion gives an indication of the affinity of the polymer to water and the degradation of the resin caused by water. The diffusion rate depends on the surface condition of the resin, i.e., airtight or ventilated, and the dispersion of microvoids in the resin. If the initial diffusion rate is quick, this suggests that the surface of the resin is porous, and the microvoids in the resin are connected.

Water diffusion in epoxy materials was measured at room temperature (290 to 298K)/75% RH, which is controlled by NaCl saturated solution (75.29% RH at 298K, according to literature [2]). The actual relative humidity ranges from 69.8% to 74.1 % RH with temperature ranging from 290 to 298K. The mass of epoxy specimens was monitored at different intervals after they were put in the environment at room temperature at 75% RH. Water sorption in the resins as a function of the square root of processing time (hours) was monitored by this gravimetric method. The specimens were periodically removed from the humid environment, wiped down, and quickly weighed on the microbalance until the percent weight did not change.

3.4 The measurement methods

3.4.1 Differential scanning calorimetry measurement

Differential scanning calorimetry (DSC) measurements were used to measure the glass-transition temperatures of epoxy materials. The glass-transition temperature is

determined as the mid-point of a temperature range over which the glass transition takes place. The glass transition temperatures of all epoxy materials were tested by a modulated differential scanning calorimeter (TA Instruments, DSC 2920) with a heating/cooling rate 10K/min from 293 to 373K. The glass-transition temperatures of the materials were measured as a function of hydration [6, 7]. From the results of the glass-transition temperatures measured by DSC, the information of the ease of chain movement in composites, the tightness of the bonds between polymer and inorganic fillers, and the change of free volume in composites [8], might be estimated.

3.4.2 Conduction current measurement

The d.c. conductivity measurements were carried out over the temperature range 292 to 298K. The applied voltages were varied from 2 to 10kV, in 2kV increments. A Glassman high voltage Inc (V_{max} : 100kV) power supply was used. The direct current values were measured by a Keithley programmable electrometer (model 617), which communicated with a PC by IEEE 488 GPIB cable. A computer program was written in LabView to realize the function of commanding and collecting the data from the Keithley 617 programmable electrometer or storing the data in the computer [Appendix I]. The specimens and the electrode system were placed in an electrically shielded box to reduce the electrical noise. The circuit diagram of the conduction current measurement system is shown in figure 3.5. For the polyethylene specimens, which had a small diameter, it was not possible to use the guard ring. The current from the bottom electrode flowed through a 10 M Ω protective resistor before the Keithley 617 programmable electrometer in case the possible breakdown damaged the meter.

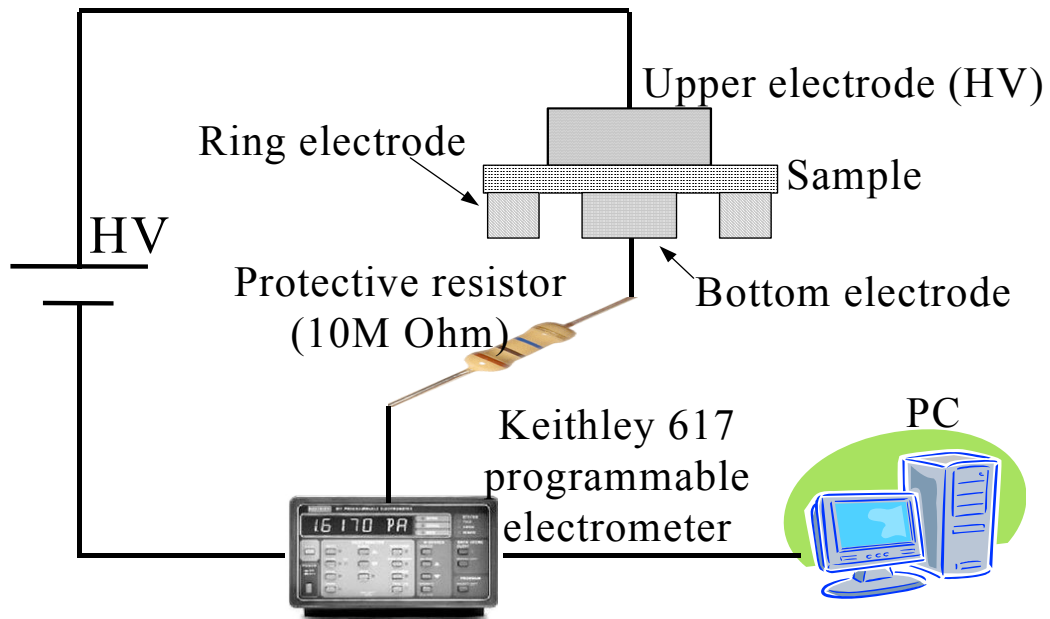


Figure 3.5. Circuit diagram of conduction current measurement

The interface of the LabView program is shown in figure 3.6. In this program, the measured objects can be set as resistance, voltage or current. The applied voltage was shown in this interface. Both the conduction currents and the logarithm of the absolute values of the conduction currents (the values of conduction currents were negative if the applied voltage was the negative polarity) were measured and calculated, and displayed on a graph in the interface of this program in real time. The data were stored in the set file paths.

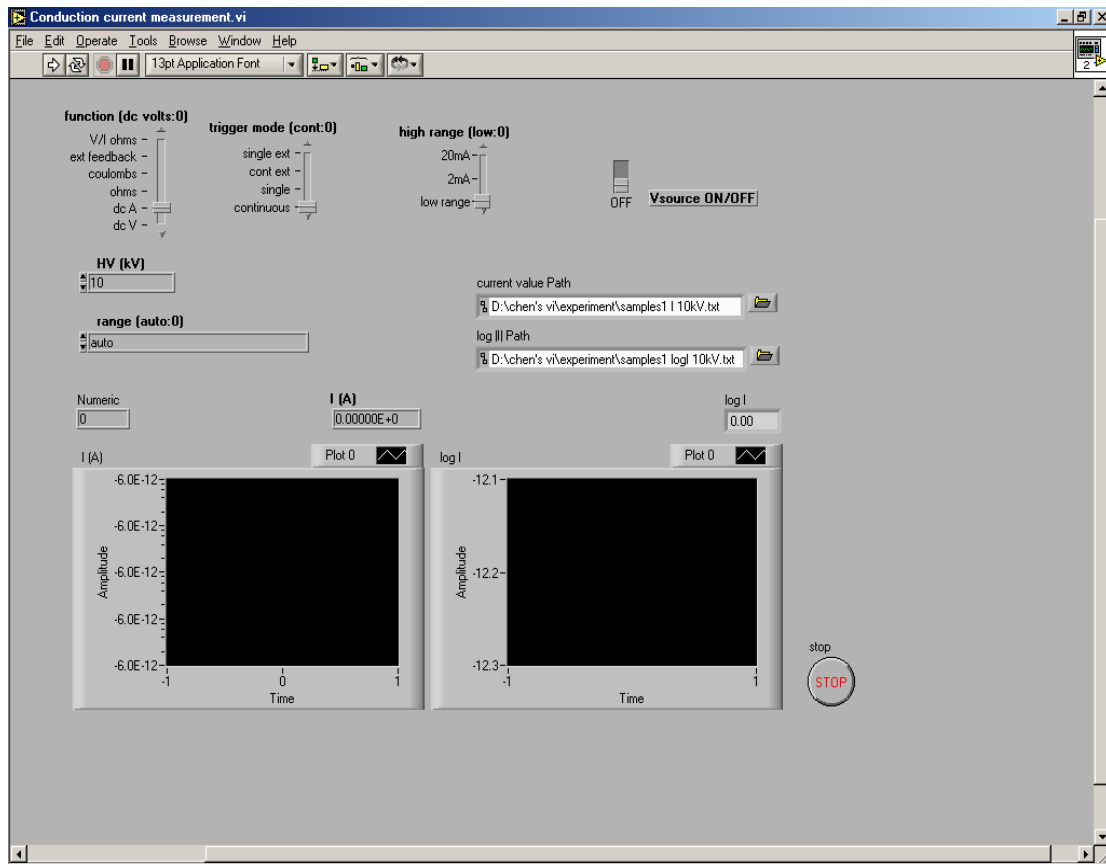


Figure 3.6. The interface of LabView program to measure/store the data of conduction currents

3.4.3 Dielectric Spectroscopy

Dielectric spectroscopy involves the study of the electrical current response of a material to an applied electric field. If the appropriate interpretation of the data is applied, it is possible to obtain structural information on a range of specimens using this technique [9 – 12].

A Solartron instrument 1255 frequency response analyser (FRA) was used [13, 14] with a Solartron 1296 dielectric interface. The measurements were based on measuring the current (amplitude and phase) in the material with respect to an ac electric field, which is a periodic function in the form of sinusoid. A digital generator produced the applied voltage with amplitude 1 V rms, which was applied to the specimen by the means of two plain electrodes. The frequency range used was 10^{-4} to 10^6 Hz. The amplifier is linked to the correlator of the FRA where the signal is integrated. The dielectric spectroscopy measurement system is shown in figure 3.7.

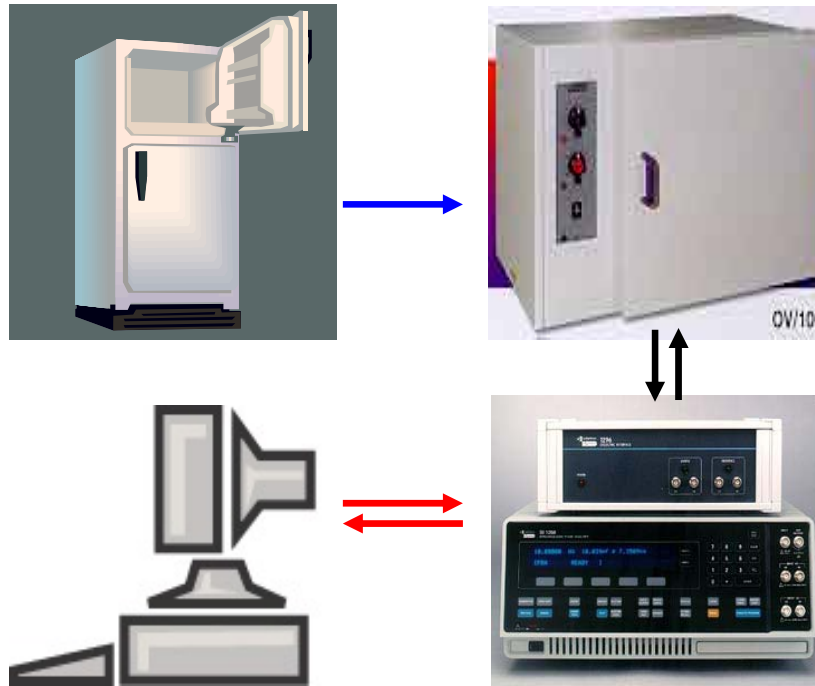


Figure 3.7. Dielectric spectroscopy measurement system, comprises Solartron instrument 1255 H.F FRA, Solartron 1296 dielectric interface, PC and Genlab oven and freezer

During the dielectric spectroscopy measurement, the FRA provides an ac stimulus signal first, and analyses the interface's response. The Dielectric/Impedance interface increases the sensitivity of the FRA. A PC provides system set up and control via easy to use software, provided by the manufacturer.

A Genlab oven with a Eurotherm temperature controller was used to control the temperature to within $\pm 0.5\text{K}$ during the dielectric spectroscopy measurements. The temperature ranged from 298 to 353K in this test. To keep a temperature close to or lower than the ambient temperature, a freezer was connected with the Genlab oven and also controlled by the Eurotherm controller to provide the cooling air.

A three-terminal parallel-plate electrode was used as the measurement electrode, in the humidity cell, shown in figure 3.4.

The analysis methods of the dielectric spectroscopy results are according to the classic dielectric theories, and have been discussed in Chapter 2 [15, 16].

3.4.4 Pulsed electro-acoustic (PEA) measurements

Space charge measurement using the pulsed electro-acoustic (PEA) technique, developed about 20 years ago by T. Maeno, Takada and co-workers [17 – 20], has become a common method for investigating dielectric properties of solid materials. The PEA method has been used for various industrial applications, such as for the evaluation of ion conductive materials [21]. PEA is a non-destructive method and used to measure dynamically net charge density as a function of distance through solid insulating material under an applied voltage [22, 23]. Typical PEA systems can measure space charge profiles in the thickness direction of specimens, with a resolution of around 10 microns, at the repetition rate of the order of 1 ms.

The way that a PEA system works is described below. When a pulsed electric field is applied to a specimen containing space charges, the sudden movement of the charges trapped in the material generates acoustic waves, which propagate in the specimen.

A piezoelectric sensor under the electrode converts the acoustic wave into an electric signal that can be observed by an oscilloscope; the amplitude and polarity of the signal is related to the charge density/polarity and the delay indicates its distance from the electrode. In this way the internal space charge distribution can be observed.

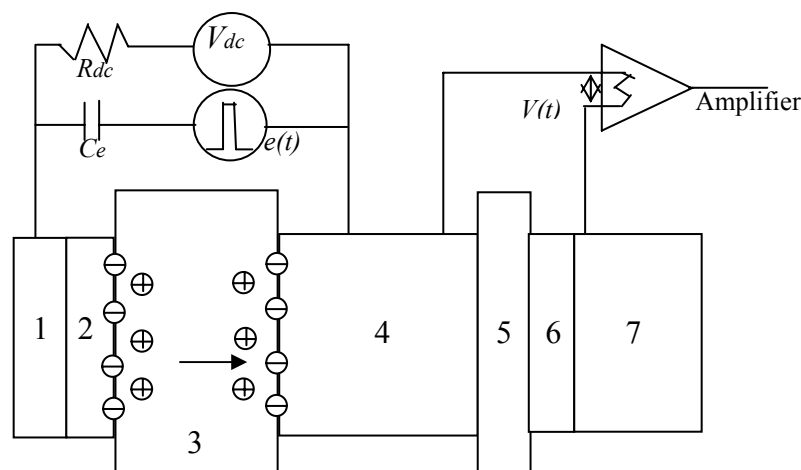


Figure 3.8. The schematic diagram of PEA system;
 Parts: 1, Electrode; 2, Semiconductor layer; 3, Charged specimen;
 4 Electrode (Al); 5, PVDF; 6, PVDF- α ; 7, Electrode (Al)
 (Redrawn from reference [21])

The pulse generator used in these studies generates a pulse up to 900 volts for a duration of 10 ns. The velocity of sound signal in polymeric material is of the order 2 $\mu\text{m}/\text{ns}$, so that a 10 ns pulse has a spatial width of 20 μm , which determines the spatial resolution in our PEA system.

The thickness range of the specimens measured by this PEA system was from 0.2 to 0.7 mm (XLPE specimens) or 0.4 to 0.6mm (epoxy specimens). The applied DC voltage was up to 12kV to generate the space charge. The pulse amplitude used was 600 – 900V.

If it is necessary, the space charge behaviour of composites at the various hydrations can be observed under the control of relative humidity. To achieve that, an enclosed chamber was designed to keep the specific relative humidity during PEA measurement carried out, as shown in figure 3.9.

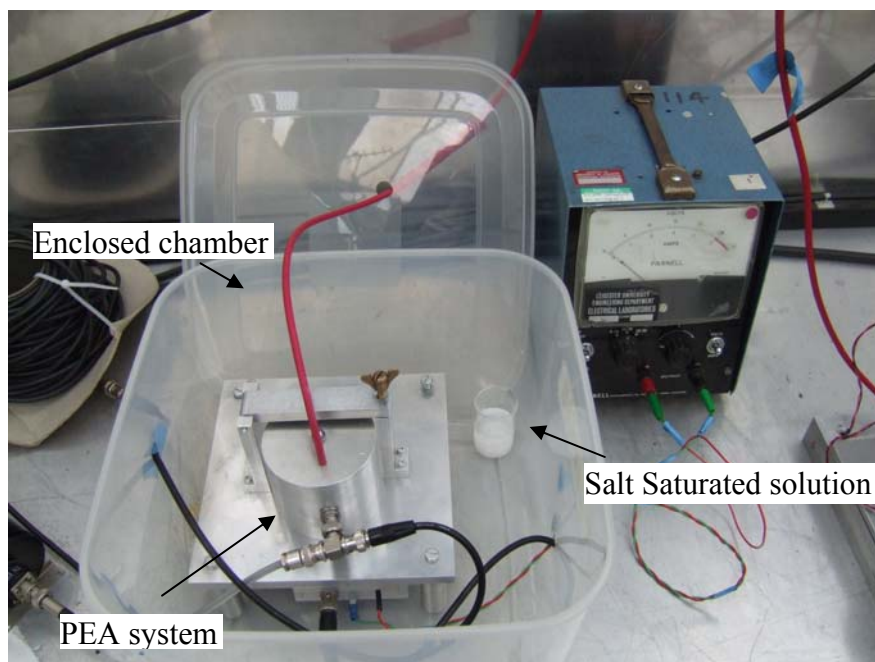


Figure 3.9. PEA measurement with relative humidity control

3.5 Summary

Crossed-linked polyethylene and epoxy resin were chosen as the polymeric matrix as they are commonly used in HV insulation applications. Either nano- or micro- silica particles were chosen as the inorganic filler. The physical, chemical and dielectric properties of the materials were measured, using SEM, DSC, conduction current measurement, dielectric spectroscopy analysis, and PEA measurement. To study the

effect of water on the epoxy composites, the following were measured as a function of relative humidity: specimen hydration, density change by water sorption and water diffusion kinetics. Moreover, the dielectric properties of the materials at various hydrations were studied by controlling the relative humidity of the environment.

The measurements were carried out by controlling variables as shown below:

1. Time domain: the conduction current measurement was carried out in the time domain, from 10 to 10^4 s;
2. Frequency domain: the dielectric spectroscopy was tested in the frequency domain (10^{-4} – 10^6 Hz);
3. Temperature domain: the dielectric spectroscopy (298 – 353K) and conduction current measurement (313K and 343K) were under temperature control;
4. Relative humidity (RH) or Hydration: the controlled relative humidity ranged from 0% (dry) to 100% (water saturated). Five relative humidity points were obtained, which were 0, 30, 50, 75 and 100% RH;
5. The average diameter of silica particle: the average diameter of silica microparticles is $\sim 40\mu\text{m}$; that of nanoparticles is from 15 (in XLPE) to 50nm (in epoxy);
6. Concentration of inorganic fillers: both the concentrations of nano- and micro-silica were 5 wt% in XLPE specimens. The concentration of epoxy microcomposites was 60 wt% (M60). Accordingly, that of epoxy nanocomposites were 3 (n3) and 9 wt% (n9);
7. Surface functionalisation: in XLPE specimens, three surface treated silica nanoparticles were applied, which were treated by Aminosilane (named as AmnPE), Hexamethyldisilazane (HmnPE) and Triethoxyvinylsilane (VinPE). For epoxy materials, epoxy specimens were filled with either surface hydrophilic or surface hydrophobic silica nanoparticles.

Chapter 4

Results

In this chapter, the main experimental results are given, which include the hydration behaviour of epoxy materials, the dielectric properties of composites, the conduction and space charge behaviour of polymeric materials.

4.1 Hydration behaviour of epoxy specimens

4.1.1 Hydration in epoxy specimens

The hydration of epoxy specimens at various relative humidities is shown in figure 4.1 at room temperature. The hydrations of the epoxy resin part in the filled composites are calculated by removing the volume of the inorganic fillers (~50 vol% in M60, ~1.5 vol% in n3 and ~4.5 vol% in n9).

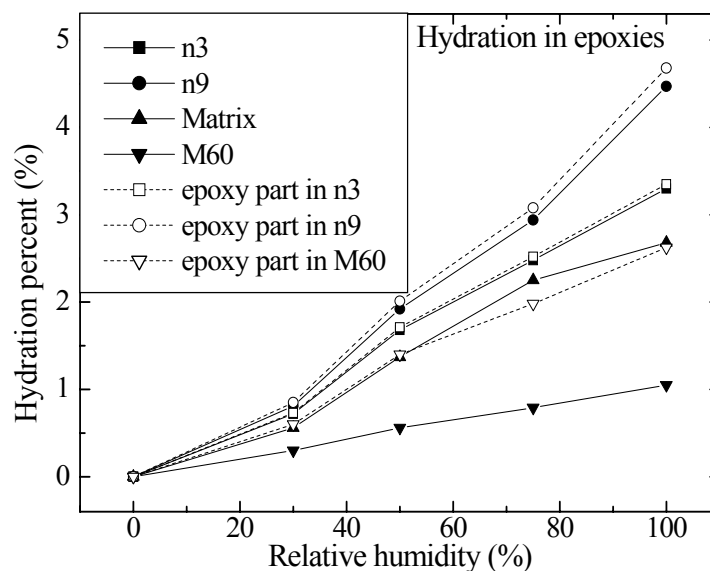


Figure 4.1. Percentage hydration (wt %) in epoxy specimens at various relative humidities after two weeks

The hydration percent, $H\%$, is expressed in mass percent (wt %) with reference to dried specimens, defined by equation 4-1:

$$H \% = \left| \frac{M_w - M_d}{M_d} \right| \times 100 \% \quad (4-1)$$

where M_w is the mass of water-absorbed specimen, (g); and M_d is the initial mass of dry specimen, (g).

In this testing, all specimens were removed from the controlled humidity environment after two weeks (>330 hours), dried superficially, and weighed. It was proven to be a sufficient time for reaching the steady state (§ 4.1.2).

The water absorption behaviour of polymer-filled composites at a humid environmental condition is determined by many factors, such as processing techniques, polymer matrix and filler characteristics, composition of the composites, and so on [1]. There are two situations for water sorption in composites filled with inorganic fillers:

- One is when there is a good interfacial adhesion established between the blend matrix and the particles. This may result in a higher density composite and less free volume around the particles. If there is a higher concentration of inorganic particles, the denser interface zones between particles and matrix means that less water can be contained in this region [1].
- Conversely, some bonds between epoxies and some fillers (such as silica and aluminium) are thermodynamically unstable or not strong enough in the presence of water molecules. The thermodynamic work in the interfaces between fillers and matrix could become negative in the presence of water from the positive value when dried. For example, the thermodynamic work for the epoxy-ferric oxide interface changes from +291 to -255 mJ/m² when there is an absorbed layer of water at the interface [2, 3]. This change from a positive to negative work of adhesion provides a driving force for the displacement of adhesive on the interfaces between particles and epoxy matrix by water [2]. It is therefore to be expected that the interfaces between the inorganic fillers and matrix might be debonded in the presence of water. The higher the concentration of inorganic particles, the more the broken bonds, and the more the water can be contained in this interfacial region.

Since silica is a non-polar material, unlike epoxy, the bonds between silica and the epoxy are not strong enough to repel water. It is the latter of the two above situations, which tends to occur in silica epoxy nanocomposites, i.e., the more the silica particles incorporated, and the more the water accumulated at the surface of the particles. By functionalising the particle surface to be hydrophobic, this situation may be overcome (§ 5.2). Hence, silica epoxy nanocomposites will normally absorb more water than the epoxy matrix and microcomposites in the same humid environment, as shown in figure 4.1. Furthermore, the absorption of water increases with the content of nano-filler. Another reason to explain the greater water absorption in silica epoxy nanocomposites is that nanocomposites have a bigger interfacial specific area than matrix and microcomposites. For example, a nanocomposite comprising 10% v/v of 10 nm diameter spherical particles has a specific area of $6 \times 10^7 \text{ m}^2/\text{m}^3$ whereas a microcomposite comprising 50% v/v of 100 μm diameter spherical particles has a specific area 2000 times less than this [4 – 7]. It is more likely for water to enter the bulk of epoxy matrix in epoxy nanocomposites by going along the interfacial region between the bulk and fillers. Moreover, the equilibrium water content depends not only on the potential space to contain water in the matrix, but also on how many hydrogen bonds are formed between water and network polar groups [8]. Obviously, nanocomposites have a much more interfacial area to generate much more likely hydrogen bonds. The same finding can be observed in figure 4.2.

During the manufacture of a composite, the inorganic fillers may produce some cracks and voids. Without such fillers, i.e., in a pure epoxy, there are fewer cracks and voids, hence less water can be contained.

For microcomposites, the hydration percent is increasing with the relative humidity in a nearly linear manner but at a lower level. The reason for the lower hydration is due to the lower specific area found in microcomposites [9].

One can see that the hydration of epoxy phase of the microcomposites is close to that of epoxy matrix. This suggests micro-fillers have little effect on the hydration of microcomposites. Conversely, the hydration of epoxy phase of the nanocomposites (both n3 and n9) is higher than that of epoxy matrix. This means that the nanofillers

do enhance water absorption in nanocomposites. The greater the concentration of nanoparticles incorporated, the more the water absorbed in nanocomposites.

4.1.2 Water diffusion in epoxy specimens

Water diffusion in epoxy materials was measured at room temperature (~ 293 K) and nominally 75% RH. The actual relative humidity ranges from 69.8 to 75.2% RH with temperature ranging from 298 to 353K [10]. This was monitored by the Digitron 2020R multifunction meter.

Diffusion is the net movement of matter down a concentration gradient due to the random movement of individual particles. The process is dependent on the imposed boundary condition [11]. When a dry planar specimen is put in a humid environment, then, after some time, a steady state is obtained in which water diffusing through the plane per unit time is zero. Within the plane, the concentration gradient is not zero. However, once a steady state is established, the concentration at any location does not change with time. This defines a steady state, and Fick's First Law is most useful in dealing with this situation [11, Appendix II].

In this experimental condition, since the relative humidity in the environment is stable ($\sim 75\%$ RH), i.e., the concentration of water in the environment C_1 is constant and independent of time; before the planar specimen reaches saturation, this flux of water J_1 across the interface at $z = 0$ can be found by Fick's law [12]:

$$J_1|_{z=0} = \sqrt{D/\pi t}(C_1 - C_{1\infty}) = \sqrt{D/\pi t}(C_1) \quad (4-2)$$

where D is the constant depending of the nature of the substances, i.e., water and epoxy plate; t is the diffusion time of water [12].

Integrating the differential equation from time 0 to t , the amount of water released M , i.e., the water absorption in epoxy specimens will change at time t , and can be found according to [Appendix II]

$$M = \int_0^t J_1 dt = \sqrt{\frac{4Dt}{\pi}}(Bc_1) \quad (4-3)$$

where B is a constant of integration.

The water diffusion behaviour in epoxy specimens is shown in figure 4.2, which is plotted as linear hydration versus the square root of time (hours).

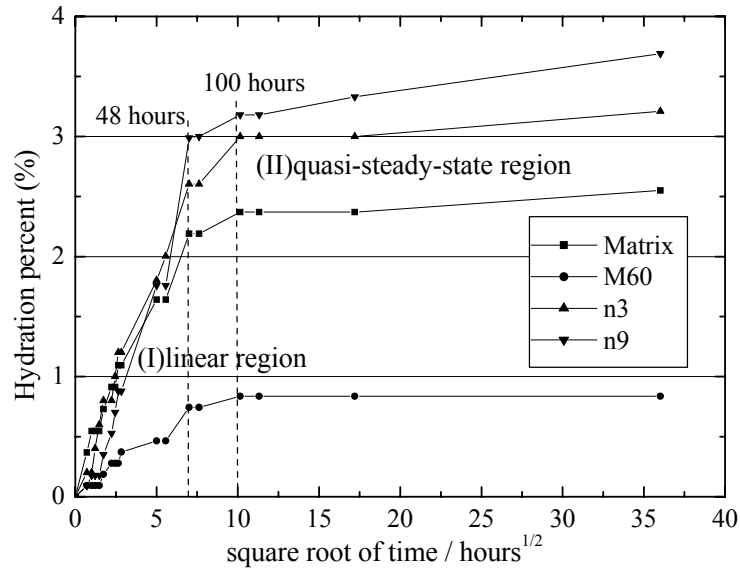


Figure 4.2. Water diffusion in epoxy specimens (75% RH, 298K)

According to equation 4.2, during water diffusion into the specimen, if Fickian diffusion behaviour is observed, one could expect a straight line on this plot of hydration against the square root of time [11]. According to figure 4.2, the hydration comes into quasi-equilibrium after 100 hours in all four epoxy specimens. This supports the credibility of the hydration results in epoxy specimens, which were measured after processing for two weeks (>330 hours).

From the initial linear portion of the curves, water diffusion coefficients can be calculated according to the following equation [13]:

$$\frac{\Delta w_t}{\Delta w_T} = \frac{w_t - w_0}{w_\infty - w_0} = \frac{4}{e} \sqrt{\frac{Dt}{\pi}} \quad (4-4)$$

where w_t , w_0 and w_∞ are the masses of the specimens at immersion time t , $t=0$ and at the equilibrium, e is the thickness of the specimen, and D the water diffusion coefficient. In table 4.1, D and the equilibrium water content are presented.

Table 4.1. Water diffusion coefficients, D , calculated with equation 4-3, and hydration of epoxy specimens at 75% RH, 298K

| Specimen | Hydration (wt%) | $D (\times 10^{-13} \text{ m}^2 \cdot \text{s}^{-1})$ |
|----------|-----------------|-------------------------------------------------------|
| Matrix | 2.37 | 3.67 |
| M60 | 0.84 | 0.38 |
| n3 | 3.00 | 5.08 |
| n9 | 3.33 | 5.17 |

The diffusion coefficients in epoxy matrix and nanocomposites are quite close; however, the coefficient in microcomposites is less than that in other materials. This might be caused by the lower hydration in microcomposites since there is a much lower percentage hydration of epoxy in M60, but the same time is needed to reach the equilibrium in various epoxy materials. Moreover, water molecules in M60 have to move a longer path from one side to the side of microparticles since the bigger size of microparticles. One more possible explanation is that some fine capillary vessels might be formed at the interfaces between nanoparticles and the matrix, which could pump the water into the bulk of epoxy materials much more easily.

The initial parts (I) of the curves in figure 4.2 are linear indicating that water diffusion occurs at the interface of the specimens. It might take much longer time to permit water molecules enter the bulk of the material, and this process is described by the latter flat portion (II) of the curves in figure 4.2. According to figure 4.2, though M60 has a lower diffusion coefficient than other epoxy specimens, the hydration in M60 keeps at a certain level once equilibrium is achieved. The concentration of microparticles in the microcomposite is much lower that of nanoparticles in nanocomposites. Once water molecules move over the surface of most microparticles, the water diffusion process is completed even though the path is longer as the microparticles have a bigger size. In nanocomposites, there appear to be two diffusion stages. During the first stage, the water molecules diffuse through the interface of specimen to realize a temporary equilibrium. Following this, they still have to continuously move across the surfaces of nanoparticles in the bulk of specimen to reach the final equilibrium. This process is the second stage of diffusion. It is the reason that the hydration in nanocomposites keeps increasing slowly after the first

stage of diffusion. As to the epoxy matrix, a possible second stage of diffusion can be observed, which may be caused by tiny voids and channels in the material.

4.1.3 Density change of the wetted epoxy specimens

The question about where the water goes once it has entered the epoxy materials, and whether this is in the bulk of the matrix or at the interface between fillers and the matrix, is important to answer in order to understand the influence of water on the mechanical and electrical properties of epoxy materials. Normally, a swelling will occur in the epoxy material after water absorption. If there is no swelling, then the implication is that the near-grain regions of the matrix are “porous” containing extra free volumes with respect to the bulk resin. Hence, water can occupy the space of ‘voids or cracks’ in the bulk resin and do not induce swelling. However, if the swelling corresponding to the extra water occurs, it hints that the water molecules may force their way between the resin and the filler by capillary action and locate them at the interfaces between the resin and the filler, or enlarge the cracks in the epoxy materials.

For the density change after water absorption, if water occupies the extra free volume in the bulk resin and does not cause a swelling, the density of composites apparently will increase because of the mass gain of water; if the swelling also occurs, it is hard to predict the density increases or decreases.

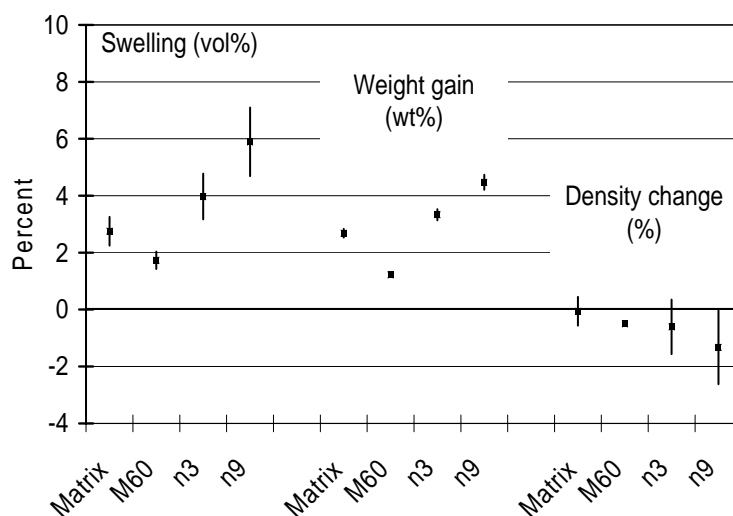


Figure 4.3. The swelling and density change of epoxy specimens by water sorption

The influence of water on the density of epoxy materials depends on two factors, one is the mass gain caused by water sorption in epoxy material; the other is the possible volume swelling of the wetted epoxies. When water enters, the weight of composites must increase; so that the volume change decides the density change. As a polymer, there always is free volume such as holes and channels in the epoxy matrix. Once water enters the matrix and occupies the free volume, there is no swelling in epoxy matrix. In this case the density of the wetted material definitely increases. The other possible location for water is the cracks produced by water since water might break the epoxy chains. In this case, swelling occurs and also there will be a weight gain by water sorption so it is difficult to predict the density change of materials.

According to figure 4.3, volume swelling occurs in all four wetted specimens. The density change in water-saturated epoxy matrix is very slight ($\sim 0.06\%$). Since the density of water ($1 \times 10^3 \text{ kg/m}^3$) is less than that of matrix ($\sim 1.25 \times 10^3 \text{ kg/m}^3$) by $\sim 20\%$, the actual slight density decrement of wetted epoxy matrix hints there was some water still occupying the voids within matrix. In the filled epoxy composites, their decreasing density suggests inorganic fillers enhanced the free volume (space) in epoxy materials, where water could be stored. From figure 4.3, it can be concluded water exists in both free volume and cracks in the epoxy materials.

Under the assumption that all the left water in epoxy nanocomposites surrounds each nanoparticle evenly over and above the water in epoxy matrix, the average thickness of water shell around particles in n3 can be calculated as $\sim 5.6 \text{ nm}$. This is quite close to that of n9, which is $\sim 5.0 \text{ nm}$. Since the effect of each nanoparticle is same, one would expect there to be the same amount of water around a single nanoparticle, no matter whether it is n3 or n9. The difference between 5.6 nm and 5.0 nm in layer thickness may be due to experimental uncertainties. However, one might expect the n9 calculation to yield a slightly lower result as there will be more overlap of interaction zones in the composite with a higher concentration of filler. This is also confirmed by the result that the water sorption in the epoxy part of n9 (4.5 vol%) is almost three times greater than that of n3 (1.5 vol%). This proves the deduction that the extra swelling in nanocomposites caused by incorporating inorganic fillers is reliable.

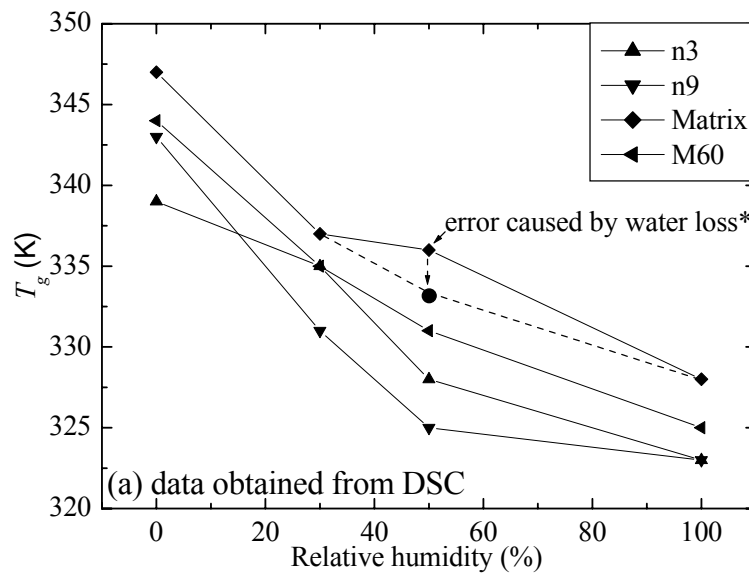
By this testing, it is concluded some water will surround the inorganic fillers besides existing in the epoxy matrix. A more detailed discussion is made in Chapter 6.

Summary of this section:

1. Nanofillers enhance water absorption in epoxy composite, however, microfillers make little difference;
2. Epoxy nanocomposites have a faster water diffusion rates than microcomposites;
3. Weak bonding between nanoparticles and the epoxy matrix may result in extra free volume at the interfaces, which water could occupy.

4.2 The glass-transition temperature of epoxy specimens

The glass-transition temperatures of epoxy specimens were measured by differential scanning calorimetry (DSC) and also by using the dielectric loss spectrum found by dielectric spectroscopy (DS). The glass-transition temperatures of epoxy specimens at various relative humidities are shown in figure 4.4.



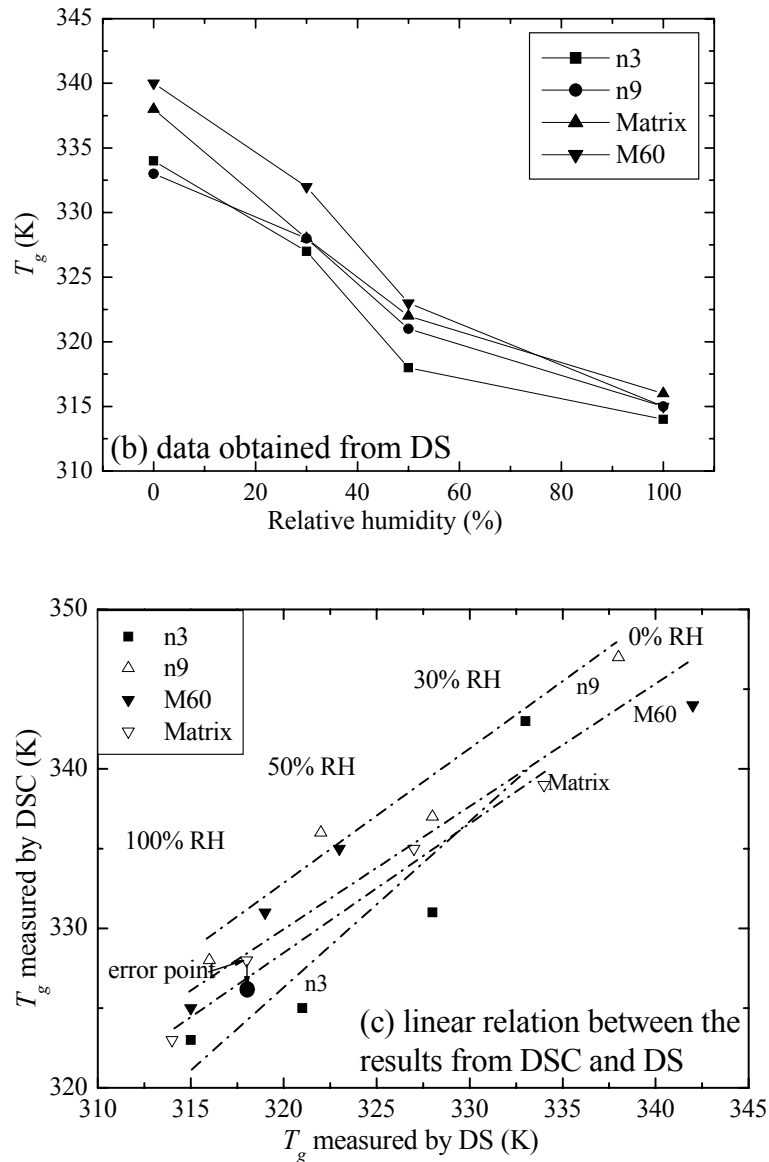


Figure 4.4. The glass-transition temperatures (T_g) of epoxy specimens, (a) measured by DSC^{*}; (b) dielectric loss spectrum (DS, at 10^4 Hz) and (c) the linear relation between the results from DSC and DS

According to figure 4.4, the glass-transition temperature of epoxy materials drops with the increasing relative humidity; this finding is confirmed by the results of both DSC and DS. Moreover, the linear relation between the glass-transition temperature results obtained by the DSC and DS measurements reflects the credibility of this finding.

^{*} An extra increment of T_g of Matrix at 50% RH is caused by the water loss in the unfilled epoxy matrix during the process of preparing and transporting the specimen for DSC measurement in Grenoble; the corrected result is shown as a dashed line

The method of obtaining the glass-transition temperature by dielectric loss spectrum is described below. A similar method of determining T_g was introduced by K. Fukao and Y. Miyamoto [14], in whose paper the electric capacitance (C') data were applied to determine T_g of thin films [14].

Figure 4.5 shows the relation between loss tangent and relative humidity for the unfilled epoxy and the n3 nanocomposites. The similar results were obtained for the n9 and M60 systems. The loss tangents at 10^4 Hz were chosen to avoid the influence of relaxation peaks, since this frequency is above the relaxation process caused by water in the mid-frequency range.

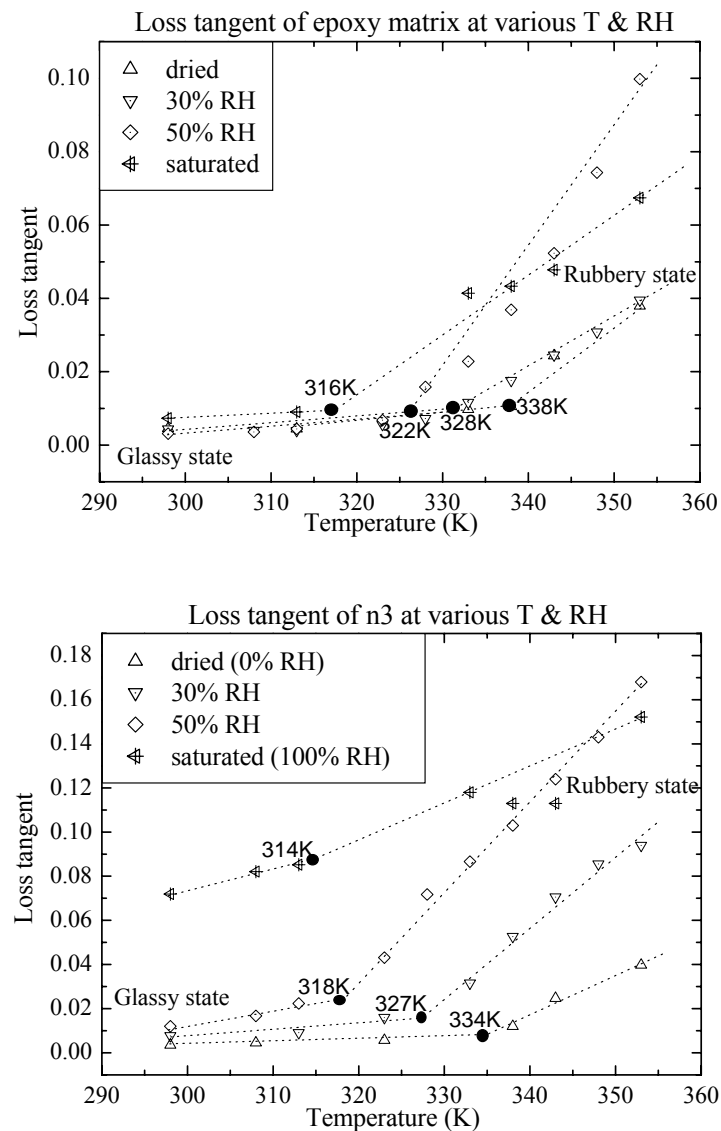


Figure 4.5. Relations between loss tangents and relative humidity at 10^4 Hz at various temperatures (Matrix and n3)

In figures 4.5, the graph of loss tangent as a function of temperature appears to comprise two straight lines with a discontinuous change in slope at the glass transition temperature. The left/lower part is in the low-temperature region, so it is believed to be in the glassy state. The right/upper one occurs in the high-temperature region, so it is likely to be the rubbery state region. If this assumption is correct, the intersection point between the extrapolated lines can be regarded as the glass transition temperature, T_g . By comparing T_g at various relative humidities, it is noted that T_g is decreasing with relative humidity increase in epoxy nanocomposites and epoxy matrix. A similar finding was obtained using the results of loss tangents at 10^2 Hz.

Summary of this section:

Both the result of T_g measured by DSC and dielectric loss spectrum can verify that the glass-transition temperature (T_g) of epoxy materials drops with the hydration. Since the same decrement (~ 20 K) of T_g among epoxy materials when the relative humidity varies from 0 to 100% RH, this suggests that the free volume in epoxy matrix is the same in all four specimens. Hence, the extra water absorbed in nanocomposites must exist in the interfacial zones around nanoparticles rather than in the region of epoxy matrix [15].

4.3 Conduction current measurement

In this test, time dependent conduction characteristics have been taken for both micro- and nano- polyethylene and epoxy composites. When a dc voltage was applied across the specimens, in nearly all cases the current at time t after voltage application varied approximately as

$$I(t) = At^{-n} \quad (4-5)$$

where $0 < n < 1$, as expected [16].

The charging current at $t \geq 10000$ s was taken as the “quasi-steady state” current, since at such times the rate of current decrease was very slow in all specimens, and the current would have been due mainly to injected electronic carriers moving in the

field established by the applied voltage and potential space charge generated by ionic charge transport at short times [17].

The charging currents $I_c(t)$ and the discharging $I_d(t)$ for a range of voltage step amplitudes V of both microcomposites and nanocomposites are shown in figure 4.6. The environmental temperature ranges from 285 to 292K.

4.3.1 XLPE

A two-electrode system (high voltage electrode – ground electrode) was used to measure the conduction current of XLPE specimens. It was not possible to apply the guard electrode because of the small specimen size. The specimens measured are ‘MPE’ (5 wt% silica microcomposites, 40 μ m average particle size) with a thickness of 0.365mm and ‘NPE’ (5 wt% silica nanocomposites, 20nm average particle size) with a thickness of 0.401mm.

For ‘MPE’, the range of poling fields was about 3 – 14 kV/mm. A flashover would occur at higher fields. The decrease of the charging currents is observed between 10 and 10⁴ s. After 10⁴ s, the conducting currents were quasi-stabilized. The lower field being applied, the longer time is required to reach the steady state. At low field (<8.2 kV/mm), the discharging currents decreased quasi linearly in a log-log plot for about 2 decades. At high field (>8.2 kV/mm), the slopes of the discharging current curves were the same as at low field at the beginning stage, which followed equation 4-5 closely, with $n \approx 0.74$ at low field (<8.2 kV/mm), or ~ 0.5 at high field (>8.2 kV/mm).

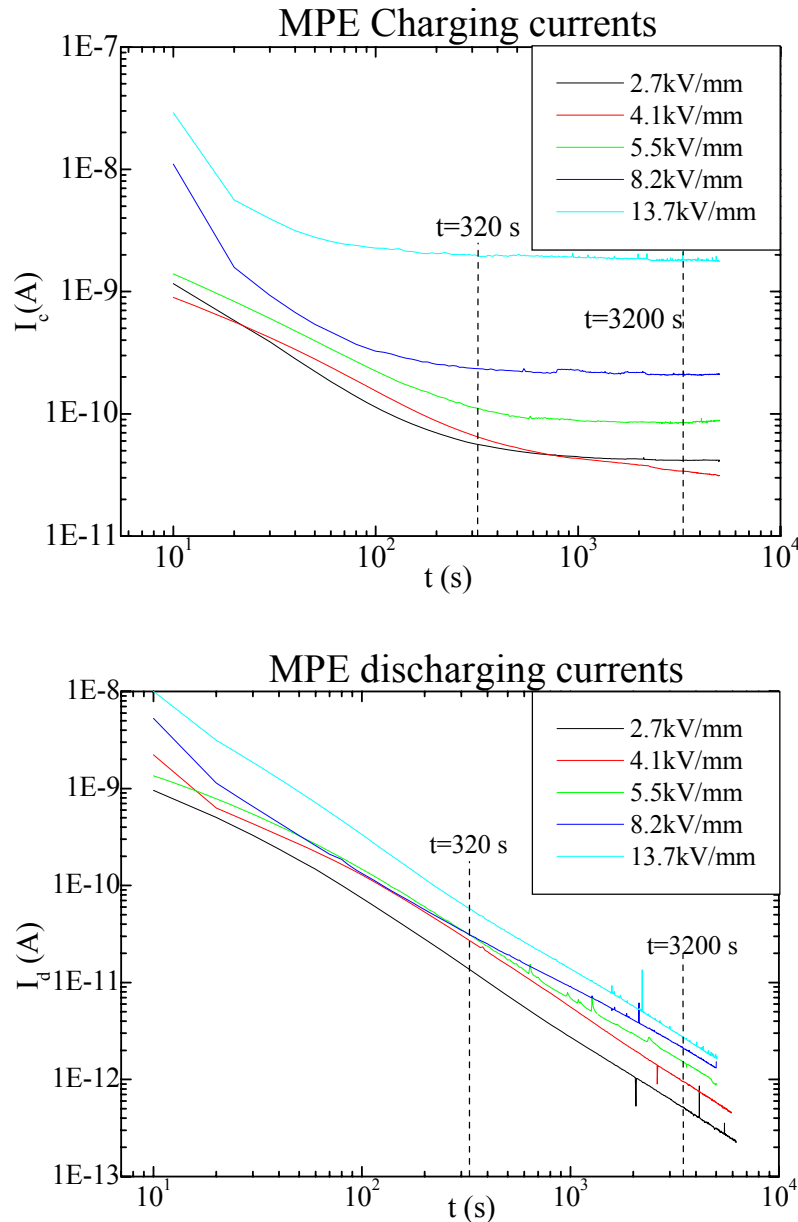


Figure 4.6. The charging and discharging currents of MPE at various fields (measured every 10s)

According to figure 4.6, at low fields (< 8 kV/mm), the quasi-stabilized charging current density of MPE increases in direct proportion to the applied field. But this relation between the quasi-stabilized charging current and the fields is no longer applied when the field is above 8 kV/mm. At the higher field, the quasi-steady state current density increases more rapidly. According to the PEA result, the threshold field for space charge accumulation in XLPE microcomposites is about 10 kV/mm. Once the external field is higher than the threshold field, space charge might be

formed and alter the local field inside the material. This causes the charging current density to deviate from ohmic behaviour at the higher field.

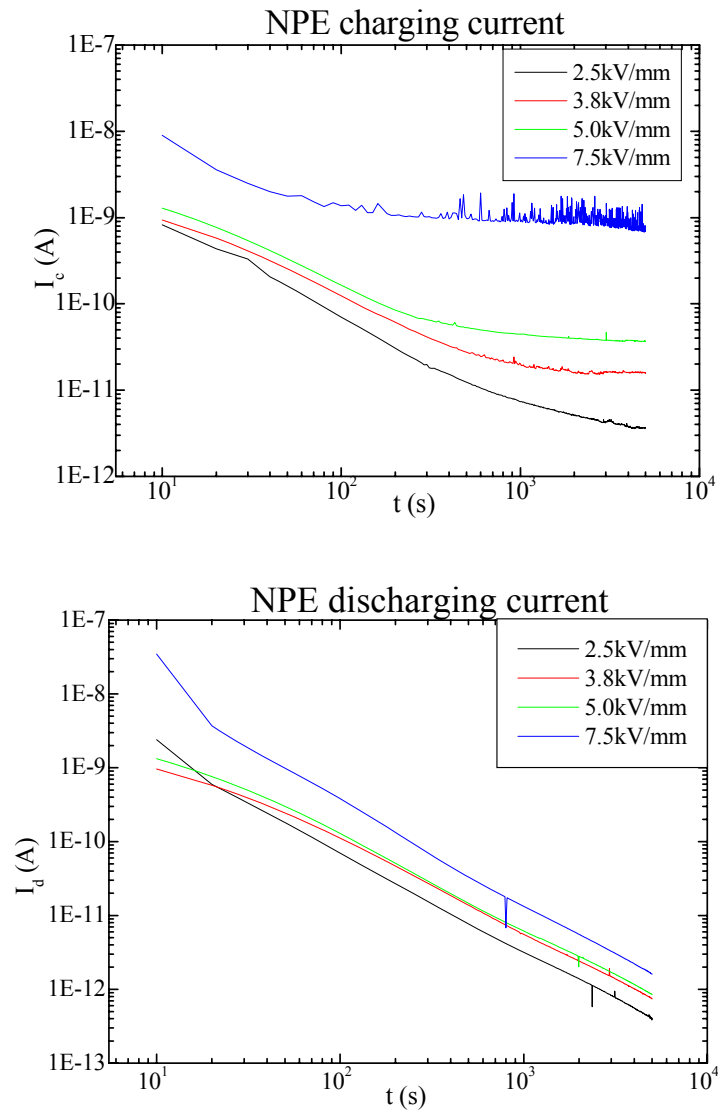


Figure 4.7. The charging and discharging currents of NPE at various fields

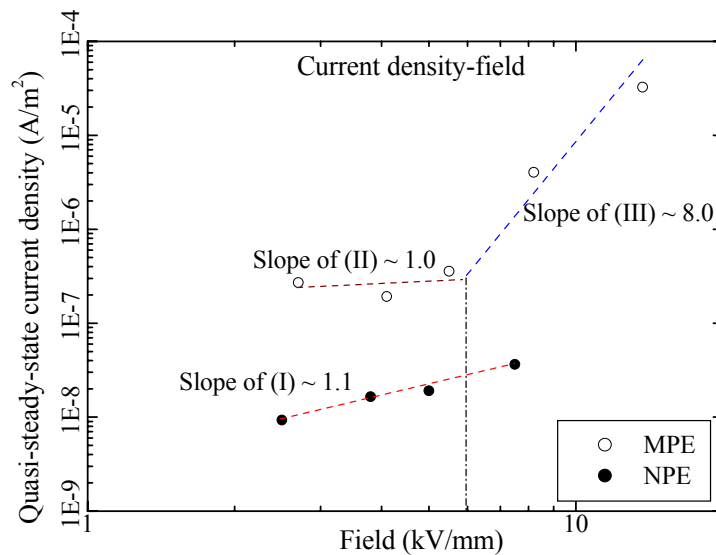


Figure 4.8. Quasi-steady state charging current density versus applied field experimental data of MPE and NPE

In figure 4.8, at the low field, nanocomposites have the slopes closing to that of microcomposites. The n of NPE in equation 4-5 ranges from 0.55 to 1 with decreasing field. The quasi-steady state charging current keeps the linear increment (ohmic behaviour) with the applied field in NPE below 7.5 kV/mm. It suggests no space charge accumulation occurred in NPE at this field. This can be confirmed by the PEA measurement, see table 4.7. The other feature is the marked decrement of quasi-steady state current density in NPE to that of MPE in one or two orders. The similar phenomenon is observed by Nelson and Hu [7].

To investigate the influence of the concentration of nanosilica on the conductivity of XLPE composites, XLPE specimens filled with 5 and 12.5 wt% nanosilica were prepared and measured in the three-electrode system. Their conduction behaviours are shown in figure 4.9.

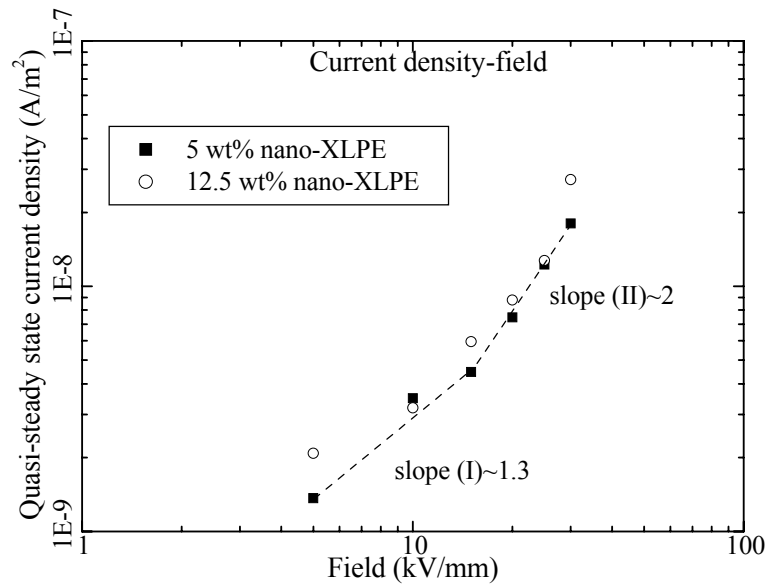


Figure 4.9. Quasi-steady state charging current density versus applied field experimental data of 5 and 12.5 wt% nano-XLPE

From figure 4.9, in the first stage (I), the slope of the curve in 5% nano-XLPE is ~ 1.3 , a nearly ohmic behaviour, as explained in figure 2.6. With the increasing applied field, the slope of the latter part (II) in the curve of 5 % nano-XLPE is almost 2, like a trap-limited SCLC behaviour. However, there is not an obviously linear relationship between field and quasi-steady state current density in the 12.5 wt% nano-XLPE; it is more like an exponential relation. This is confirmed in figure 4.10, which is drawn as $\ln J$ versus \sqrt{E} for both 5 and 12.5% nano-XLPE. The curve of 12.5% nano-XLPE behaves a quite good linear relationship between $\ln J$ and \sqrt{E} during the whole field range given. Hence, the conduction mechanism of nanocomposites is transiting to Schottky emission with increasing content of nanoparticles. At high field, above 15 kV/mm, it is possible that 5 wt% nano-XLPE also behaves as Schottky emission, but only at high fields. The quasi-steady state current densities of nanocomposites with various concentrations are not very different. This suggests that both 5 and 12.5 wt% are a high concentration for nanofillers.

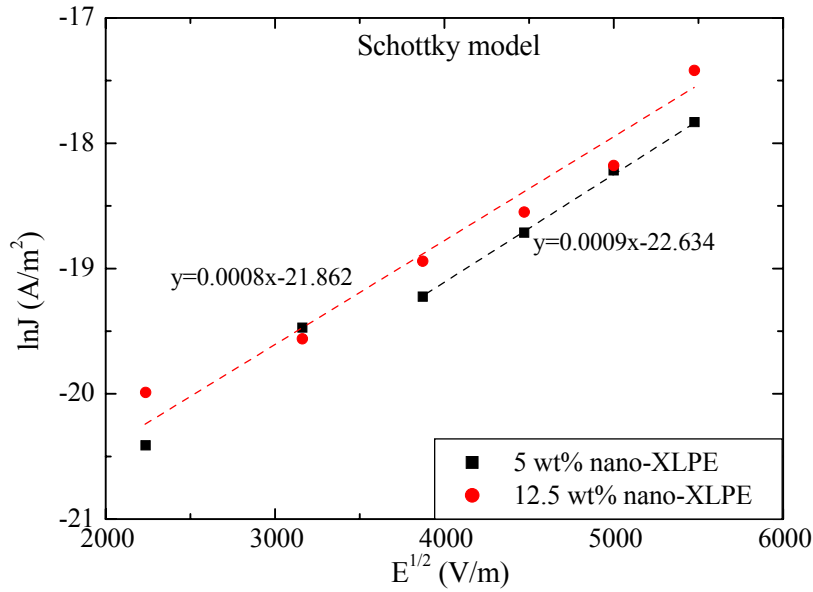


Figure 4.10. $\ln J$ versus \sqrt{E} experimental data of 5 and 12.5 wt% nano-XLPE

According to the expression for Schottky emission, equation 2-30, the slope of the curve $\ln J$ versus \sqrt{E} is equal to $\frac{\sqrt{e^3 / 4\pi\epsilon_r\epsilon_0}}{kT}$, where ϵ_r is the relative permittivity of insulator, which is assumed as 2.3 for XLPE base resin.

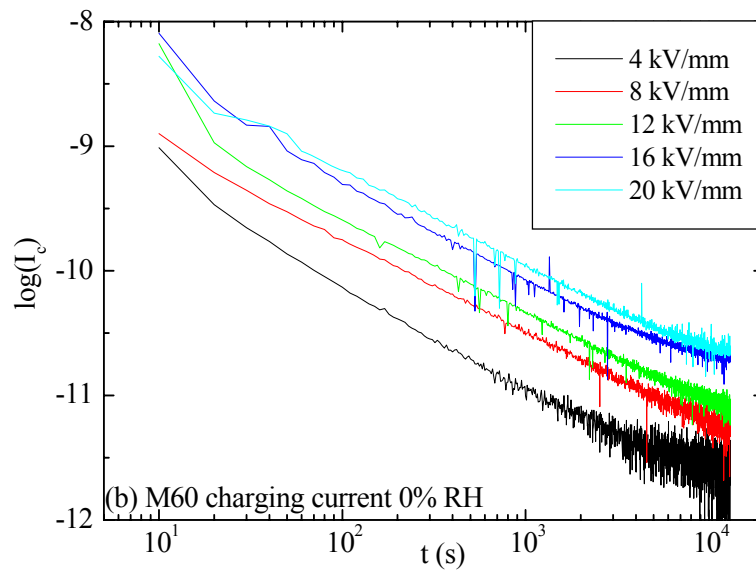
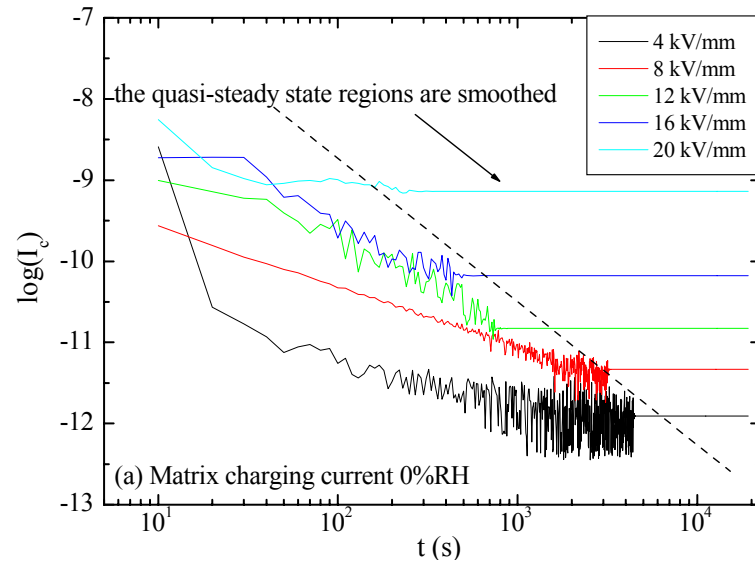
From figure 4.10, the slope can be obtained for the curve $\ln J$ versus \sqrt{E} for both 5% and 12.5% nano-XLPE as 0.0009 and 0.0008, respectively. These are close enough to be assumed identical within experimental uncertainties. The calculated permittivity ϵ_r of 5% and 12.5% nano-XLPE is 2.53 and 3.51, respectively, by assuming XLPE base resin with a permittivity of 2.3. This suggests that the permittivity of nano-XLPE increases with the increasing concentration of nanofillers. This is predicted by Effective Media theory. The height of the barrier ϕ_B in 5% and 12.5% nano-XLPE is 1.21 and 1.19 eV, respectively, again these are very close.

4.3.2 Epoxy materials

The three-electrode system, as shown in figure 3.5, is used to measure the conductivity of epoxy specimens (Matrix, M60, n3 and n9) at 0% RH and 75% RH. The measurements were carried out in the temperature range of 285 to 292K. There

was a lot of apparent noise superimposed on the quasi-steady state currents in these experiments; the graphs show the average of the logarithm of the current.

I. Epoxy composites under 0% RH, room temperature



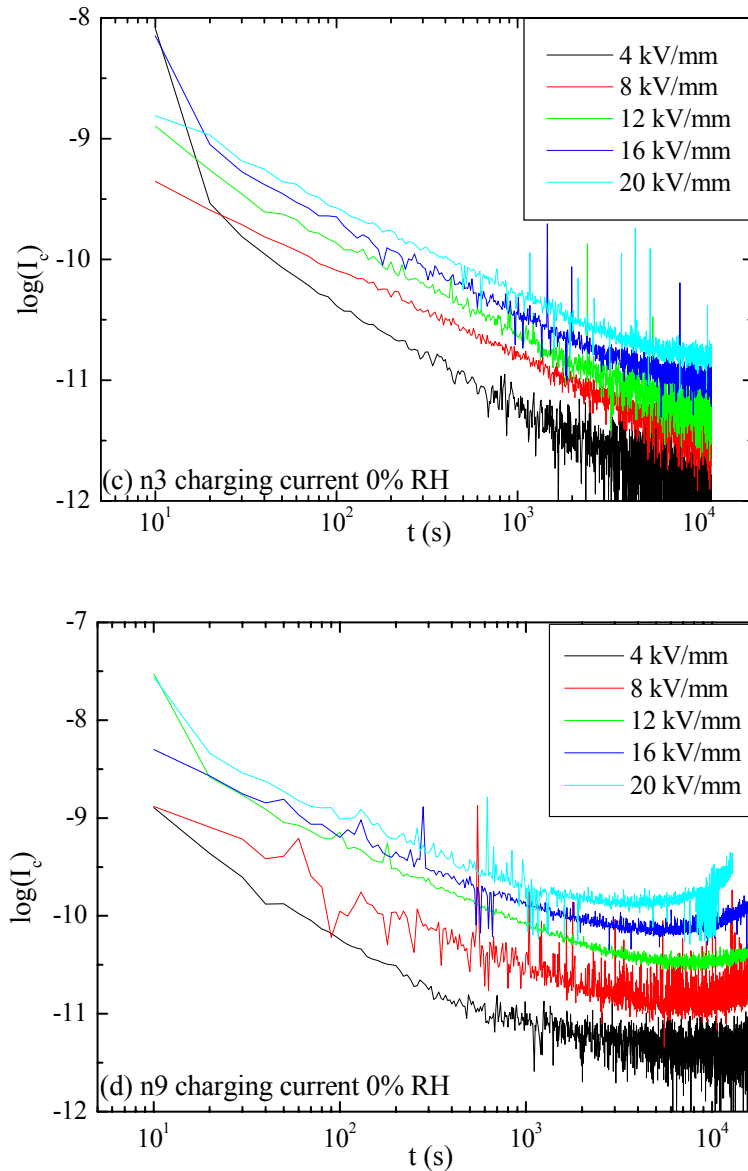
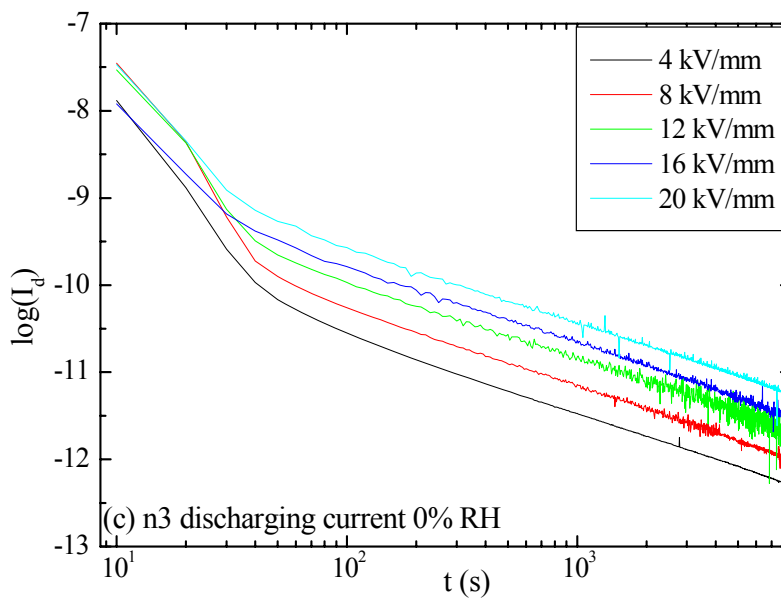
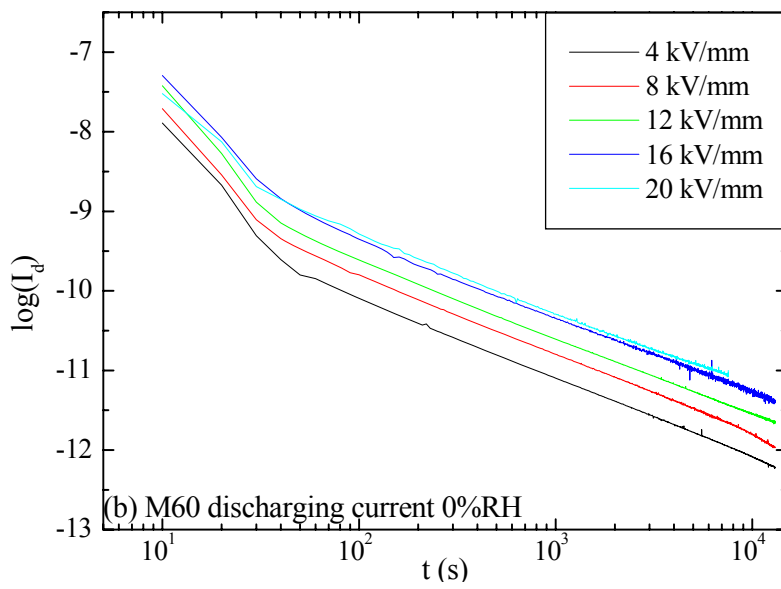
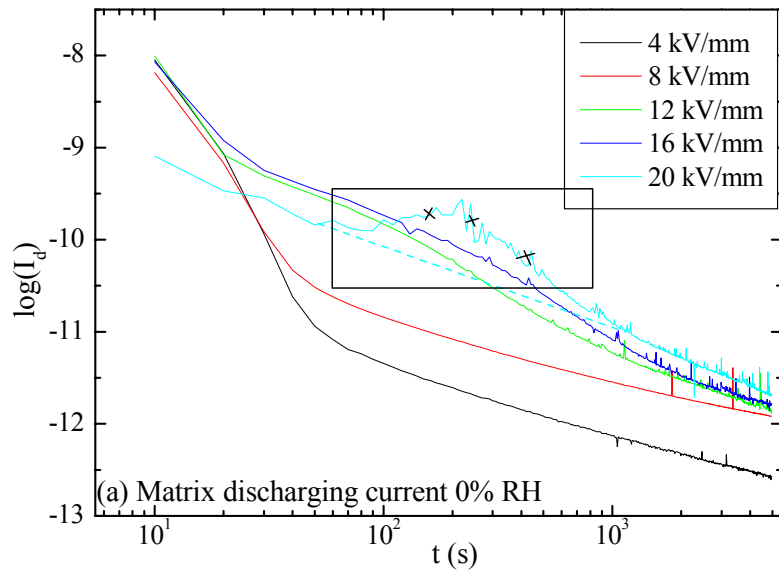


Figure 4.11. The charging currents of dried epoxies under various fields

According to the curves of charging current, the charging currents of Matrix and nanocomposites more quickly reach quasi-stabilisation. However, a longer time is required in M60. Where the quasi-stabilised current is seen to increase at long times, this may be caused by temperature fluctuations in the laboratory.



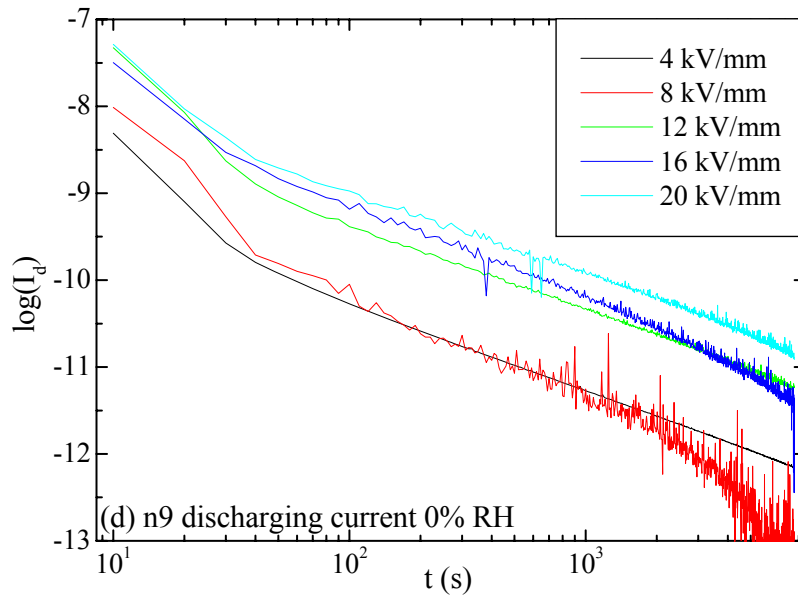


Figure 4.12: The discharging current of dried epoxies under various fields, (a) Matrix, (b) M60, (c) n3 and (d) n9

The n values in equation 4-5 of epoxies are provided in table 4.2, which include the values from both charging and discharging processes.

Table 4.2. The values of n in charging and discharging processes

$$(I(t) = At^{-n}) (0\%RH)$$

| Specimens | Values of n in $I(t) = At^{-n}$ | |
|-----------|-----------------------------------|-------------|
| | Charging | Discharging |
| Matrix | 0.7~0.9 | 0.67~0.93 |
| M60 | 0.75~0.98 | 0.98~1.0 |
| n3 | 0.76~0.94 | ~0.88 |
| n9 | 0.87~1.0 | ~0.98 |

This suggests, under a low loading of nanofillers, the conduction behaviour of nanocomposites is close to epoxy matrix. However, once beyond a concentration threshold (for example, the percolation threshold), the conduction behaviour of nanocomposites will change. As to M60, since the volume concentration is much beyond the threshold (~19 vol%), the discharging current drops more rapidly than that

of the matrix. The threshold field for space charge accumulation in epoxies is about 8 – 10 kV/mm according to these tests, see table 4.9.

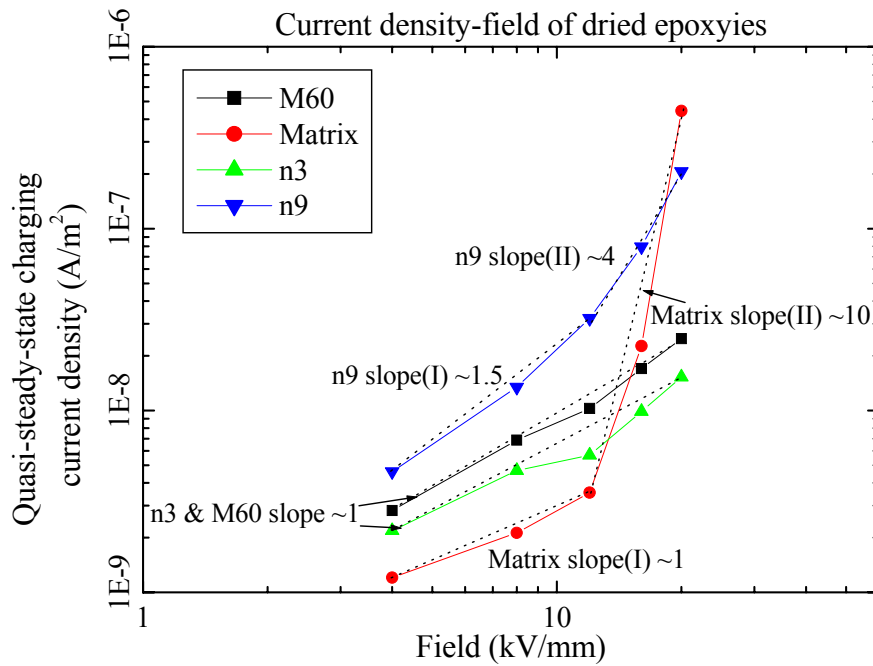


Figure 4.13. Quasi-steady state charging current density versus applied field experimental data of dried epoxy specimens

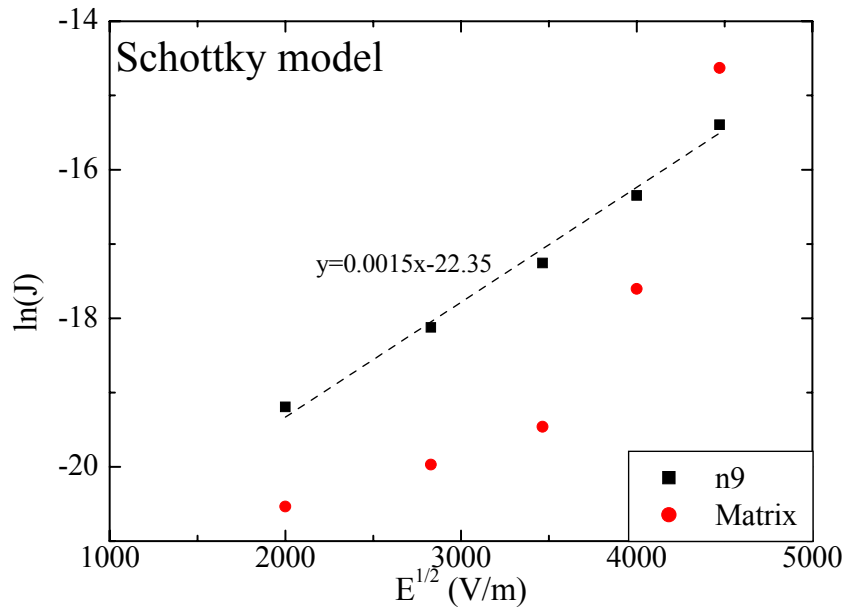


Figure 4.14. $\ln J$ versus \sqrt{E} experimental data of 9 wt% epoxy nanocomposites

According to figure 4.14, Schottky emission is not seen in the epoxy matrix since there is not a linear relationship between $\ln J$ and \sqrt{E} . In figure 4.13, two conduction processes in epoxy matrix can be observed, which are ohmic (lower field) and trap-filled limit (higher field).

In the higher loaded epoxy nanocomposites, i.e., n9, Schottky emission dominates the conduction process (figure 4.14). This is similar to what happens in XLPE nanocomposites (figure 4.10). The permittivity of n9 calculated from the slope of the curve $\ln J$ versus \sqrt{E} is ~ 1 by assuming the epoxy matrix has a permittivity of 3.5. This result is much lower than the value expected. This is possibly caused by the weak interfacial bonding between nanosilica and epoxy matrix and the irregular surface of nanoparticles [18]. The height of barrier ϕ_b in n9 is ~ 1.33 eV calculated from the intercept of the curve $\ln J$ versus \sqrt{E} . The close value of barrier height in composites filled with nanosilica (1.19 – 1.21 eV in nano-XLPE, and 1.33 eV in epoxy nanocomposites) hints that the type of nanofiller controls the barrier height in nanocomposites.

II. Epoxy composites under 75% RH, room temperature

The method above also is used to analyse the conduction mechanisms within wet epoxy materials (75% RH). In table 4.3, the values of n in both charging and discharging processes of wet epoxy materials are given.

Table 4.3. The values of n in charging and discharging processes

$$(I(t) = At^{-n}) (75\% \text{ RH})$$

| Specimens | Values of n in $I(t) = At^{-n}$ | |
|-----------|-----------------------------------|-------------|
| | Charging | Discharging |
| Matrix | ~ 0.5 | 0.7~0.8 |
| M60 | 0.5~0.67 | 0.9~1.5 |
| n3 | 0.7~0.9 | 0.8~0.95 |
| n9 | 0.54~0.85 | 0.9~1.6 |

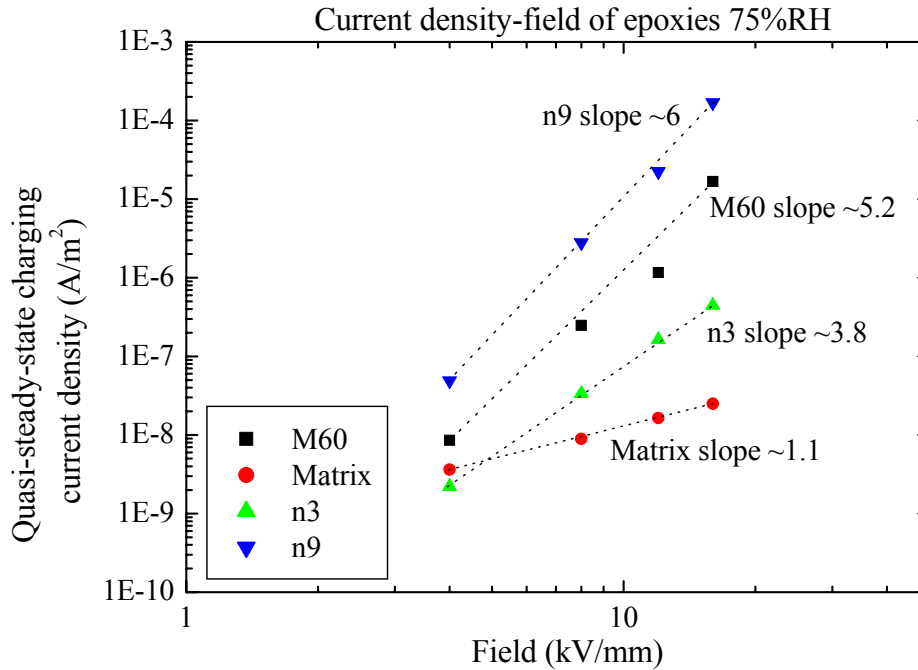


Figure 4.15. Quasi-steady state charging current density versus applied field experimental data of epoxy specimens at 75%RH

According to figure 4.15, the quasi-steady state conducting currents of all epoxies treated at 75%RH appear to be the straight lines with the applied field in log-log. The slope of the curve for matrix is about 1.1, which means no space charge was formed under 16 kV/mm. This is in agreement with table 4.9. But space charge can accumulate within the other wet specimens since their slopes are higher than one. The conduction mechanism to this phenomenon is not clearly understood. One possible explanation is that the absorbed water will increase the mobility of charge and make the materials to be more conductive.

(III) Epoxy composites under 323K and 0% RH

According to §2.7.1, the injected electrons from electrodes need to overcome a potential barrier to cross from electrode into insulator. Crossing the barrier depends on applied electric field and the interface defects [19]. These processes are greatly influenced by temperature. In figure 4.16, $\ln J$ (at 323K) is plotted as the function of the square root of E , according to Schottky emission.

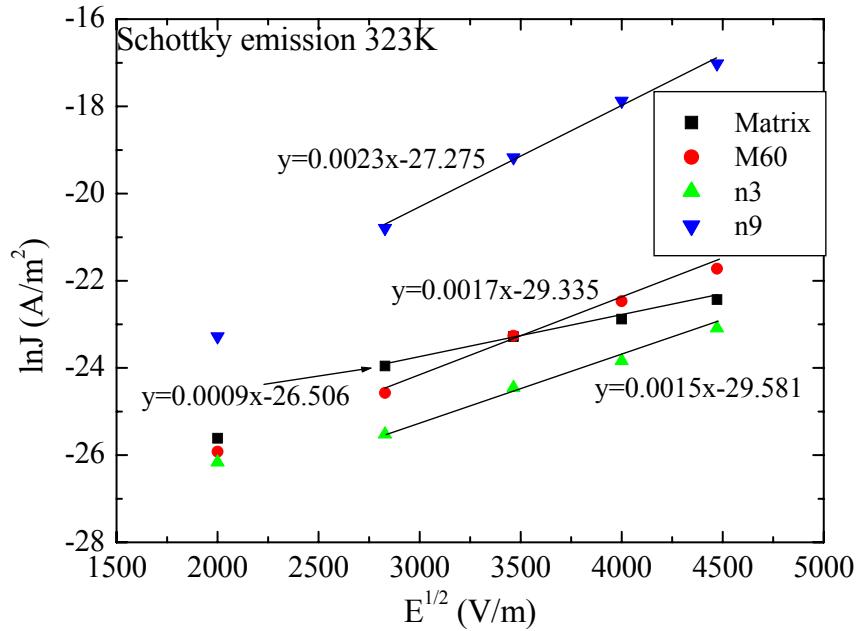


Figure 4.16. The quasi-steady state current densities of epoxy materials at 323K

According to the Schottky emission expression, the permittivity and barrier height of epoxy materials can be calculated from the slope and interception of the curves in the above graph. The permittivity of epoxy matrix at room temperature is assumed as 3.5.

Table 4.4. The permittivity and barrier height of epoxy materials at 323K*

| Specimens | ϵ_r | ϕ_B (eV) |
|-----------|--------------|---------------|
| Matrix | 2.59 | 1.45 |
| M60 | 0.73 | 1.53 |
| n3 | 0.93 | 1.54 |
| n9 | 0.40 | 1.47 |

*(Calculated by Schottky expression, assumed ϵ_r of epoxy matrix at room temperature is 3.5)

Again, the barrier heights of epoxy materials are similar to each other. This suggests that the type of inorganic filler decides the barrier height. However, permittivity is unlikely to be less than one. One possibly reason to cause such wrong is the experimental uncertainties. Moreover, the error may also be due to the pressure contact rather than metallised contact in this testing, which will cause a lower permittivity calculated. This deviation from the effective media theory suggests that

interfacial polarisation dominates the dielectric permittivity of epoxy nanocomposites [20].

(IV) Epoxy composites under 343K (0% RH)

The relationship between $\ln J$ and the square root of field for dry epoxy materials at 343K are presented in figure 4.17.

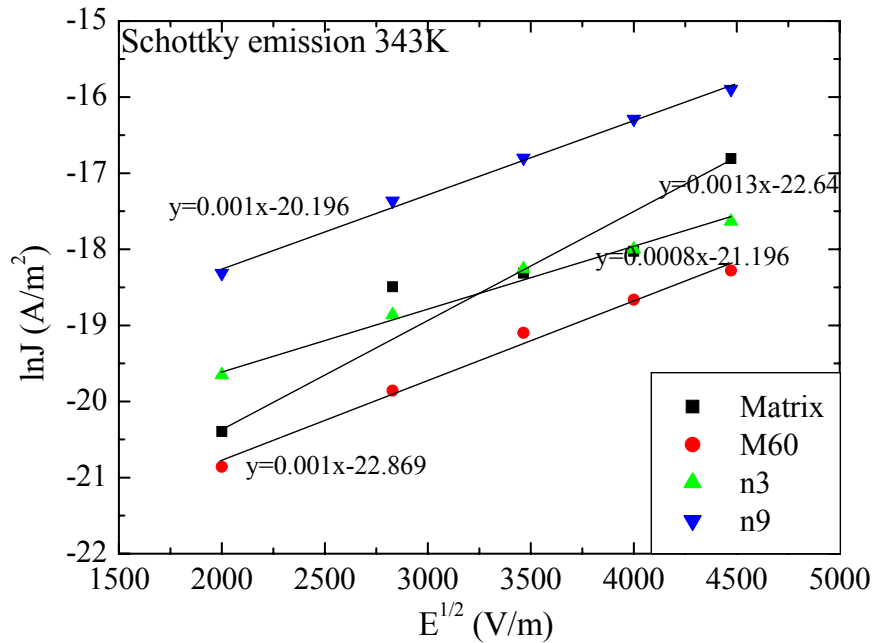


Figure 4.17. The quasi-steady state current densities of epoxy materials at 343K

Table 4.5. The permittivity and barrier height of dry epoxy materials at 343K*

| Specimens | ϵ_r | ϕ_B (eV) |
|-----------|--------------|---------------|
| Matrix | 1.24 | 1.43 |
| M60 | 2.09 | 1.44 |
| n3 | 3.27 | 1.39 |
| n9 | 2.09 | 1.36 |

(Calculated by Schottky expression, assumed ϵ^ of epoxy matrix at room temperature is 3.5)

The results at 343K show a similar regular with that at 323K, except the permittivities are higher than the results at 323K, which is because the more dipoles can join the polarisation at the higher temperature.

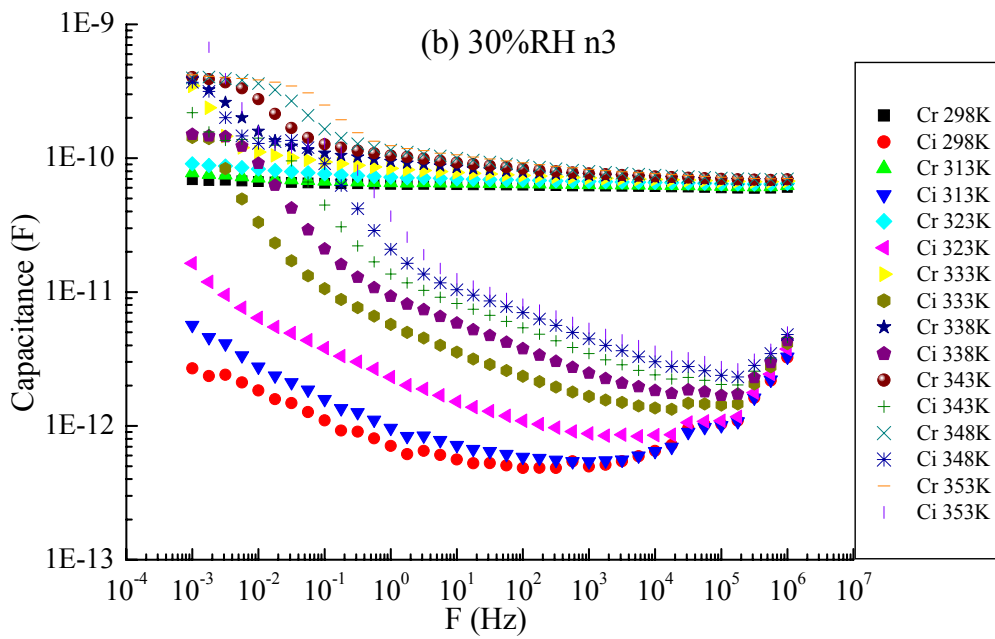
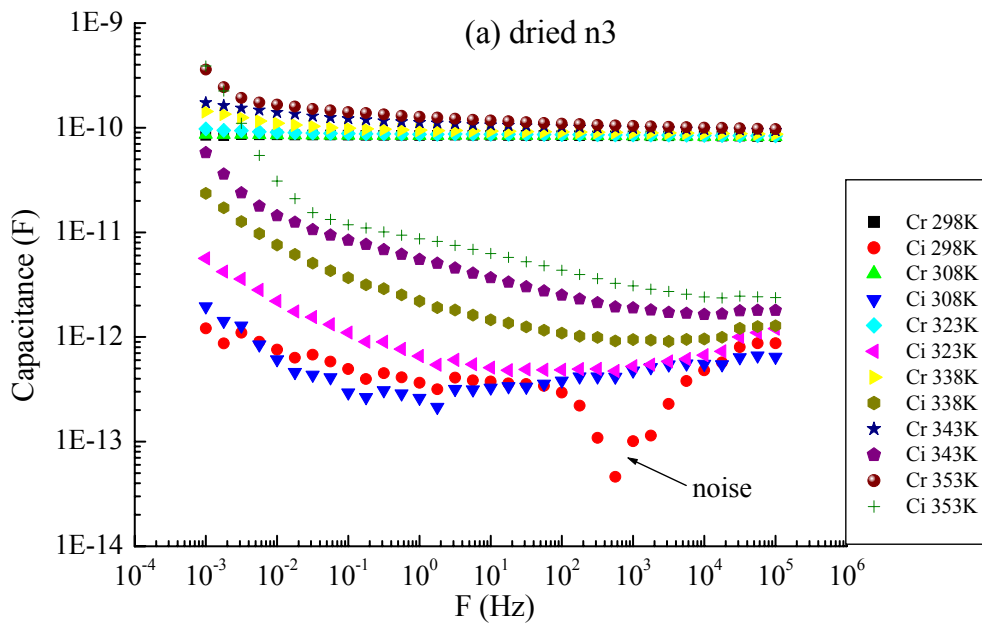
Summary of this section:

1. Composites with low concentration have a similar charging/discharging behaviour to the polymer matrix. High concentrations of inorganic fillers will alter the conduction behaviour of composites;
2. The quasi-steady state current deviates from the low-field linear relation when the applied field is higher than the threshold field for space charge accumulation;
3. The more the inorganic fillers filled, the discharging current of composites drops more rapidly because the particles make the charges disperse more easily;
4. In nanocomposites, the conduction mechanism is changing to Schottky emission with increasing concentration of nanofillers.

4.4 Dielectric spectroscopy of epoxy materials

The dielectric spectra of epoxy specimens at various temperatures and relative humidities were measured [Appendix III]. The real and imaginary parts of capacitance are used to describe the dielectric behaviour of composites rather than dielectric permittivity and loss as this does not require an accurate measurement of the dimensions of the specimen.

4.4.1 The overall dielectric properties of n3 epoxy specimens



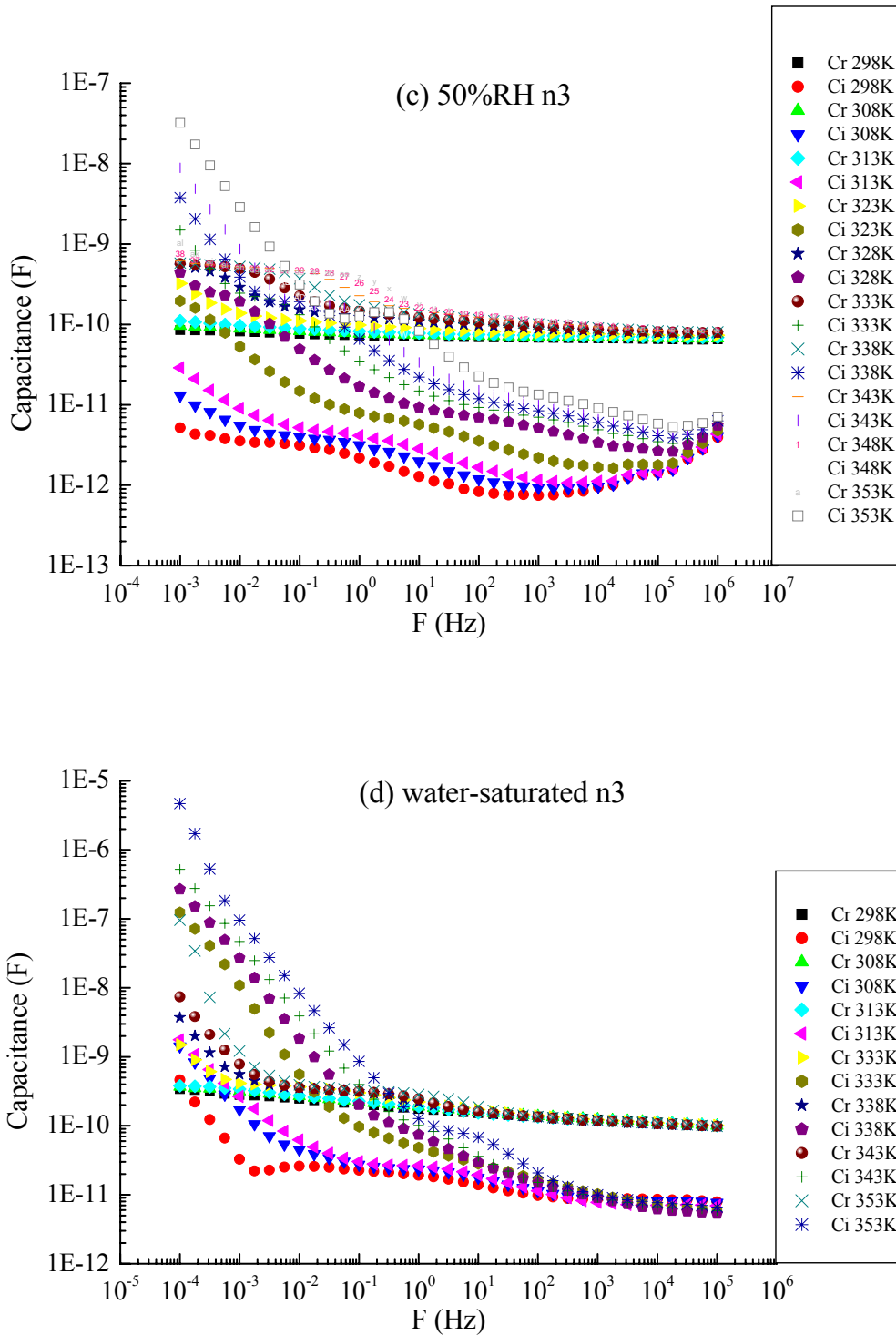


Figure 4.18. The dielectric spectrum of n3 at various relative humidities and temperatures, (a) 0% RH, (b) 30% RH, (c) 50% RH and (d) 100% RH

Figure 4.18 shows the dielectric behaviour (real and imaginary parts of capacitance, C' and C'') of n3 between 298 and 353 K at various values of RH. The reproducibility

of the data was confirmed by measuring several specimens. In dried n3 specimens (figure 4.18a), there were some noises at high frequencies ($10^2 - 10^4$ Hz) at 298K. For the comparison, the noises were not removed by changing the electrodes.

When the frequency is below 10^{-2} Hz, the true conduction can be observed in all dry epoxy specimens, i.e., $C' \propto \omega^0$, $C'' \propto \omega^{-1}$ [21]; this is shown more clearly in figure 4.19 (a). This is typical of a material possessing mobile charge carriers, which one would expect for an ideal capacitor in parallel with an ideal conductor; i.e., it shows that there is a constant “leakage resistance” with a classical (frequency independent) conduction mechanism. However, with increasing temperature, once the hydration in nanocomposites reaches a certain level, the dielectric behaviour at low frequencies will change to a quasi-DC/LFD process, i.e., $C' \propto C'' \propto \omega^{n-1}$ [22 – 24], more clearly shown in figure 4.19 (b). In figure 4.19 (b), at high temperature and high hydration, the value of C' of n3 is not independent of frequency and the C' and C'' curves are, in fact, parallel with a ratio $C''/C'=73$ and a slope is -0.995 in reasonable agreement with equation 2-20 [23], This behaviour is typically observed when charge carriers have some limited freedom of movement, and under the influence of the electric field, follow tortuous paths that do not allow transport right through the material. It seems likely that the carriers are moving through partially interconnected interaction zones that surround the particles. This transition in n3 is presented in figure 4.19.

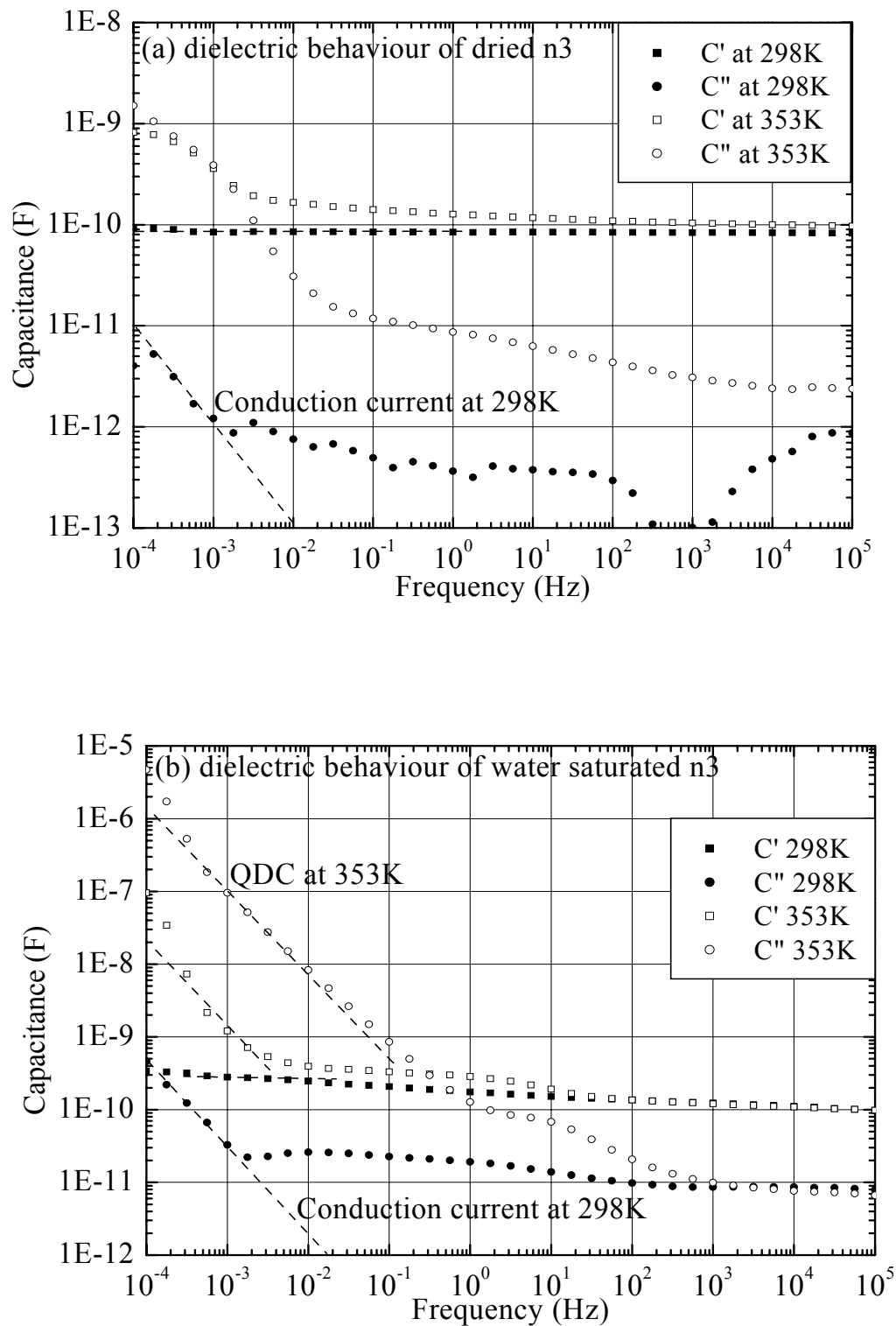


Figure 4.19. Dielectric behaviours of dried (a) and water-saturated (b) n3 at 298K and 353K

A similar low frequency phenomenon was observed in unfilled epoxy, M60 and n9. However, at the same relative humidity, the minimum temperature at which QDC occurs in n9 is lower than that in other specimens. Also, QDC could occur in n9 at a lower relative humidity than other epoxy specimens at the same temperature. The transition temperature and RH of epoxy specimens from conduction to QDC are given in table 4.6 (The complete dielectric spectra for all four specimens at all temperatures and humidities are included in Appendix III).

Table 4.6. The transition temperature/RH of epoxy specimens from conduction to QDC

| Specimens/Conditions | 0% RH | 30% RH | 50% RH | 100% RH |
|----------------------|------------|------------|------------------------|------------------------|
| Matrix | conduction | conduction | conduction | $\geq 348\text{K QDC}$ |
| M60 | conduction | conduction | conduction | $\geq 353\text{K QDC}$ |
| n3 | conduction | conduction | conduction | $\geq 343\text{K QDC}$ |
| n9 | conduction | conduction | $\geq 338\text{K QDC}$ | $\geq 333\text{K QDC}$ |

Obviously, QDC starts at a lower temperature in nanocomposites than in epoxy matrix and M60. The higher the concentration of nanofillers, the lower the temperature and hydration required for QDC.

4.4.2 The activation energy (E_a) at low frequencies

Master plots were used to calculate the activation energy at low frequencies (lower than 10^{-2} Hz). The theory of master plots was introduced in detail in § 2.4.8. Figure 4.20 shows the master plot (for the low frequency process) and activation energy of dry n3.

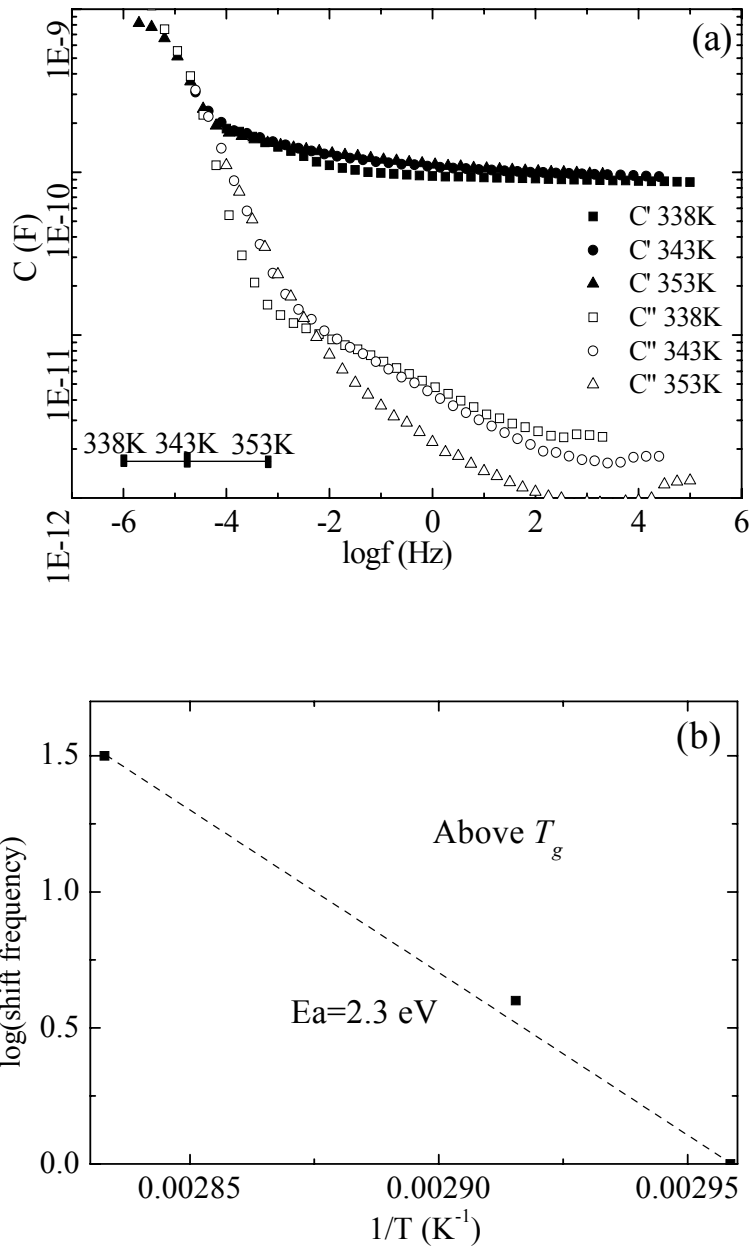


Figure 4.20. The master plot (a) and activation energy (b) of dry n3

The activation energy values of the relaxation process in epoxy materials at low frequency (below 10^{-2} Hz) and above 338K are given in figure 4.21.

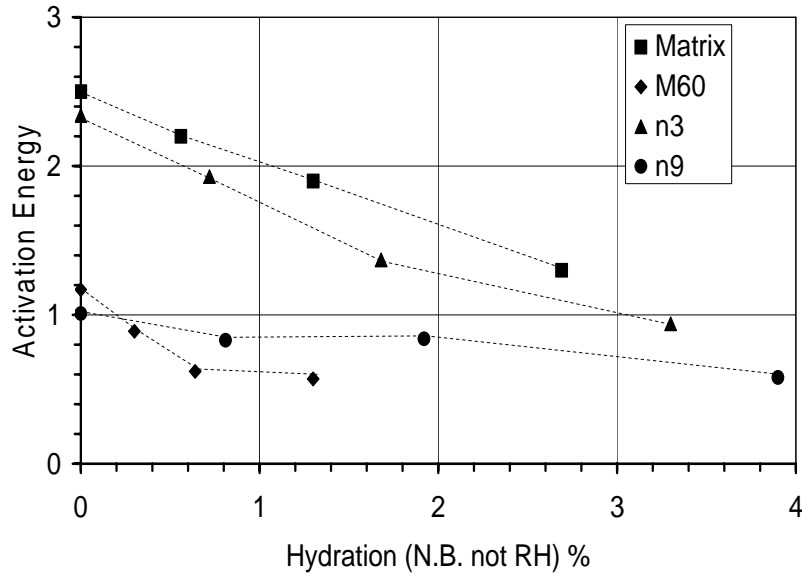


Figure 4.21. The activation energies of epoxy materials at various hydrations

According to figure 4.21, the activation energy of the relaxation process at the low frequencies drops with increasing hydration (relative humidity), suggesting the channels in the percolation network are dilated. As more water enters the epoxy material, the epoxy becomes more flexible and more of the water exists in a free state [21]. This then leads to a reduction of the activation energy with increased hydration. Moreover, the activation energy of the filled composites is lower than that of matrix. This might suggest that free volume in composites with fillers is increased by incorporating inorganic fillers, and the more filler is added, the bigger the free volume in the composites; this can be seen by comparing n3 and n9. Such results are in agreement with the conclusion from saturated specimens.

4.4.3 The relaxation process caused by bound water

Currently, at least two states of water have been observed in the epoxy network these are depicted as free water and bound water [9, 25, 26]. One possible state of water in these composites occurs when water molecules infiltrate the polymer structure, interact with adjacent bond sites, and form hydrogen-bonded clusters; this is the so called “bound” water. The other one is “free/liquid” water, which occupies the free volume holes or cracks in composites, and is relatively free to move.

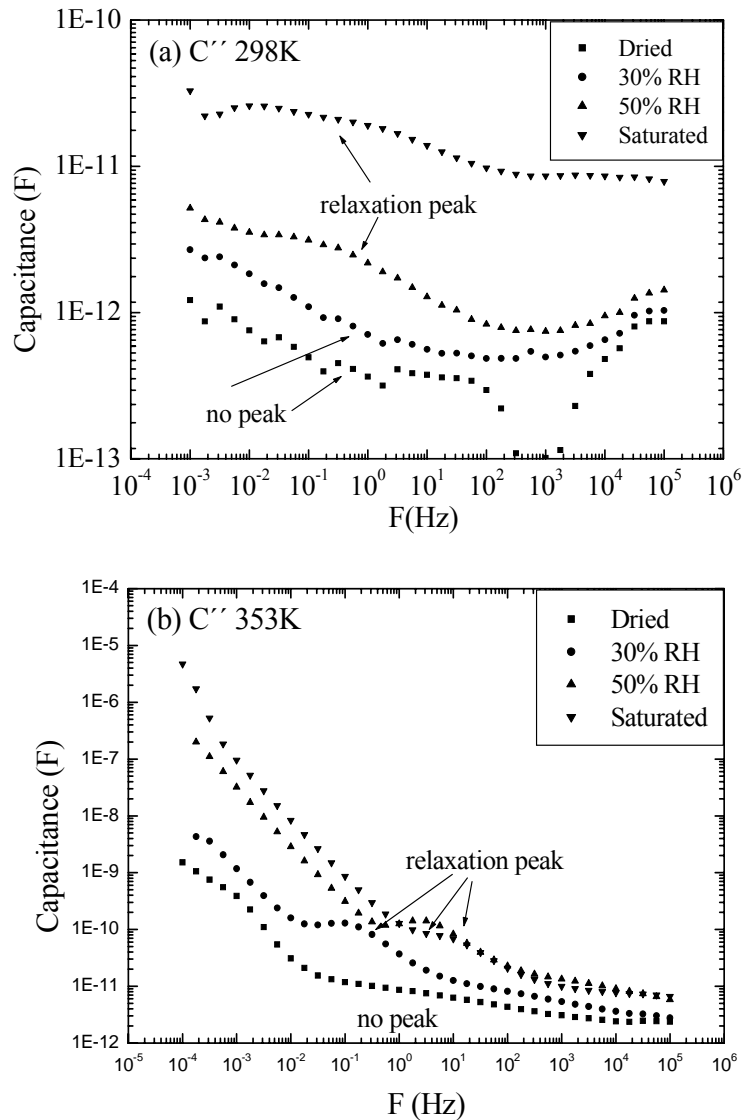


Figure 4.22. Imaginary capacitance of n3 at 298K (a) and 353K (b)

The relaxation peak in the middle frequency range, i.e., 10^{-2} to 10^2 Hz, seems to be linked with the water within epoxy specimen, since it cannot be observed in any dried specimen [27], as shown in figure 4.22. This relaxation process becomes stronger with increasing temperature and relative humidity. Figure 4.22 (b) shows, at high temperature (353K), even at low relative humidity, i.e., 30% RH, that this relaxation peak can be observed in dielectric spectrum. However, at lower temperatures, it only can be observed at higher relative humidity, above 50% RH for instance.

The mid-frequency relaxation shifts to higher frequencies with increasing temperature, and causes an increase of dielectric loss at the power frequency (50 Hz).

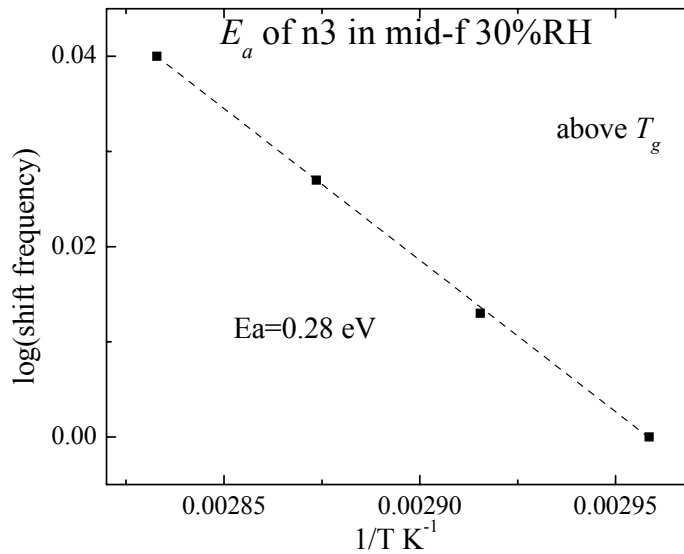


Figure 4.23. E_a of the mid-frequency process in n3 at 30% RH

The activation energy of the relaxation process caused by water at the mid-frequency range in water saturated 3 wt% nanocomposites is 0.28 eV , calculated by master plots, in figure 4.23. The activation energy reflects the strength of local interactions around a water molecule.

It is known that, the activation energy of H-bond is 0.052 eV , and that of liquid/free water is about 0.21 eV [28]. Hydrogen-bonding considerations and X-ray data for the liquid suggest that the immediate environment of a water molecule in liquid water is much like that of a water molecule in ice, with an approximate tetrahedral arrangement of four neighbours, i.e. there are four H-bonds associated with a water molecule in liquid water or “free” water [29]. However, in water saturated epoxy specimen, the number of H-bond associated with a water molecule is about 5, i.e., one more H-bond than liquid water, which is connected with Si. Hence, it is the bound water causes the mid-frequency relaxation. Moreover, the hopping time of free water is about $7 \times 10^{-10} \text{ s}$ [29], the response frequency of 10^9 Hz is too high to be the mid-frequency relaxation observed in dielectric spectrum. This is the other evidence that the mid-frequency relaxation is caused by bound water, which also is supported by Jelinski [30, 31].

4.5 PEA measurement

In this section, space charge profiles, the threshold field for space charge accumulation, and the local field distortion by space charge are presented.

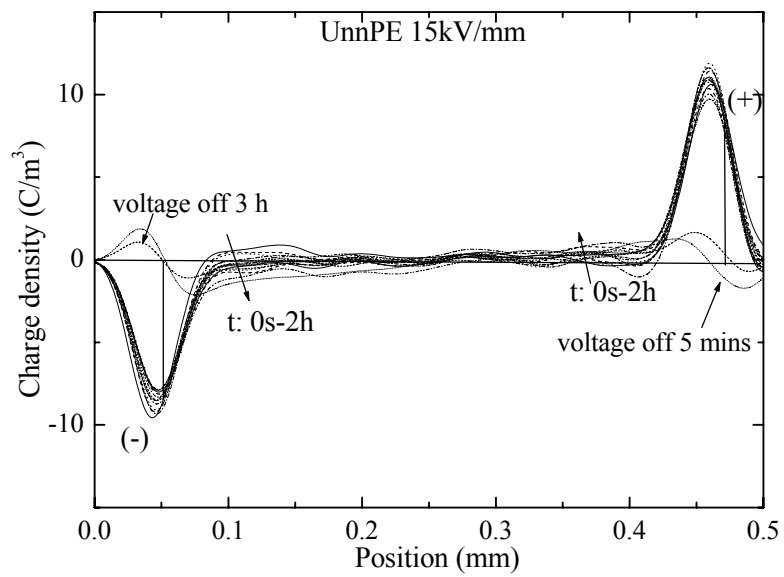
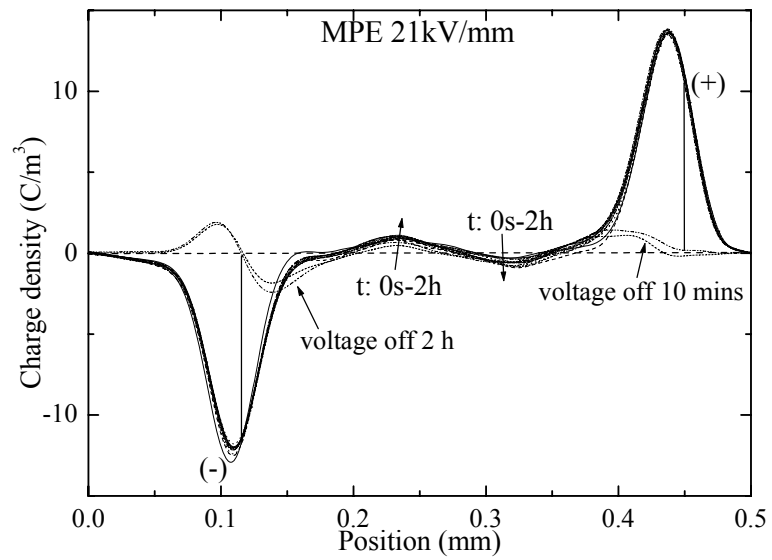
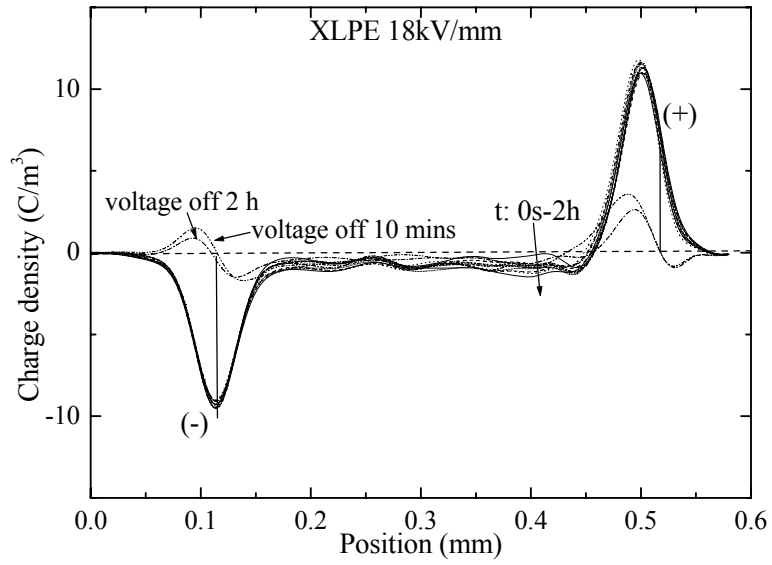
In order to explore the field required to cause space charge to accumulate, the following experiment has been carried out. The voltage across a film-shaped specimen, 0.3 – 0.7 mm thick, was gradually increased. Without space charge accumulation, such a specimen would behave like an ideal capacitor and the charge on the electrodes, q , would be proportional to the applied voltage, v , since, for a perfect capacitor:

$$q = v \times C \quad (4-6)$$

where C is the capacitance of the specimen. However, if space charge accumulates within the specimen, then the electrode charge deviates from equation 4-6. In the case of homocharge accumulation, the charge on the electrode will decrease, whereas, in the case of heterocharge accumulation, the electrode charge will increase. By using a pulsed-electroacoustic (PEA) space charge measurement system, the electrode charge was measured as the applied voltage. The voltage was increased in 1 kV steps. In this test, every voltage step test was carried out immediately following the previous voltage step to reduce the time effect [6].

4.5.1 Space charge behaviours of polyethylene specimens

The results from space charge measurements by PEA on XLPE specimens are summarised in figure 4.24.



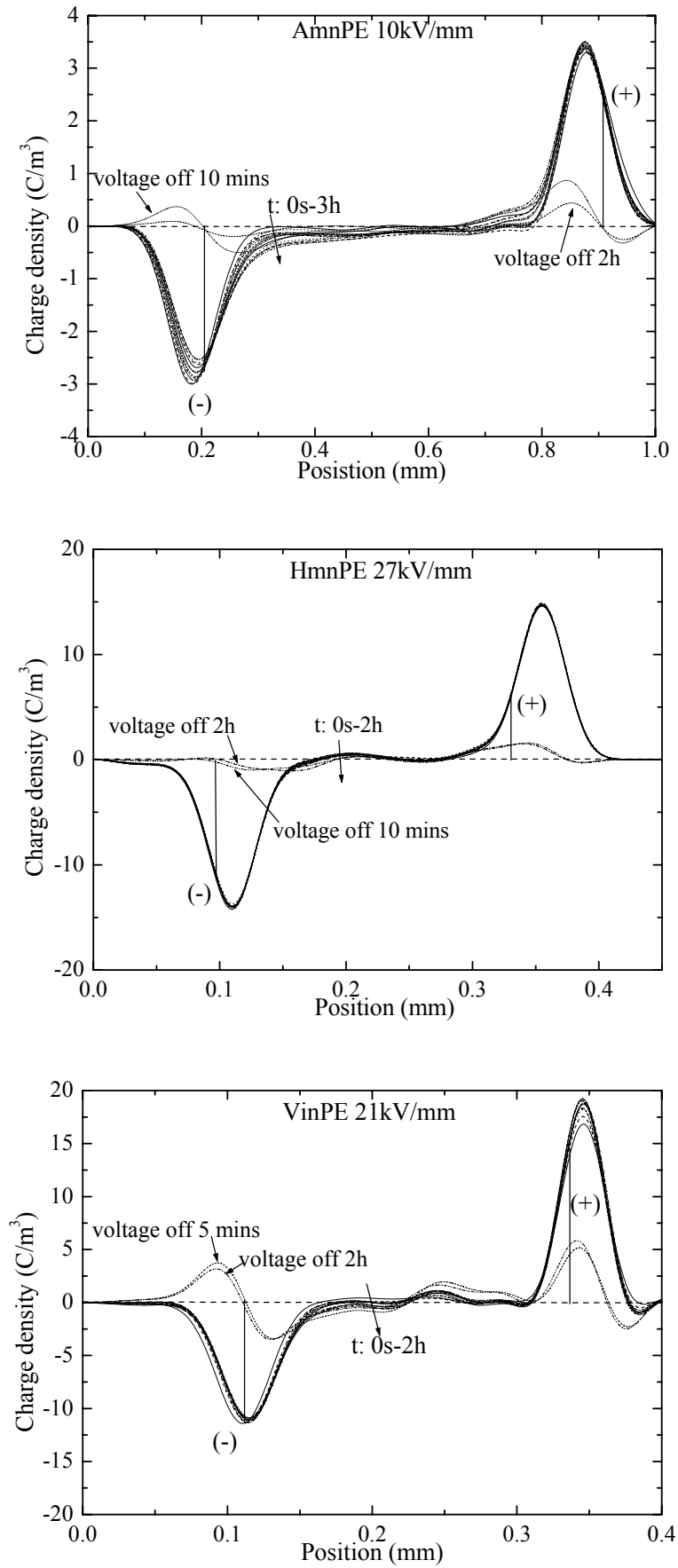


Figure 4.24. The space charge profiles of XLPE specimens

According to figure 4.24, under the external applied field we can summarise the behaviour of the different XLPE composites as follows:

| | |
|---------------------|-------------------------------------------------------------------------------------------------------------------------------------------------------------------------------------------------------------------------------|
| XLPE matrix | Negative charges accumulated, injected from the cathode. Homocharge appeared within the sample near the interface, and the charge density increased with increasing time of field applied. |
| XLPE microcomposite | The charge inside specimen was changing the polarity when time increases. Homocharges accumulated at the inner interface. |
| UmnPE nanocomposite | Both positive and negative charges can be detected. Homocharge appeared near the inner interface |
| AmnPE nanocomposite | Only 10kV/mm can be applied on AmnPE since its thickness, the charge density inside the specimen was very low. Homocharge accumulated at inner interface of the specimen, which charge density increased when time increases. |
| HmnPE nanocomposite | Homocharge accumulated inside the specimen, which charge density increased with increasing time. Charge density was low even at the high field. |
| VinPE nanocomposite | Homocharge accumulated at inner interface. Both negative and positive charges were detected within the specimen. When the amount of negative charges increased with increasing time, positive charges decreased. |

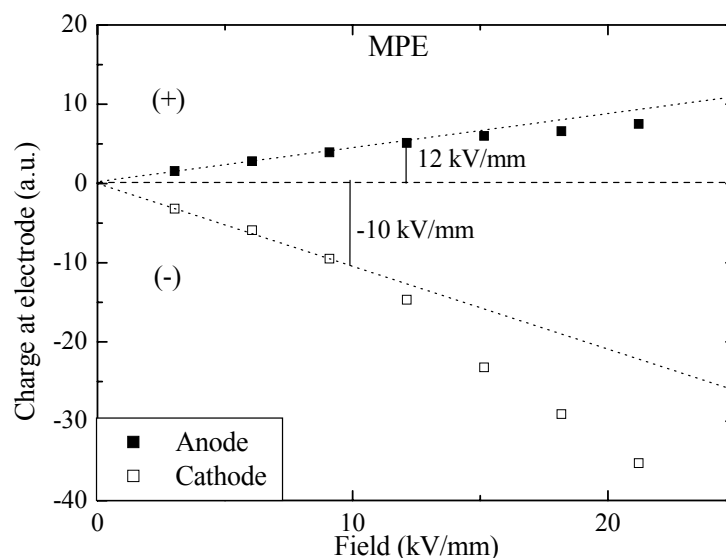


Figure 4.25. The threshold fields for space charge accumulation at anode and cathode within MPE

The threshold fields for space charge accumulation at both electrodes within MPE are determined in figure 4.25. The dotted lines show the linear relationship expected by equation 4-6. However, there is a deviation from linearity for the anode field at approximately 12 kV/mm, and 10kV/mm for the cathode field in figure 4.25. The same method was used to determine the threshold fields for space charge accumulation within other XLPE specimens. The results for all the XLPE specimens are shown in table 4.7.

Table 4.7. Space charge threshold field values for a range of XLPE specimens at room temperature

| Specimens | Field at anode (kV/mm) | Field at cathode (kV/mm) |
|-----------|------------------------|--------------------------|
| XLPE | 13 | 12 |
| MPE | 12 | 10 |
| UmnPE | 13 | 14 |
| AmnPE* | >12 | >12 |
| HmnPE | 26 | 23 |
| VinPE | 25 | 26 |

*The aminosilane treated material did not reach its threshold before flashover occurred

One can note that treated nanocomposites display considerably higher fields before the space charge initiation. According to the space charge profiles within treated nanocomposites, homocharge initially accumulated near the cathode when the external voltage was applied. However, after longer times, heterocharge has replaced homocharge to exist near cathode. For nanocomposites, only homocharge is induced near cathode. This also is observed by Nelson and Hu [7]. It can be explained as the nanoparticles cause scattering in the composite so energetic electrons are slowed and will get trapped in front of the cathode, thus generating these charges that were recorded. This contrasts with microcomposites where the large distance between particles does not contribute too much scattering and thus allow impact ionisation. The residual positive ion charge is seen in PEA studies for the composite [32].

It is known that particles act as electrical defect centres in filled polymers and distort the local electrical field [6], like in HmnPE, figure 4.26. The local field within the samples is distorted by space charge. The calculated field profile is calculated by

considering both the negative and positive charges. The results of local field distortion are given in table 4.8.

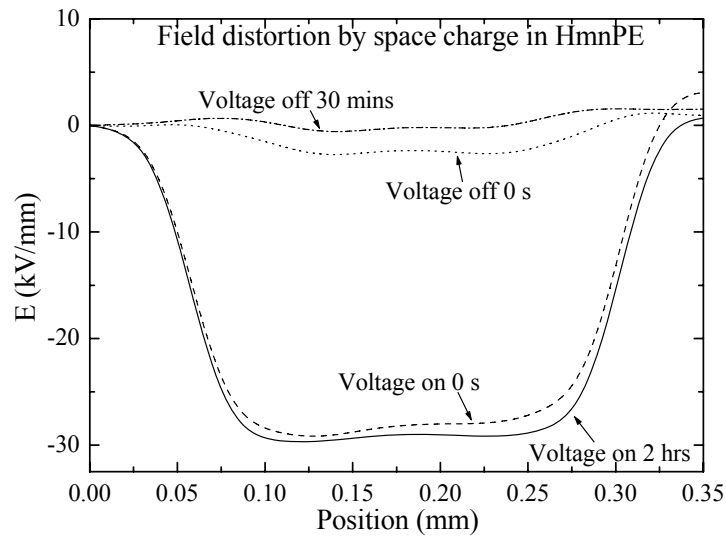


Figure 4.26. Field distorted by space charge accumulation in HmnPE (27 kV/mm)

Table 4.8. Field induced by space charge for a range of SiO₂-XLPE specimens

| Specimens | XLPE | MPE | UnnPE | AmnPE | HmnPE | VinPE |
|--------------------------------------------------------|------|------|-------|-------|-------|-------|
| Applied field (kV/mm) | 18 | 21 | 15 | 10 | 27 | 21 |
| Max value of positive charge (C/m ³) | 3.5 | 1.1 | 1.2 | 0.9 | 1.5 | 5.0 |
| Max value of negative charge (C/m ³) | -1.7 | -1.8 | -2.1 | -0.5 | -1.1 | -3.4 |
| Field induced by space charge (kV/mm) | 5.6 | 1.2 | 5.8 | 0.78 | 2.6 | 2.3 |
| E _{max} inside specimens (kV/mm) | 22.3 | 21.8 | 19.0 | 11.4 | 29.7 | 22.3 |
| The field distortion degree caused by space charge (%) | 31 | 5.7 | 39 | 7.8 | 9.6 | 10.0 |

According to table 4.8, the fields inside specimens of XLPE and UnnPE have a bigger field distortion caused by space charge accumulation (or a great amount of space charge accumulated within specimens), the electrical field distortion degree is about

31 – 39%. However, the fields inside specimens of MPE, HmnPE and VinPE only have a slight field distortion, less than 10% field distortion degree. It is clear that the functionalised nanocomposites have a lower degree of space charge formation than the other materials. Compared with the results of the threshold field of space charge formation, it is noticeable that the higher threshold field of space charge formation within the functionalised nanocomposites indicates that less field distortion occurs.

4.5.2 Space charge accumulation in epoxy specimens

Both the space charge behaviours of dry and wet (at 75% RH) epoxies were measured by PEA in this research. The profiles of space charge with epoxy materials were quite complicated because the charge decay within epoxies is much faster. Figure 4.27 shows the profile of space charge within dried n3, under 12 kV/mm. The threshold field for space charge accumulation is quite important as an indication of ageing [33]. Usually, build up of space charge within polymer is not desirable. With the higher threshold field for space charge accumulation, it is more difficult to build up space charge within polymer. This method is used frequently by G. C. Montanari [34]. These threshold field results of epoxies are not as clear as they are for XLPE because of the complicated space charge profiles in epoxy materials, see figure 4.27.

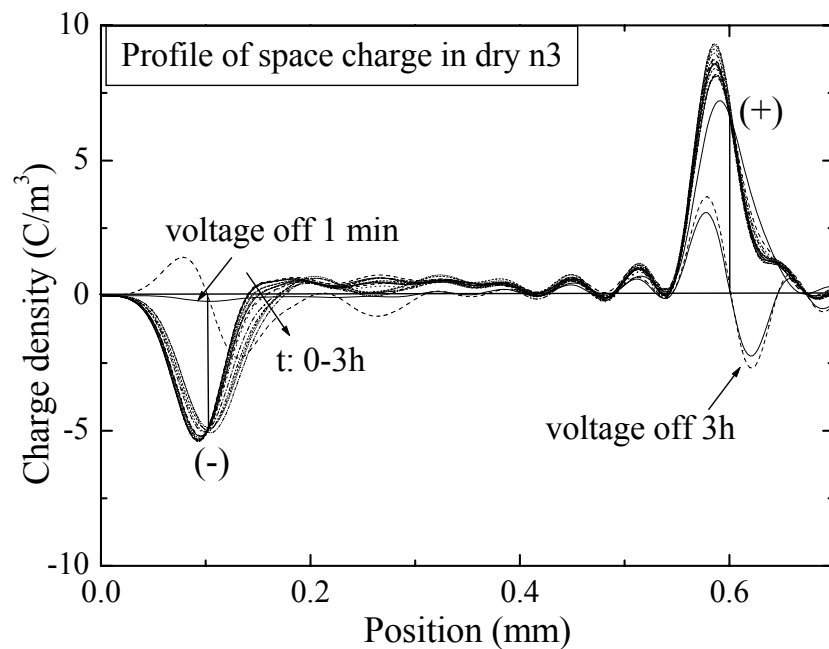


Figure 4.27. Profile of space charge in dry n3 (12 kV/mm)

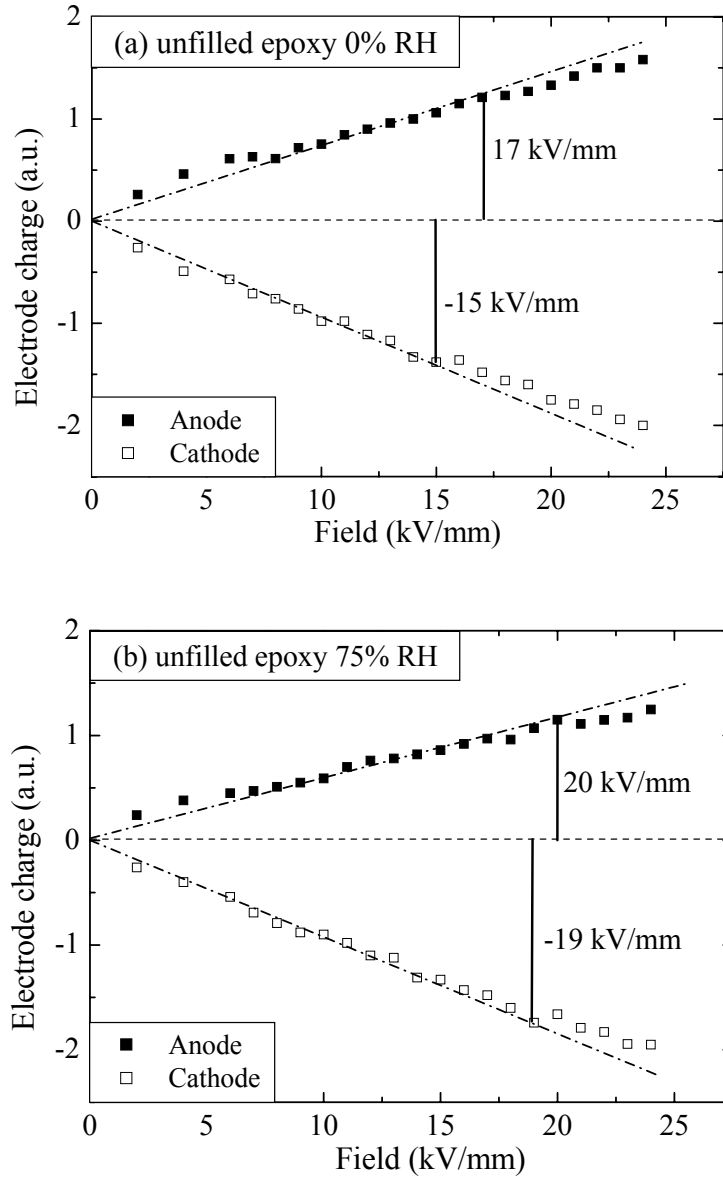


Figure 4.28. Space charge threshold characteristic of unfilled epoxy at electrodes under various humidities, (a) 0% RH, (b) 75% RH

Table 4.9. The threshold field of epoxies at electrodes

| Specimens | Threshold field at anode under 0% RH (kV/mm) | Threshold field at cathode under 0% RH (kV/mm) | Threshold field at anode under 75% RH (kV/mm) | Threshold field at cathode under 75% RH (kV/mm) |
|-----------|----------------------------------------------|------------------------------------------------|-----------------------------------------------|-------------------------------------------------|
| Matrix | 17 | 15 | 20 | 19 |
| M60 | 15 | 18 | 21 | 15 |
| n3 | 19 | 17 | 24 | 20 |
| n9 | 24 | 19 | 24 | 22 |

The threshold fields for space charge accumulation within unfilled epoxy resin both at anode and cathode, at 0% RH (figure 4.28 a) and 75% RH (figure 4.28 b) are shown. The threshold field results of epoxy materials are given in table 4.9. According to table 4.9, it is more difficult to build up space charge within the wetted epoxy materials since they are more conductive. In general, the threshold fields for space charge accumulation within wetted materials were higher than that within dry materials.

Chapter 5

Interfaces and Nanodielectrics

In nanodielectrics, the interface, which is established between two dissimilar but uniform macroscopic phases, is itself invariably a system in which at least one dimension is in the nanometric range [1]. It is logical to consider that such interfaces also play important roles in determining the general characteristics of the polymeric composite. In this chapter, the influence of interfaces between inorganic nanofillers and the polymer matrix on the dielectric and mechanical properties of nanocomposites is discussed.

Once the polymeric matrix is filled with inorganic particles, a new phase is established. This interface phase has different properties to both the matrix and the particle [2]. This phase has different dielectric, mechanical, thermal and chemical properties, and tends to affect the properties of composite. Smaller nanoparticles have relatively thicker interface region leading to a greater influence of the interface phase. In nanocomposites, the role played by the surface is very crucial. For example, in nanocrystals considered as 2nm diameter spheres, 50% of the atoms are located on the surface [2]. The high reactivity of nanoparticle surfaces leads to a high level of surface physical and chemical defects. In addition, the local (atomic and molecular) and long-range (Coulombic) forces [3] between nanoparticles are responsible for a strong agglomeration, thus inhibiting the dispersion of nanoparticles in polymer matrix. To overcome this, it is possible to control of the surface chemistry either during the particle synthesis process or by surface chemical modification afterwards [4]. Figure 5.1 shows the volume fraction of interface region as a function of the diameter of nanoparticle (assumed to be spherical) for 10 vol% filling. However, it must be noted the result from this figure 5.1 is under these assumptions, e.g., no overlapping of interface zones, no agglomeration of nanoparticles, all nanoparticles same size, etc. Otherwise, the volume fraction of interface region will be greatly overestimated or underestimated.

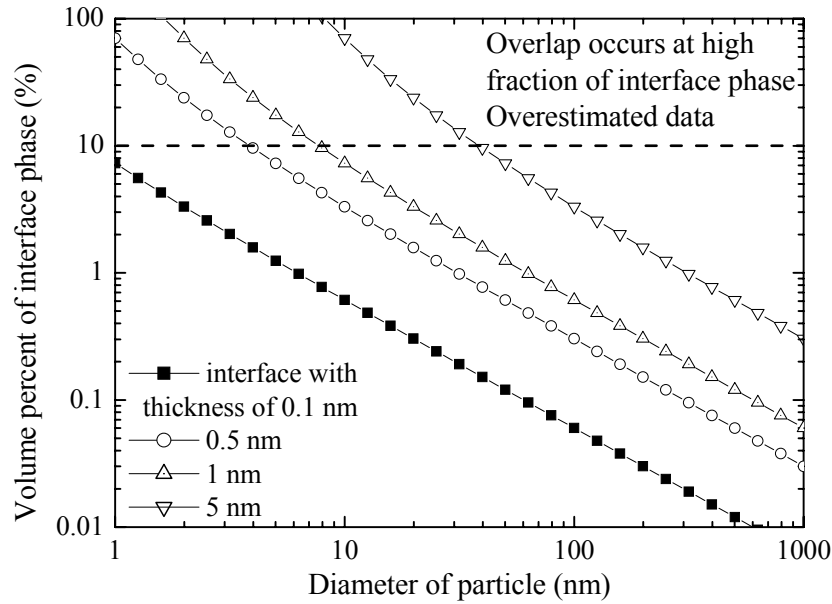


Figure 5.1. The volume percent of interface phase in composites (10 v/v% filled)

According to figure 5.1, if nanocomposites are filled with 10 vol% nanoparticles with diameter of ~45 nm, the volume fraction of interface regime will reach to 10% even if its thickness is only 5 nm. In this case, it is clear that the interface phase will play a key role in determining the properties of nanocomposites.

5.1 Interfaces and space charge behaviour of polyethylene

According to the results of §4.5.1, the untreated nanocomposite exhibits similar space charge behaviours for the polyethylene matrix and the microcomposite. There is no profound enhancement on the dielectric behaviour by incorporating microfillers. However, once the surface-treated nanoparticles are used, the threshold field for space charge accumulation is enhanced considerably (table 4.7). This suggests that no space charge can be formed within surface treated nanocomposites unless a higher field is applied. The higher threshold field for space charge accumulation might be caused by the modified surface condition of nanofillers and the new functional groups/defects around surface chemical treated nanosilica. It is believed that these defects can help the dispersion of internal charge within composites. FTIR results from reference [5] in figure 5.2 show that the particles are chemically bonded to the polymer in the vinylsilane-treated nanocomposite unlike the untreated nanocomposite, where no such bonding exists.

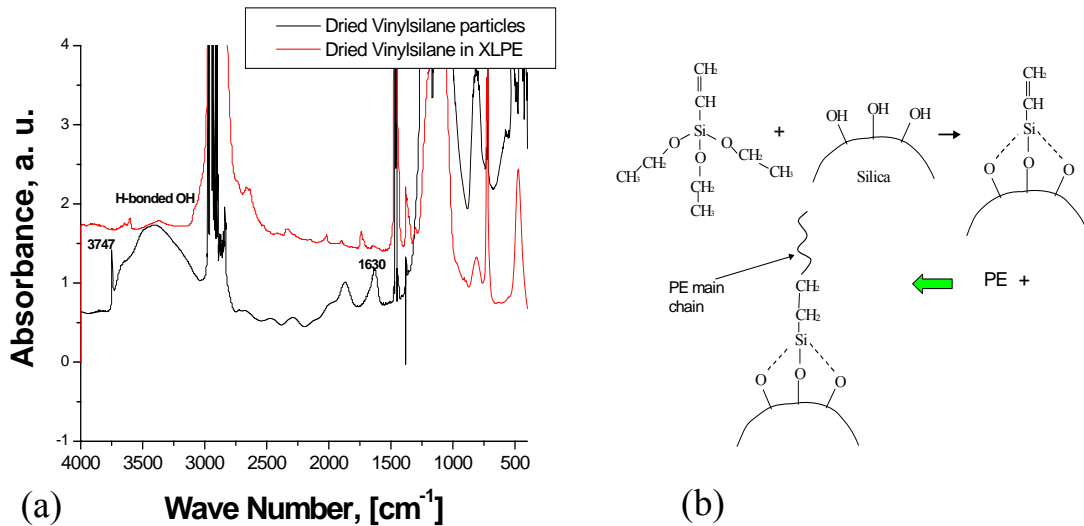


Figure 5.2. IR measurement (a) and schematic diagram of the possible chemical reaction on interface chemistry (b) of XLPE filled with vinylsilane nanoparticles (drawn by Keith Nelson, from [5])

Figure 5.2 (a) shows FTIR spectra of vinylsilane-treated particles and vinylsilane-treated nanofillers in XLPE indicating that the surface treatment resulted in covalent bonding between the nanoparticles and the XLPE [5]. There are two significant differences between these spectra: once the particles are added to the XLPE, (1) many of the features of the particles (such as free silanol groups at 3747 cm^{-1} and a broad peak centred around 3500 cm^{-1}) are missing, and (2) some new features are added. A peak at $1580 - 1680 \text{ cm}^{-1}$ representing carbon-carbon double bond ($-\text{C}=\text{C}-$) which was present in the vinylsilane-treated particles (from the vinyl group) is replaced by the peak at $2860 - 2970 \text{ cm}^{-1}$ representing the single bond of carbon ($-\text{CH}_2-\text{CH}_2-$) [6]. This leads one to conclude that vinyltriethoxysilane is chemically bonded to the silica particle on one end, and to the polyethylene on the other [5]. A schematic of the possible chemical reaction of the silica particle with vinylsilane treatment with the XLPE is shown in figure 5.2 (b) [5].

In the case of microcomposites, the silanol groups can undergo hydrogen bonding as shown to create an interfacial dipole since the bigger diameter of the microparticles make the space for two neighbouring hydrogen bonds [5]. This structure of microparticles causes the weak bonding between inorganic fillers and polymeric matrix. This has a detrimental influence on the mechanical and dielectric properties of

composites [5]. The radius of curvature implied by a nanoparticle does not readily permit this and results in the structure on the right in figure 5.3 [5]. Hence, it is possible for surface treated nanocomposites to have a stronger bonding between nanofillers and XLPE matrix than microcomposites [5].

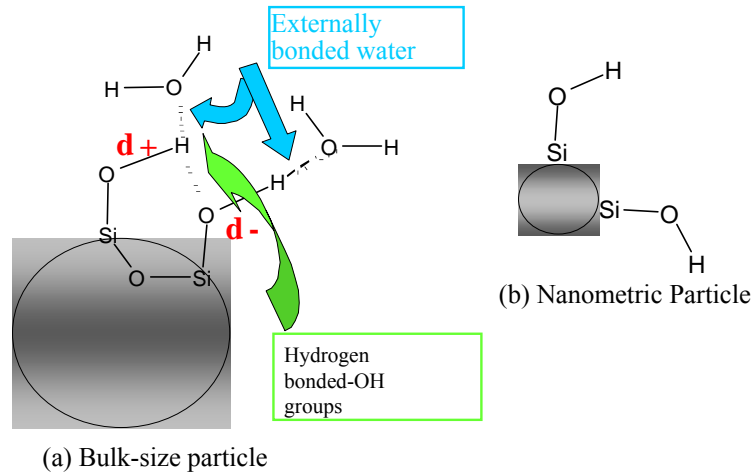


Figure 5.3. Suggested interface chemistry between micro- and nanosilica
(drawn by Keith Nelson, from [5])

A strong bonding between inorganic filler and polymer matrix is necessary to produce the good mechanical and electrical properties. The denser structure, modified surface condition and polarity of those cross-linked polyethylene specimens filled with surface chemical treated nanosilica are helpful to retard the accumulation of space charge so that a higher threshold field required inducing space charge within surface functionalised XLPE nanocomposites [5].

5.2 Interfaces and water sorption in epoxy nanocomposites

Normally, water is regarded to be ubiquitous in the degradation processes of many composites filled with inorganic fillers. Water may plasticize and cause structural relaxation in the composites, swell the composites, and therefore degrade the mechanical and electrical properties of the composite [7]. Water can also precipitate the chemical reactions in the composite as well as forming cracks and nanovoids, which are not desirable. In most situations, eventual degradation of the interfaces between the polymer matrix and inorganic filler is the primary reason for failure of

composite [7]. After water absorption, a continuous or discontinuous water region might be formed in the composites and reduce their mechanical strength. Also the directional water transport (e.g. through cracks) from the surface of composites, through the bulk of polymer, to the interfaces between matrix and inorganic filler by diffusion could provide a potential driving force under a concentration gradient [7]. Osmotic force, temperature differences, and chemisorption or physisorption at the interfaces might enhance the accumulation of water at the interfaces [7].

Sensitivity of epoxy composites to humidity is a serious matter of concern. Sorption of water may cause irreversible damage to the material. Also, there is a great body of evidence supporting the accumulation of water at the interfaces/surfaces in composites [7]. The accumulation of water at the interfaces is strongly dependant on the amount of absorbed water and relative humidity in the environment. Funke and Haagen noticed that coatings can absorb more water than non-bonded films due to significant water accumulation at the interfaces [8]. Nguyen *et al.* and Linnossier *et al.* observed accumulated water at the interfaces of coatings bonded to SiO₂-Si substrates utilizing Fourier transform infrared multiple internal reflection (FTIR-MIR) [9, 10]. Bowden and Throssell found that on aluminium, iron, and SiO₂ surfaces, these layers can be up to 20 molecular layers thick (or 5 – 6nm) at ambient temperatures and humidity [11]. Takahashi, using “ac impedance spectroscopy” (essentially dielectric spectroscopy), found that at a relative humidity of 80% the interfacial capacitance increased abruptly, suggesting the formation of water clusters in the bulk and at the interfacial region [12, 13]. Using neutron reflectivity, Wu *et al.*, measured the concentration of D₂O at a polyimide-silicon wafer interfaces and found that the deuterated water concentration at the interfaces was 17% (by volume) compared to 2 – 3% in the bulk polyimide adhesive [14].

The results of hydration and swelling in wetted epoxy nanocomposites in §4.1.1 and §4.1.3 reveal the water shells exist surrounding nanoparticles. In a normal humid environment (30 – 75% RH), the thickness of such water shell in n₃ and n₉ is 1 – 3 nm, or 5 – 10 water molecules. This is in agreement with the findings of Nguyen and Brown [9, 11, 15, 16].

There are two paths for water transport in composites, one is water diffusion into the bulk of the polymer matrix, and the other is water migration to the interfaces through

pinholes, pores, defects, and local inhomogeneities in the adhesive [9]. Inhomogeneities or non-bonded areas may exist at the interfaces and speed up the transport of water and serve as sites for the accumulation of water [7]. When water reaches the interfaces between polymer matrix and inorganic filler, the bonds between the matrix and fillers are disrupted suddenly by secondary molecular interactions of water (van der Waals and hydrogen bonding) [9]. The bonding between the matrix and fillers becomes poor in the presence of water, and this situation can be exacerbated by high temperature. This will cause structural relaxation, mechanical and electrical problems in composites.

To avoid that, two obvious solutions are suggested. The one is, surely to strengthen the bonding between the matrix and fillers and establish a better interfacial adhesion between the blend matrix and the particles by choosing appropriate inorganic fillers carefully. This may result in a higher density composite, less free volume around the particles, so that less water can be stored in composites. However, sometimes an appropriate filler is difficult to find or uneconomical. The other solution is inhibiting water from reaching the interfaces between the matrix and fillers in adequate quantity. Normally, the commercial silica filler is slightly hydrophilic and tends to adsorb with water. When silica nanoparticles are incorporated into epoxy resin, the situation becomes even worse. According to the results in §4.1.1, the epoxy part in epoxy nanocomposites can absorb more water than epoxy matrix does. This suggests that the commercial silica nanoparticles enhance the water sorption in the composite. However, if the surface of nanosilica is changed to a hydrophobic state, the particles are likely to push water out of the epoxy material. If this works in this desirable way, the water sorption behaviour of nanocomposites should be considerably improved.

To test the effectiveness of the second solution, a surface functionalised nanosilica is chosen as the replacement of the common silica nanofiller. This nanosilica is produced by Degussa AG, Germany, and the production code is “AEROXIDE® LE 3” with the average diameter of ~15nm, which was calculated from the specific area published in the manufacturer’s data sheet. The key specification of these goods is its hydrophobic surface, which is obtained by unspecified chemical treatments. 3 wt% of surface modified nanosilica were incorporated into the same epoxy material, as described in §3.1.2, and referred as “bn3”.

In the processing of “bn3”, it is more difficult to mix hydrophobic nanoparticles into epoxy resin evenly. It is believed that the different chemical surface behaviour between epoxy material (hydrophilic) and nanoparticles (hydrophobic) causes the incompatibility between them. Lots of voids and cracks can be observed even by eyesight in the specimens.

The hydration in the hydrophobic epoxy nanocomposites at 100% RH (water-saturated)/ room temperature ($\sim 293\text{K}$) after 15 days is $\sim 1.5\%$, much lower than that of n3, which is $\sim 3.3\%$. This is despite the fact that the diameter of the hydrophobic nanoparticles is much less than that of the unfunctionalised particles (15nm as opposed to 50nm). Without the functionalisation they would therefore cause the composite to absorb considerably more – approximately five times – the amount of water. The hydration in bn3 is even less than that in epoxy matrix, which is $\sim 2.68\%$, because of the less fraction of epoxy matrix. This confirms the hydrophobic surface of nanofillers does work in reducing the water sorption in epoxy materials.

In figure 5.4, the relative permittivity of water-saturated n3 and bn3 at 343K are shown. Comparing the low frequency behaviours, QDC polarisation is observed in water saturated n3 at 343K, whereas only true conduction can be observed in bn3 under the same conditions. At the higher temperature of 353K, down to frequencies of 10^{-3} Hz, no QDC is observed in the dielectric spectroscopy of “bn3” at relative humidity (100%), figure 5.5. It is possible that, at lower frequencies, QDC may be observed. The possible explanation is that the low hydration in “bn3” cannot provide a thick enough “water shell” to realize the overlap and percolation. This point will be discussed more extensively in Chapter 6.

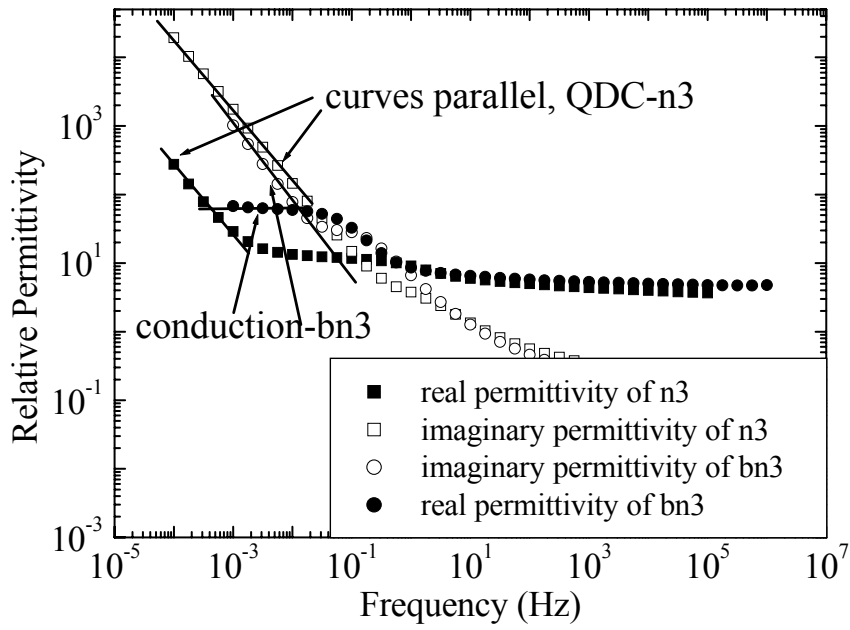


Figure 5.4. The relative permittivity of water saturated n3 and bn3 at 343 K

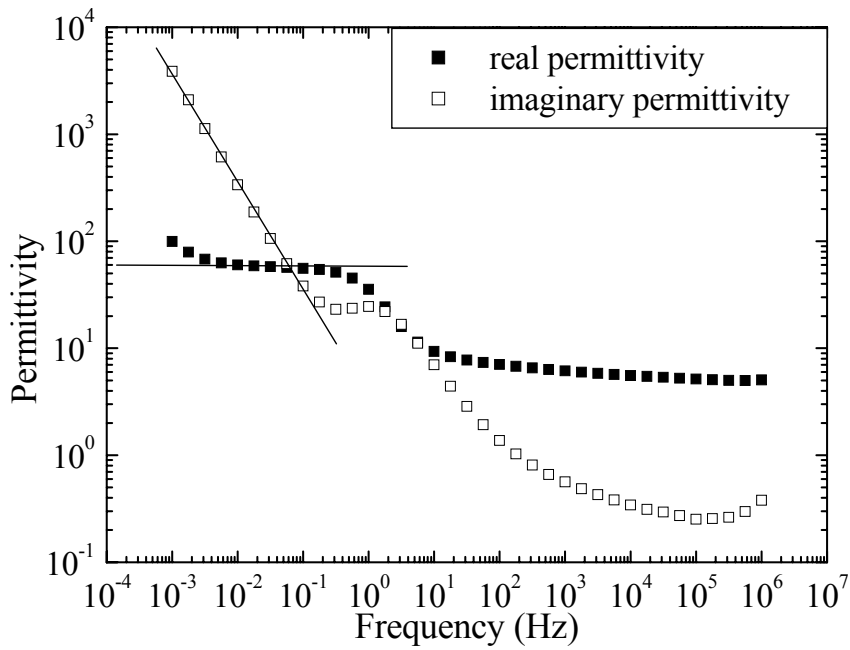


Figure 5.5. Dielectric spectrum of bn3 at 100% RH and 353K

The activation energies at low frequencies of “bn3” and other epoxy nanocomposites are shown in table 5.1.

Table 5.1. The activation energies at low frequencies of epoxy nanocomposites

| RH (%) \ Ea (eV) | bn3 | n3 | n9 |
|-----------------------|------|------|------|
| 0 (Dried) | 0.82 | 2.34 | 1.01 |
| 100 (Water saturated) | 0.57 | 0.94 | 0.58 |

Since the incompatibility between surface-hydrophobic nanosilica and hydrophilic epoxy matrix, the free volume increases with increasing concentration of hydrophobic particles, especially at the interfaces between surface-hydrophobic nanoparticles and epoxy matrix. The activation energy reflects this variation.

Chapter 6

Water Shell Model and Percolation Phenomenon

In this chapter, the mechanisms of the different dielectric behaviours of epoxy nanocomposites with hydration are discussed. The aspects include: the location and forms of water within nanocomposites, the origin of the quasi-DC dielectric behaviour, and the different dielectric behaviours of nanofiller and microfiller.

6.1 The water shell surrounding the nanoparticles

In §4.1, the water existing in the matrix was defined as “free/liquid water”. The results of hydration measurements showed the nanocomposites studied can absorb up to 60% water more than epoxy matrix.

In §4.2, the glass transition temperatures (T_g) of all epoxy specimens, measured by both DSC and dielectric spectroscopy, show a nearly proportional reduction with the amount of water in the resin (~20K reduction from dry to fully water-saturated specimens), figure 4.3. This shows that for all epoxy specimens the amount of water in the resin is almost independent of the concentration of particles or filler size. However, it was observed that there was up to 60% water extra in the nanofilled specimens. It is not possible for the extra water to have been located in the bulk resin of nanocomposites, otherwise their T_g would be reduced by an additional ~12K for the water saturated case. The most obvious implication is that the extra water is located around the nanoparticles, i.e. in the interface zones.

Further evidence for the water surrounding the nanoparticles was provided in §4.4.3, activation energy measurements showed that the water was bound.

The results of swelling in composites after water sorption have shown that the epoxy matrix can hold about 2.68 wt% of water. However, the mass concentration of water in epoxy nanocomposites is greater than the water sorption of the epoxy part in nanocomposites. One reasonable explanation is that the extra water exists around nanoparticles or at the interface region to form the water layers surrounding nanoparticles. This situation is described in figure 6.1.

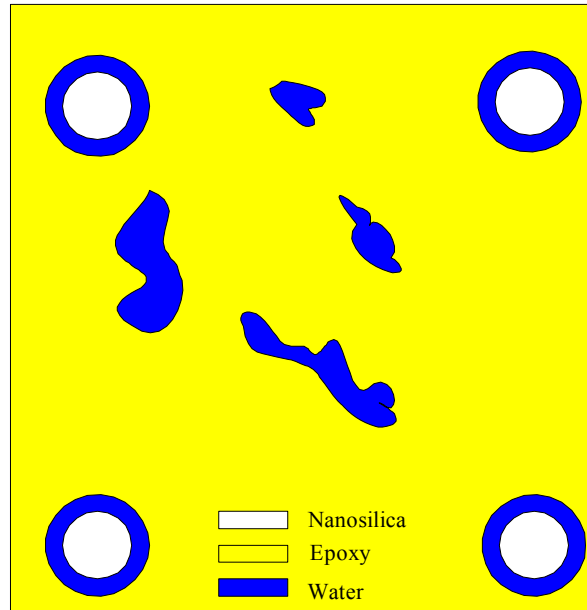


Figure 6.1. Schematic diagram of water in epoxy nanocomposites

Under this assumption, some water will surround such nanoparticles as assumed above; the rest of the water exists in the epoxy matrix in the form of “free” or “liquid” water. In any case, the link between silica and epoxy is more likely to be broken by water and the adhesion of the epoxy to the silica also becomes weakened so that the mechanical behaviour of epoxy material deteriorates.

Since the density of silica is nearly double with that of epoxy matrix, its volume percent is ~1.5 % or roughly 1/64th of the volume. In other words, the distance between one nanoparticle and its neighbour particle is about seven times bigger than the average size of particles in a perfect dispersion. If the size of nanoparticles is same, e.g., 50 nm, the distance between one particle and its neighbours will be 300 – 350 nm. For a given humidity, assuming that pure epoxy absorbs $x\%$ of water and nano-filled epoxy absorbs $y\%$ of water, the extra water absorbed by the nano-filled

epoxy is therefore $(y-x)$ %. Hence, the thickness of each water shell can be calculated in this way.

For example, for the water saturated condition of n3, in the case (100%RH), $x\%=2.68$ %, $y\%=3.33$ %.

Supposed the density of pure epoxy is 1.2×10^3 kg/m³, the density of silica is 2.65×10^3 kg/m³, and 3wt% is roughly 1.5% by volume.

The average diameter of nano-SiO₂ is 50 nm ($r=25$ nm).

The volume of a single particle (V_p) = 6.54×10^{-23} m³.

Hence, 1m³ of nanocomposite has 0.015 m³ nanoparticles inside.

The nanocomposite weighs 1.1675×10^3 kg, and contains $0.015 / (6.54 \times 10^{-23}) = 2.29 \times 10^{20}$ nanoparticles.

After swelling caused by water, 1 m³ n3 should be swollen to $(0.015 + 0.985 \times 1.0275) = 1.027$ m³, where 2.75% is the swelling percent of water saturated epoxy matrix.

However, the measured volume of 1 m³ n3 after water saturated is 1.040 m³ (the volume swelling in water saturated n3 is 3.97%, figure 4.3). The extra volume is the volume of such water surrounding nanoparticles.

If all the extra water is divided evenly on the surface of every particle, then the thickness of water layer in n3, $d = 5.6$ nm. By the same calculation, the thickness of water layer in n9 is 5.0 nm. These are very close and assumed to be the same within experimental error.

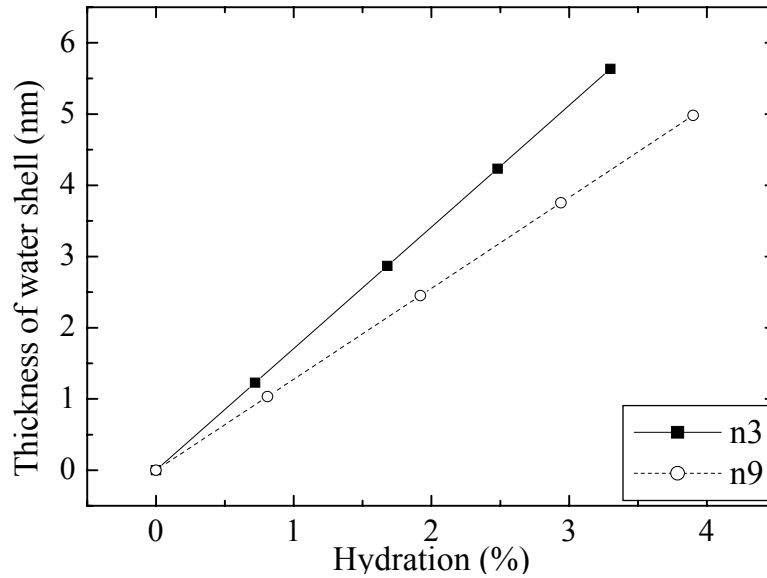


Figure 6.2. Calculations of the thickness of a water shell around spherical nanoparticles in n3 and n9

The thickness of a water shell around each nanoparticle in n3 and n9 at various hydrations is shown in figure 6.2. It is noted that the characteristic thickness of water surrounding a nanoparticle is directly proportional to the hydration.

Even the distance between each particle in a perfect dispersed system seems too far, i.e., ~300nm in n3 or ~200nm in n9. The distance between most particles in nanocomposites is much shorter than that because of the randomly positioned particles and, in an imperfect composite, because of agglomeration. Also, the actual area of influence of one nanoparticle should include its interfacial region, which has a radius of over 100nm (Debye effect), according to reference [1]. Moreover, water around nanoparticles has a greater mobility and greatly expands its influence region once water is activated at high temperature. Hence the influence region of nanoparticles (nanoparticle, its interfacial zone and water shell) is likely to overlap at high temperature and high hydration, so that to form the channels for the charges carriers in composites to flow. Under the consideration of the “isolated island” of nanoparticles, the conduction mechanism in such system is more likely to be Quasi-DC or LFD rather than a real conducting system. This point will be discussed extensively in § 6.2.

6.2 Water shell model

The above calculation shows the thickness of water shell surrounding nano-particles is 5.3 ± 0.3 nm at saturated condition. However, at low relative humidity (not water saturated), the thickness of water layer is only 1 – 3 nm in n³ by calculating the weight difference of dried and wetted specimens, figure 6.2. Since the size of single water molecule is 0.278 nm [2], the thickness of water layer is about 5 – 10 water molecules. This deduction is confirmed by Fourier transform infrared-multiple internal reflection (FTIR-MIR) spectra by Nguyen [3]. Bowden and Throssell also found that on aluminium, iron, and SiO₂ surfaces, these layers can be up to 20 molecular layers thick at ambient temperatures and humidity [4]. To describe the real situation describing how water exists in epoxy nanocomposites, a “water shell” model is proposed. The multiple shells model, originally proposed by Lewis [5] and developed by Tanaka [1], a nanoparticle plays a role of “core”. To cover the “core”, the water in nanocomposites can be divided into three layers. The first layer of water (5 – 10 water molecules) may be firmly bound to the nanoparticle. Beyond that, water may be loosely bound by van der Waals Forces as the second layer with a thickness of ~25nm. The concentration of water in this second layer may be sufficient to allow this to be conductive. The rest of the water will be “free” and exists in the bulk of the matrix with a thickness of ~50nm. The first and second water layers are likely to provide a channel for charges and carriers. Figure 6.3 is an attempt to illustrate this. The nanoparticle is shown in grey in the centre surrounded by the first layer of water (shown in black). Water also surrounds this first layer in high concentration as interconnected regions – this is the conductive layer (2) and is indicated in the figure by a white line. Outside this, the water is in a lower concentration which may not be conductive.

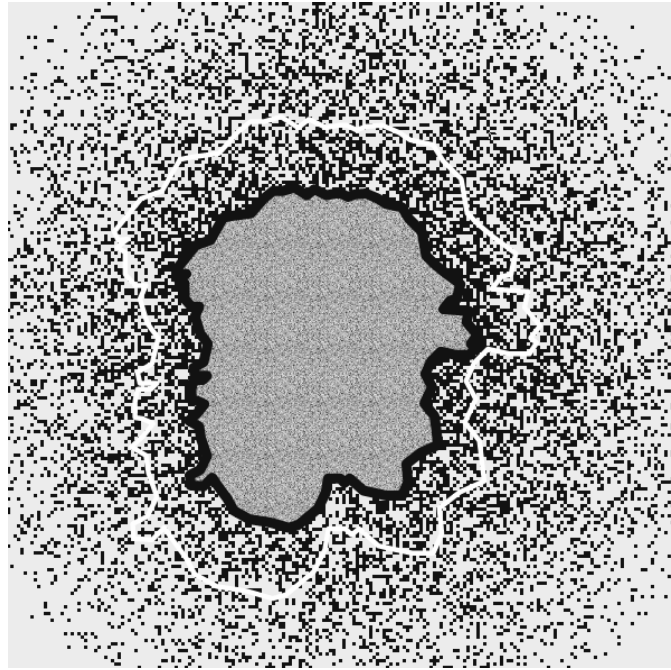


Figure 6.3. Water shell surrounds nanoparticles

Quasi-DC behaviour at low frequency is typically observed when charge carriers have some limited freedom of movement and, under the influence of the electric field, follow tortuous paths that do not allow transport right through the material. At low temperature and low hydration, water cannot provide the channels for carriers to go through the bulk of nanocomposites because of the low activity/mobility (at low temperature) or low content (at low hydration) of the water, where the carriers go through. However, at high temperature (above T_g) and high hydration, the situation is just like the prediction by the water shell model as in figure 6.4 (d). The paths for charges and carriers are formed by the overlapping water layers surrounding nanoparticles. It seems likely that the carriers are moving through partially interconnected interaction zones that surround the particles. This phenomenon has been observed by dielectric spectroscopy in §4.4.

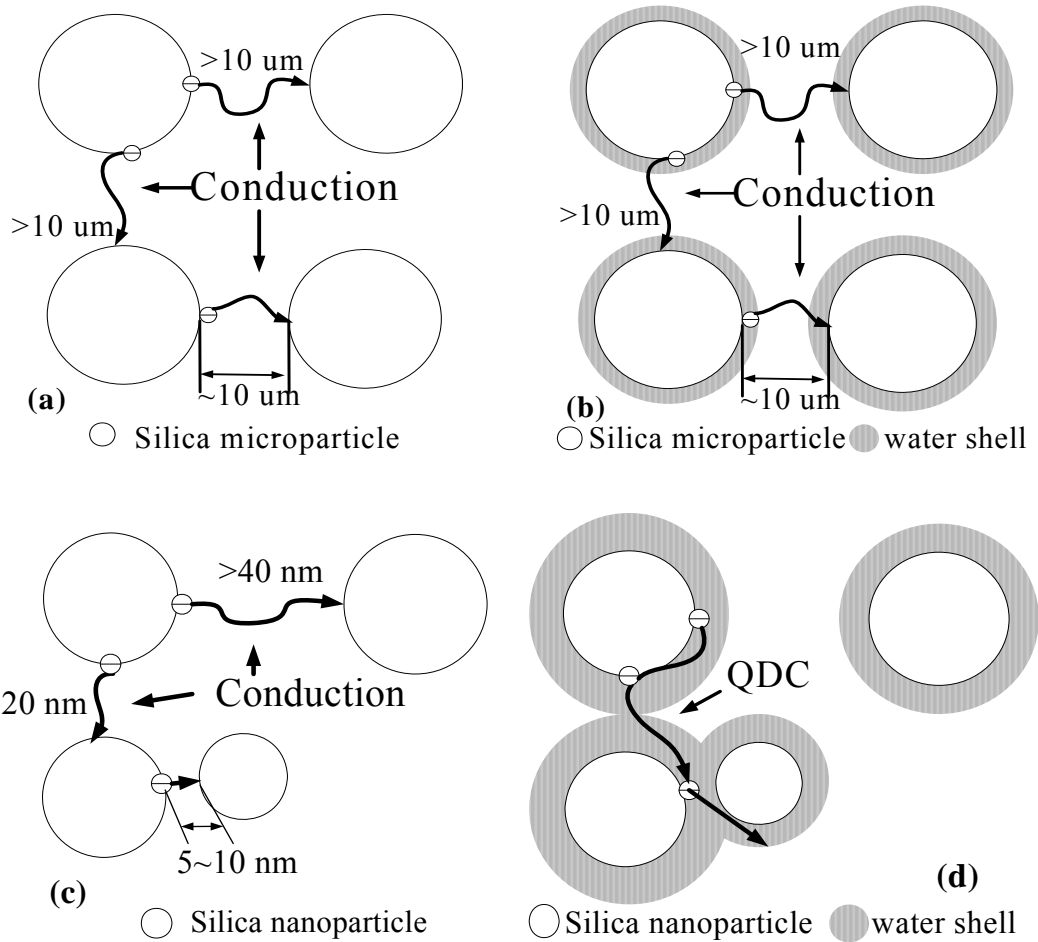


Figure 6.4. The water shell as the path for carriers in micro- (low concentration) and nano-composites

In low concentration microcomposites (for example, less than 20 vol%), figure 6.4 (a, b), the gap between two particles is too far for their interaction zones to overlap, and only conduction current can be found in microcomposites by charges carriers going through the matrix. As for nanocomposites, figure 6.4 (c, d), under the dry condition, the situation in nanocomposites is similar to that in microcomposites, however, once enough water enters the nanocomposites, the water layers surrounding nanoparticles might overlap and provide the paths for charges and carriers. This causes the QDC behaviour at low frequencies. The higher the content of nanoparticles, the shorter the distance between particles, and the lower the hydration required to make the water shells around nanoparticles overlap. According to table 4.6, indeed QDC occurs in n3 at higher relative humidity or temperature than in n9.

6.3 Percolation phenomenon in nanocomposites

In a composite in which the particles are well dispersed, unless they are arranged to be “self-repelling” the distance between the particles will be distributed according to a Poisson distribution [6]. The probability, P , that one interaction zone will overlap with one of its neighbour’s (for low concentrations) is then given by equation 6-1 for spherical particles and shown in figure 6.5, where t is the zone thickness and d the average particle separation [6]. So for a 50% probability of overlap, t/d would be 0.347 and a 50 nm particle would require an interaction zone thickness of 17.3 nm [6].

$$P = 1 - \exp \left\{ - \frac{2t}{d} \right\} \quad (6-1)$$

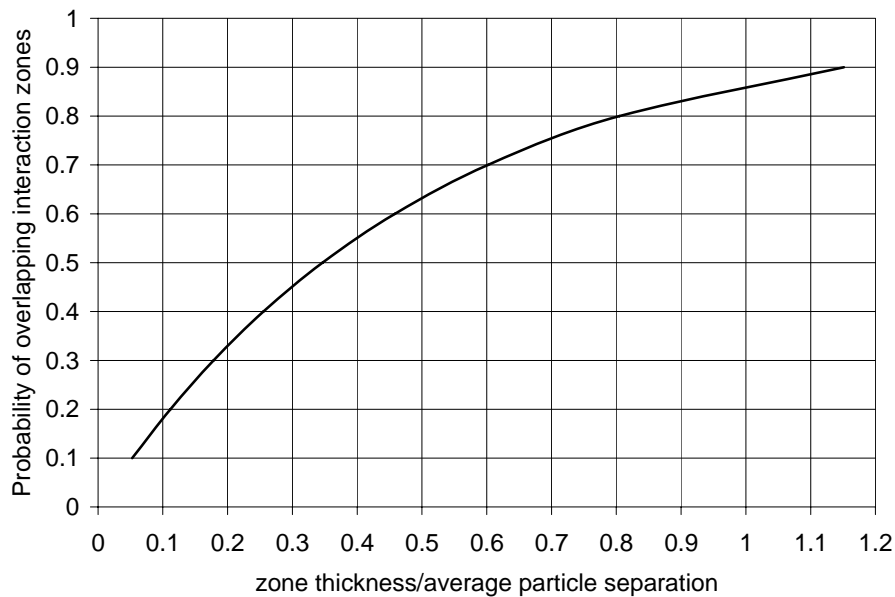


Figure 6.5. Probability of interacting particle zones (from [6])

For charge carriers to percolate through overlapping shells, the volumetric concentration of zone and spherical particle must exceed 19% [7]. Figure 6.6 shows the required ratio of shell thickness to particle radius as a function of volumetric concentration of particle for complete percolation to occur [6]. For n9, the volumetric concentration is approximate 4.5%. Thus, for these 25 nm radius particles, the thickness of layers 1 and 2 must exceed 15 nm for full percolation [6]. One would therefore expect extended charge carrier movement but at a sub-percolation level [6].

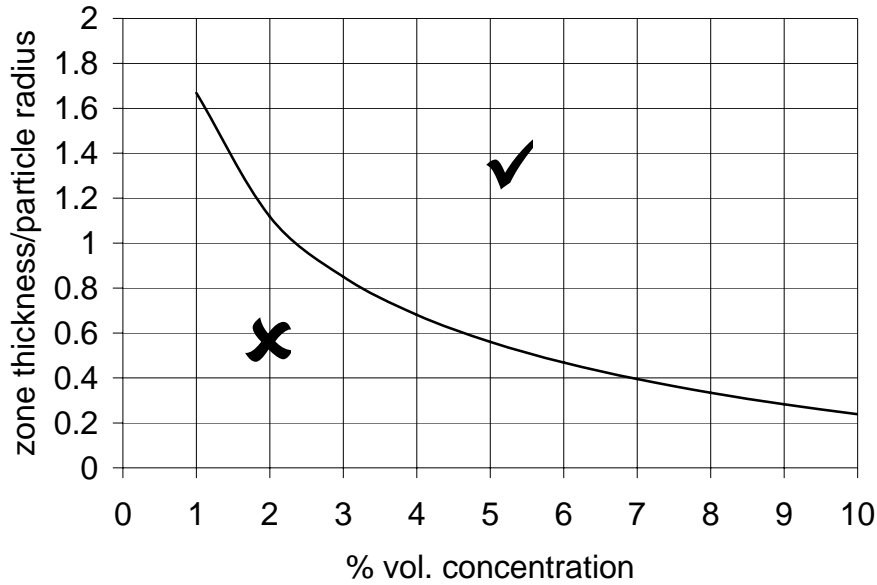


Figure 6.6. Percolation occurs on the “✓” side of the line (from [6])

At low levels of RH and at lower concentration of particles, the shells would not be expected to overlap much and conduction could be largely determined by the conduction through the epoxy matrix between the particles. This would result in a low frequency dielectric characteristic in which $C' \propto \omega^0$, $C'' \propto \omega^{-1}$. This is observed in all systems at lower RH levels, table 4.6. In figure 4.21, the higher activation energies observed at low levels of RH in the matrix are similar to that for n3, in which the volumetric concentration of particles is $\sim 1.5\%$. In n3, percolation through overlapping water shell will be less common. So drift velocity for charge transport will be determined by the carrier movement through the epoxy (where it is much difficult) rather than through percolation overlapping water shell. However, in n9, percolation is much more likely and the activation energy is therefore lower.

If both epoxy matrix and inorganic filler (with their interfacial phase) are considered as capacitive, it could be assumed as an elementary assumption they are in series to compose the system of epoxy composites, like that shown in figure 6.7.

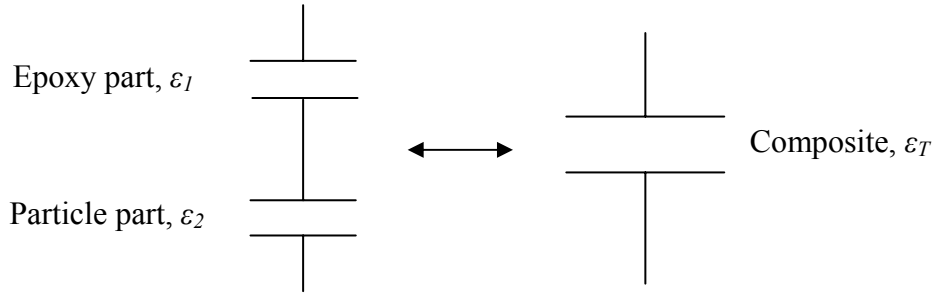


Figure 6.7. The equivalent circuit sketch of epoxy composites

According to figure 6.7, the below relation can be obtained

$$\frac{1}{\varepsilon_T' - i\varepsilon_T''} = \frac{p}{\varepsilon_1' - i\varepsilon_1''} + \frac{1-p}{\varepsilon_2' - i\varepsilon_2''} \quad (6-2)$$

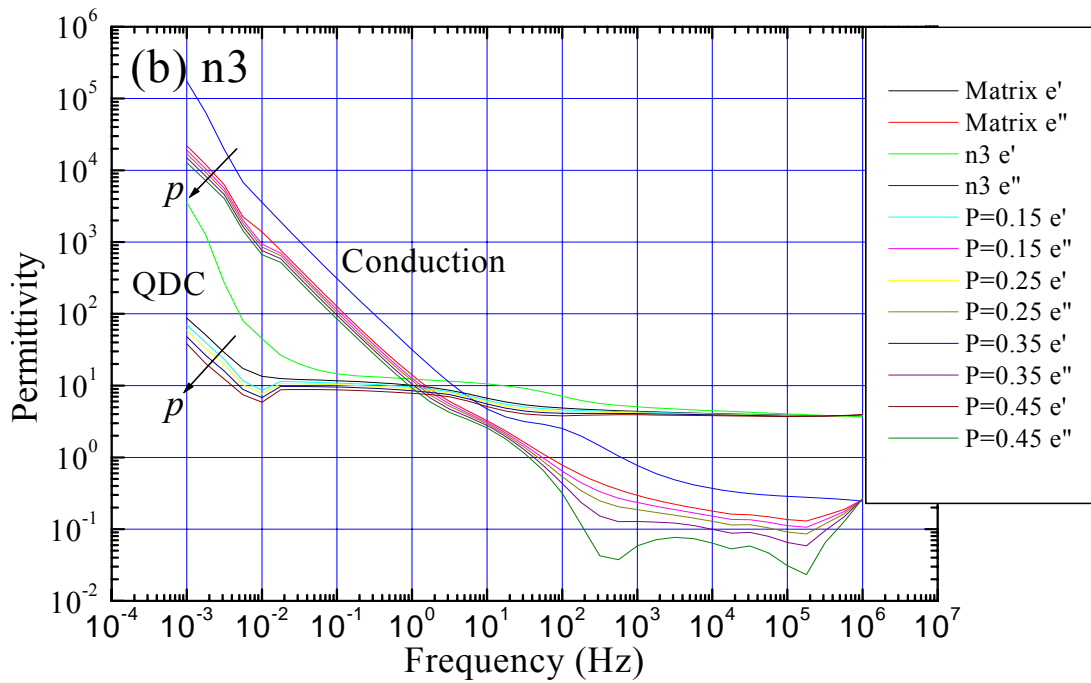
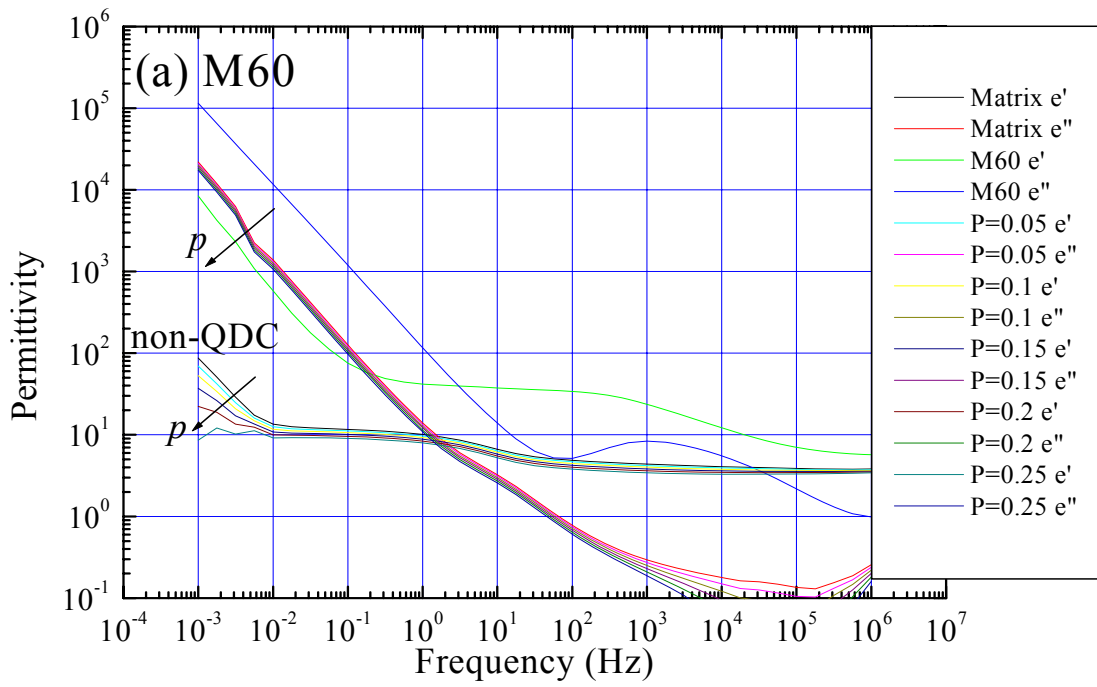
where p ($0 < p < 1$) is a ratio coefficient to describe the contribution of epoxy part. The contribution of particle part is $(1-p)$.

$$\text{Hence, } \frac{1}{\varepsilon_2' - i\varepsilon_2''} = \frac{1}{1-p} \cdot \left(\frac{1}{\varepsilon_T' - i\varepsilon_T''} - \frac{p}{\varepsilon_1' - i\varepsilon_1''} \right) \Rightarrow$$

$$\varepsilon_2' = (1-p) \cdot \frac{(\varepsilon_T' \varepsilon_1' - \varepsilon_T'' \varepsilon_1'')(\varepsilon_T' - p\varepsilon_1') + (\varepsilon_T'' \varepsilon_1' + \varepsilon_T' \varepsilon_1'')(\varepsilon_T'' - p\varepsilon_1'')}{(\varepsilon_T' - p\varepsilon_1')^2 + (\varepsilon_T'' - p\varepsilon_1'')^2} \quad (6-3)$$

$$\varepsilon_2'' = (1-p) \cdot \frac{(\varepsilon_T'' \varepsilon_1' + \varepsilon_T' \varepsilon_1'')(\varepsilon_T' - p\varepsilon_1') - (\varepsilon_T' \varepsilon_1' - \varepsilon_T'' \varepsilon_1'')(\varepsilon_T'' - p\varepsilon_1'')}{(\varepsilon_T' - p\varepsilon_1')^2 + (\varepsilon_T'' - p\varepsilon_1'')^2} \quad (6-4)$$

The dielectric behaviour of filled epoxy composites, i.e., n3, n9 and M60, at 100%RH and 353K are known, which are “ ε_T^* ”. Compared to the data of Matrix (ε_1^*) at 100% RH and 353K, the dielectric behaviour of particles in composites can be calculated by equations 6-3, 4. By adjusting the value of p , and using the raw data of epoxy matrix (ε_1' and ε_1'') and nanocomposites (ε_T' and ε_T'') at 100% RH and 353K, the dielectric behaviour of particle part in nanocomposites (the interfacial part is also included as the particle part) at 100% RH and 353 K can be calculated by equations 6-3, 4. Under the real condition, $\varepsilon_2' > 0$ and $\varepsilon_2'' > 0$, and the value of p should be chosen appropriately to maintain this requirement.



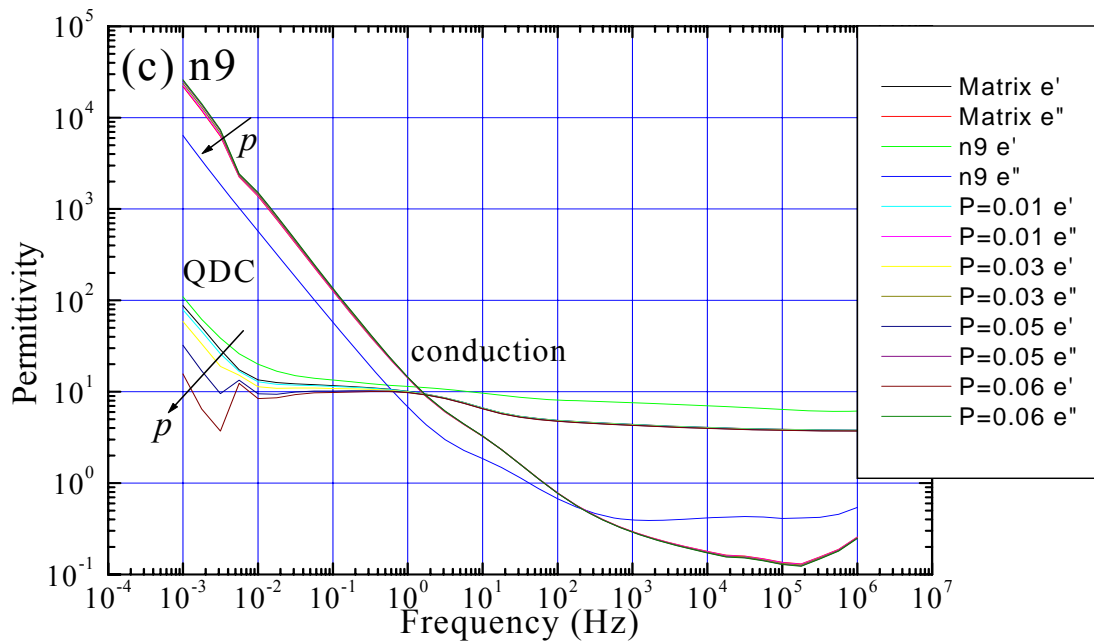


Figure 6.8. The permittivity of fillers predicted by effective media theory,
a) M60, b) n3 and c) n9

Figure 6.8 shows, for 353K and 100% RH, calculated real and imaginary permittivities for (a) the microparticle system, (b) the n3 nanoparticle system and (c) the n9 nanoparticle system, according to equation 6-3, 4. In figure 6.8 (a) it is not possible to find a QDC behaviour for any value of p , whereas in figure 6.8 (b) and (c), QDC is observed for all possible values of p .

At high temperatures, the nanoparticles surrounded with a water shell have the same behaviour with the epoxy matrix, i.e., QDC at low frequencies. However, unlike nanoparticles, no matter what values of p were used, the dielectric relaxation of microparticles and their interface phase at low frequencies could not be QDC. This hints that the QDC occurring in M60 at low frequencies (under higher relative humidity and temperature) is unlikely to be due to microparticles.

6.4 Ageing

On the basis of this work, Rowe [8] has proposed an “alternative scenario” for ageing composite materials in which the interfaces between the particles and the host material gradually weaken. In this case, the water may weaken the interfaces between the epoxy and silica. This accumulation of water modifies the mechanical strength,

the dielectric behaviours and the electrical strength of these tiny regions [8]. Since this degradation is diffuse and occurs at all interfaces at the same time, it can be thought of as ageing in the true sense [6]. Gradually a network of semi-interconnected pathways builds up through the labyrinth of filler particles. If percolation through these degraded regions occurs, Figure 6.9, then an electrical pathway forms that may lead to breakdown [8].

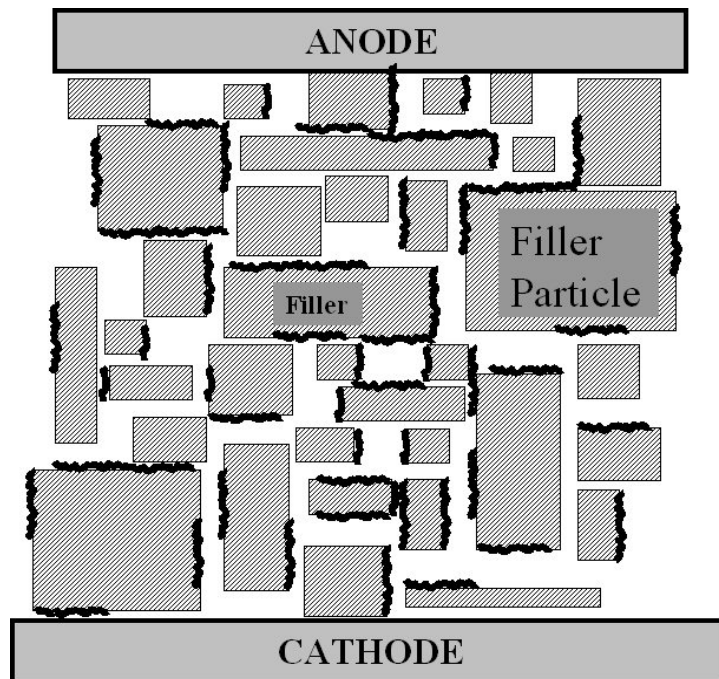


Figure 6.9. Representation of the “Alternative Ageing Scenario”, showing water degraded, filler interfaces (drawn by Rowe, from [8])

This “alternative ageing scenario” for highly filled HV insulation is fundamentally different from other explanations of ageing [8]. In particular, the ageing precursor is not dependent upon the electrical field, charge, etc. It is only after the damage has been started by the water, which is inevitably present, that electrical degradation starts to occur [8].

Chapter 7

Conclusions and Future Work

7.1 Conclusions

The work carried out during the course of this study sought to accomplish a better understanding of the dielectric properties of nanocomposites and the factors that affect them, especially the conditions at the surfaces of nanofillers. To accomplish this, commercial and surface functionalised nano-silica fillers were incorporated in XLPE and epoxy materials. It was found that the surface functionalisation of nanofillers has a profound effect on the dielectric behaviour of XLPE nanocomposites. For example, the threshold field for space charge accumulation within XLPE nanocomposites was considerably enhanced by incorporating surface chemical modified nanosilica. For epoxy nanocomposites, the replacement of surface hydrophilic nanosilica by surface hydrophobic fillers can reduce considerably the water sorption of epoxy nanocomposites. So far, interfaces have been determined as the key role in determining the dielectric properties of nanocomposites in this research.

The hydration behaviour of epoxy nanocomposites and the influence of water on the swelling, glass transition temperature, and dielectric behaviours of epoxy materials were investigated thoroughly in the course of this work. Both DSC and dielectric spectroscopy showed the glass-transition temperature of epoxy materials decreased as the hydration increased and, in all cases, corresponded to a drop of approximately 20K as the relative humidity was increased from 0% to 100%. This implied that for all the specimens, the amount of water in the resin component of the composites was almost identical. It was therefore concluded that the extra 60% of water found in the 9 wt% nanocomposites was not in the resin component of this composite; if it were, the T_g would have been reduced by an extra 12K for the same increase in humidity. For this reason, the extra water was considered to be located around the surface of the nanoparticles. This was confirmed by measuring the hydration isotherms of the specimens and the swelling and density change as water was absorbed. Further

evidence was found from the activation energy of the “mid-frequency” relaxation process in the dielectric spectra which showed, by calculating the activation energy, that the water found in the epoxy nanocomposites was bound rather than free. The thickness of water layers around nanoparticles can be calculated from hydration tests.

The diffusion of water into the specimens was shown to obey Fick's law initially. However, nanocomposites have an additional diffusion process related with the nanoparticles. The epoxy nanocomposites were also shown to have a larger water diffusion coefficient than microcomposites.

The dielectric spectroscopy measurements showed different conduction and quasi-DC behaviours at very low frequencies ($<10^{-2}$ Hz) with activation energies dependent on the hydration. These observations led to the development of a model in which a “water shell” is formed around the nano-particles. In this model, it was deduced that the QDC behaviour at low frequencies in wetted epoxy nanocomposites was due to the overlap of the water shells around nanoparticles and a percolation phenomenon. The multiple shell model, originally proposed by Lewis and developed by Tanaka, has been further developed to explain low frequency dielectric spectroscopy results in which percolation of charge carriers through overlapping water shells occurs. At 100% relative humidity, water is believed to surround the nanoparticles to a depth of approximately 5 – 10 monolayers as the first layer. A second layer of water is proposed that, although dispersed, is sufficiently concentrated to be conductive. If all the water had existed in a single layer surrounding a nanoparticle, this layer would have been approximately 5nm thick at 100% RH. The calculations, based on the Effective Media Theory, showed microfillers made no contribution to QDC behaviour of epoxy microcomposites. On the basis of this work, S. W. Rowe has proposed an “alternative scenario” from the effect of humidity on the dielectric behaviours of epoxy nanocomposites, for ageing composite materials in which the interfaces between the particles and the host material gradually weaken.

Conduction current measurements showed that the conduction mechanisms within the polymer matrix and nanocomposites were different. Space charge measurements, using the PEA technique, showed that the wetted epoxy specimens have a higher threshold field for space charge accumulation than the equivalent dry specimens, presumably because they are more conductive.

7.2 Future work

Further research may be required in, but not limited to, the following areas.

1. Measurement of mechanical properties

In the current research, the focus has been on the dielectric properties of both XLPE and epoxy nanocomposites. Although, it was concluded that the bonding between nanofillers and polymer matrix become weakened by the water accumulation at the interfaces. Moreover, the decreased glass-transition temperature with increasing humidity supported that point. It may be possible to obtain more direct evidence through testing the mechanical properties.

2. Chemical description of the surface condition of surface hydrophobic nanofillers

So far, the mechanism that causes the surface hydrophobicity in the nanosilica particles used in the epoxy resin is not clear. The functional groups on the surface of this nanosilica are unknown. To direct future work, a precise chemical description of the surface condition of nanofillers would be desirable.

3. Ageing test

In the end of this research, both “water shell model” and “alternative scenario” are proposed to explain the electrical properties of epoxy nanocomposites after water sorption. Although there is not lack of ageing testing on composites, it would be better to do some ageing measurements on the current specimens. The theory for composite ageing can be explained more convincingly by ageing measurements under various conditions, i.e., temperatures, electrical fields, and relative humidities. Interface degradation measurement

Interfaces have been determined as having a key role in determining the properties of nanocomposites. If interface degradation can be observed, it would be helpful to improve the understanding of the ageing behaviour of composites. Dr. Rowe and his colleagues have designed a series of methods to observe the interface degradation

(Private communication, March 2007). Their research will achieve a better understanding of the ageing of nanocomposites.

5. Conduction mechanisms in nanocomposites

The mechanism of conduction within nanocomposites is not clear yet. Although several models can give close descriptions of the conduction phenomenon in nanocomposites, none of them have given a precise prediction. It may be useful to have further work in this area.

6. Mathematical work on the “water shell model”

Currently, the “water shell model” is a physical model. It can explain the QDC phenomenon found in water-absorbing nanocomposites utilising percolation theory. However, more mathematical work should be done to predict the probability that percolation occurs. In systems like nanocomposites, several factors have been determined: the dispersion of nanoparticles (probably a Poisson distribution), the thickness of water shell (including the interface zone) around nanoparticles, the dielectric properties (dielectric permittivity, conductivity, etc) of the nanoparticles, the dielectric properties of the polymeric matrix, and the dielectric properties of the interfacial region.

Obviously, there would need to be a lot more experimental and theoretical work to push this research further. Work on nanodielectrics is young but progressing fast. It is expected that it will continue to have a significant impact on science and engineering.

Appendix I

LabView program for conduction current measurement

This program is based on the driver of Keithley 617 multifunction meter. Both the real and absolute values of conduction current through the specimen can be measured and recorded as the paths specified. Also the results can be shown in the two graph windows real time.

Firstly, the function of Keithley 617 meter should be chosen as “dc A” since the current is measured. Secondly, Trigger mode is “continuous” for a long time measurement. Lastly, the paths to store the real and absolute values of conduction current should be specified.

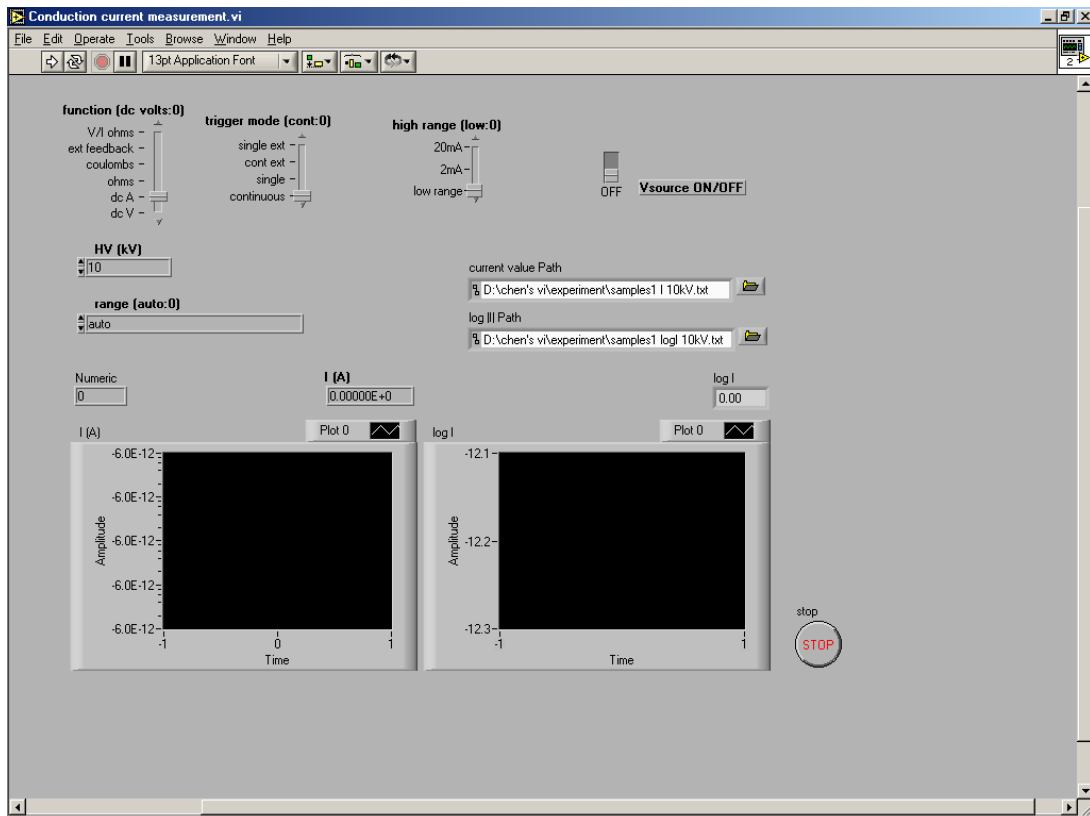


Figure AI.1. The interface of LabView program for conduction current measurement

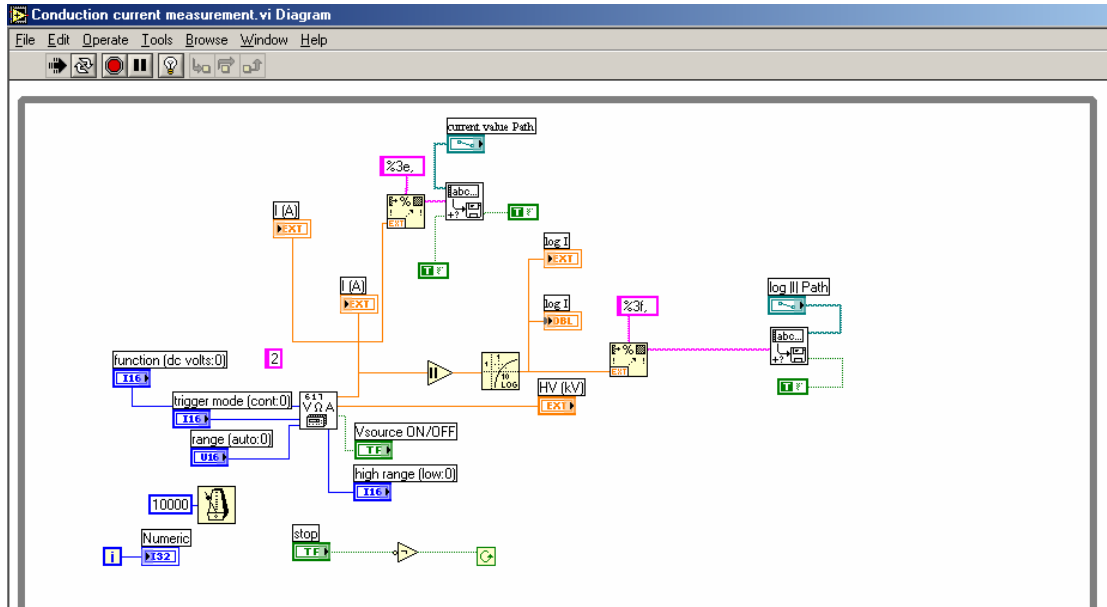


Figure AI.2. The diagram of LabView program for conduction current measurement

The “clock” can be set to adjust the sampling time. In this experiment, 10000 ms (10 s) is applied as the interval time between each sampling point. The GPIB address of Keithley 617 is chosen as the default value, i.e., 2.

In the driver program of Keithley 617, which diagram is shown in figure AI.3. The data from GPIB is continuously being collected and transferred into the specified file path to store.

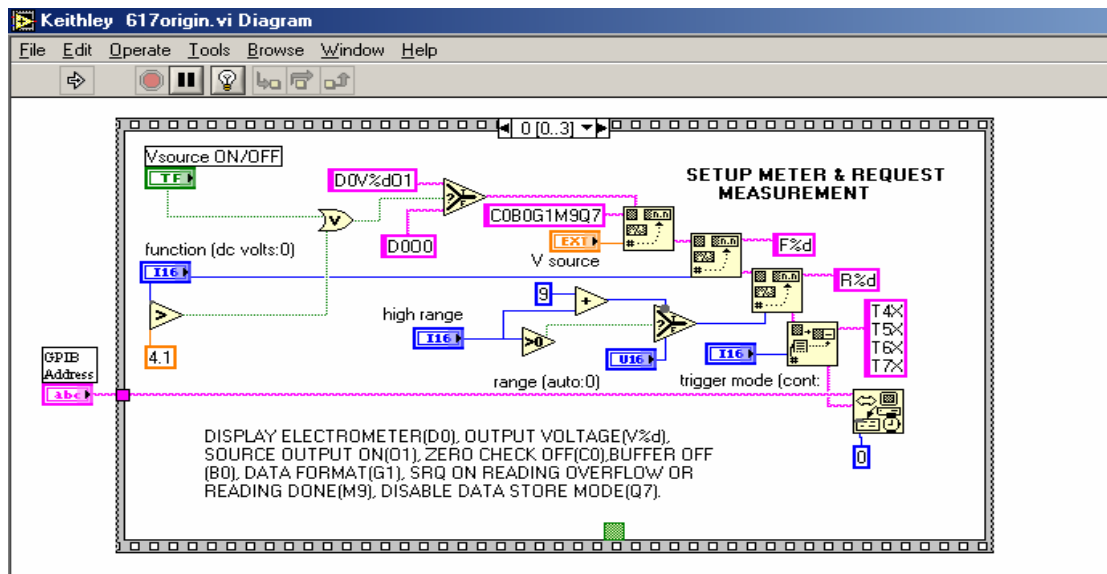


Figure AI.3. The diagram of driver program of Keithley 617

Appendix II

The deduction of the water diffusion equations

This appendix is cited from reference [1].

(I) The physical situation

The most diffusion problems can be described by the three models in figure AII.1. At small times, diffusion will occur only near the left-hand side of the membrane (a). As a result, at these small times, the diffusion will be the same as if the membrane was infinitely thick (b). At large times, the results become those in the thin film (c).

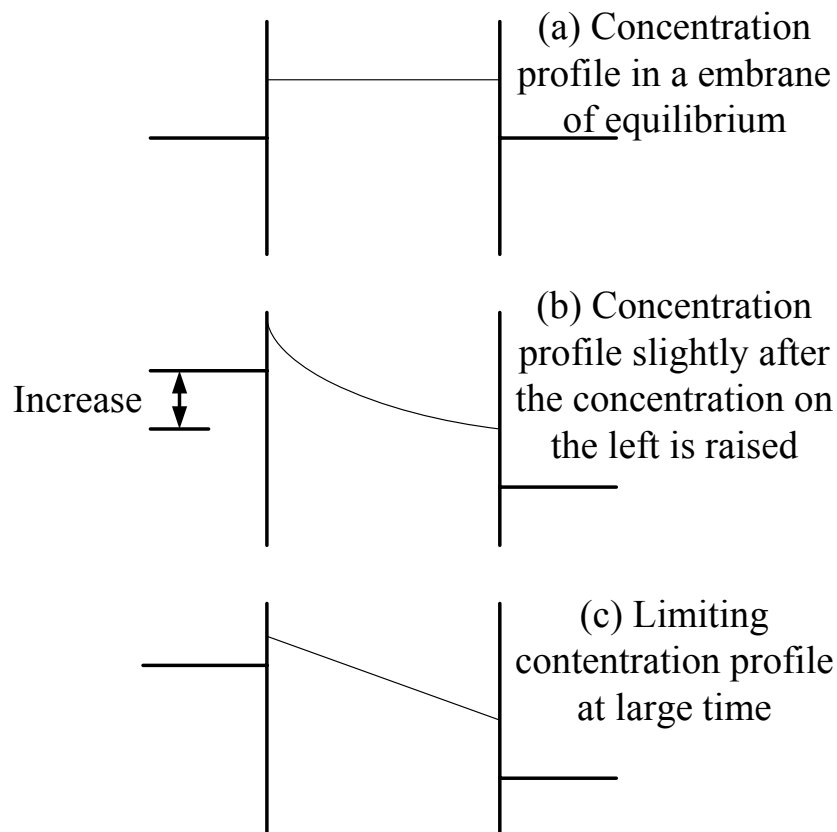


Figure AII.1. Unsteady- versus steady-state diffusion

The moisture diffusion in a polymer film/plate in a steady-humidity environment is schematically sketched in figure AII.2. In this case, the outer side of the polymer plate is suddenly increased to a higher constant value. Diffusion occurs in the region to the inside of the plate. In the current experimental setting, the diffusion occurs at the both sides of the epoxy plate. However, it can be investigated from one side.

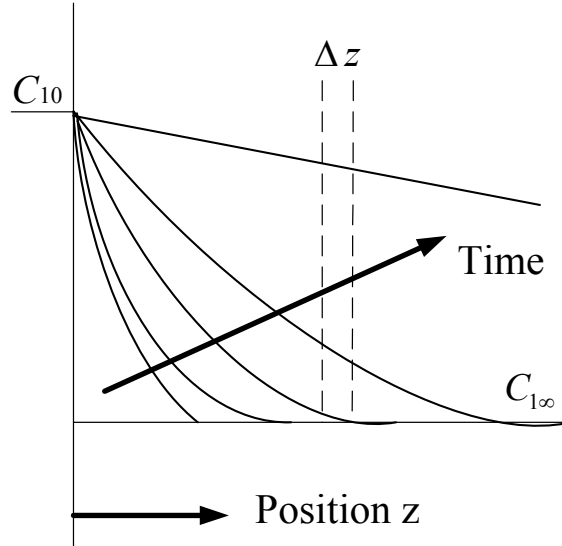


Figure AII.2 The relation between concentration and time in free diffusion

The plate initially contains a uniform concentration of water $c_{1\infty} = 0$, at time zero, the concentration at the interface is suddenly and abruptly increased. The increased produces the time-dependent concentration profile that develops as moisture penetrates into the plate. The water absorption in the epoxy plate can be expressed in this way:

(Water accumulation in volume $A\Delta z$)

= (Rate of diffusion into the layer at z)-(Rate of diffusion out of the layer at $z + \Delta z$)

In mathematical terms, this is

$$\frac{\partial}{\partial t}(A\Delta z c_1) = A(j_1|_z - j_1|_{z+\Delta z}) \quad (\text{AII-1})$$

This equation is divided by $A\Delta z$ to find

$$\frac{\partial c_1}{\partial t} = \left[\frac{j_1|_{z+\Delta z} - j_1|_z}{(z + \Delta z) - z} \right] \quad (\text{AII-2})$$

If $\Delta z = 0$, then $\frac{\partial c_1}{\partial t} = \frac{\partial j_1}{\partial z}$ can be obtained by using the definition of the derivative.

Combining this equation with Fick's law, $J_1 = Aj_1 = -AD \frac{\partial c_1}{\partial z}$, and assuming that the diffusion coefficient is independent of concentration, then

$$\frac{\partial c_1}{\partial t} = D \frac{\partial^2 c_1}{\partial z^2} \quad (\text{AII-3})$$

This equation is sometimes called as Fick's second law. It is subject to the following conditions:

$$t = 0, \text{ all } z, c_1 = c_{1\infty}$$

$$t > 0, z = 0, c_1 = c_{10};$$

$$z = \infty, c_1 = c_{1\infty}$$

It is noted that both c_{10} and $c_{1\infty}$ are constants. Since the concentration $c_{1\infty}$ is constant since it is so far from the interface as to be affected by events there; and the concentration c_{10} is kept constant by adding water at the interface.

(II) Mathematical solution

To solve the equation AII-3, a new variable is defined,

$$\zeta = \frac{z}{\sqrt{4\pi t}} \quad (\text{AII-4})$$

Hence, equation AII-3 can then be written as

$$\frac{dc_1}{d\zeta} \left(\frac{d\zeta}{dt} \right) = D \frac{d^2 c_1}{d\zeta^2} \left(\frac{\partial \zeta}{\partial z} \right)^2 \text{ or } \frac{d^2 c_1}{d\zeta^2} + 2\zeta \frac{dc_1}{d\zeta} = 0 \quad (\text{AII-5})$$

Appendix II: The deduction of the water diffusion equations

One integration of equation AII-5 gives $\frac{dc_1}{d\zeta} = ae^{-\zeta^2}$, where a is an integration constant. A second integration and use of the boundary conditions gives

$$\frac{c_1 - c_{10}}{c_{1\infty} - c_{10}} = \text{erf}\zeta \quad (\text{AII-6})$$

where $\text{erf}\zeta = \frac{2}{\sqrt{\pi}} \int_0^\zeta e^{-s^2} ds$, which is the error function of ζ . This is the desired concentration profile giving the variation of concentration with position and time.

The flux can be found by combining Fick's law with equation AII-6:

$$j_1 = -D \frac{\partial c_1}{\partial z} = \sqrt{D/\pi t} e^{-z^2/4Dt} (c_{10} - c_{1\infty}) \quad (\text{AII-7})$$

One particularly useful limit is the flux across the interface at $z = 0$:

$$j_1 |_{z=0} = \sqrt{D/\pi t} (c_{10} - c_{1\infty}) \quad (\text{AII-8})$$

This equation has been used to calculate the amount of water released into the epoxy plate with time t in §4.1.2.

One integration of equation AII-7 from $t = 0$ to t gives

$$M = \int_0^t J_1 dt = \sqrt{\frac{4Dt}{\pi}} (Bc_1) \quad (\text{AII-9})$$

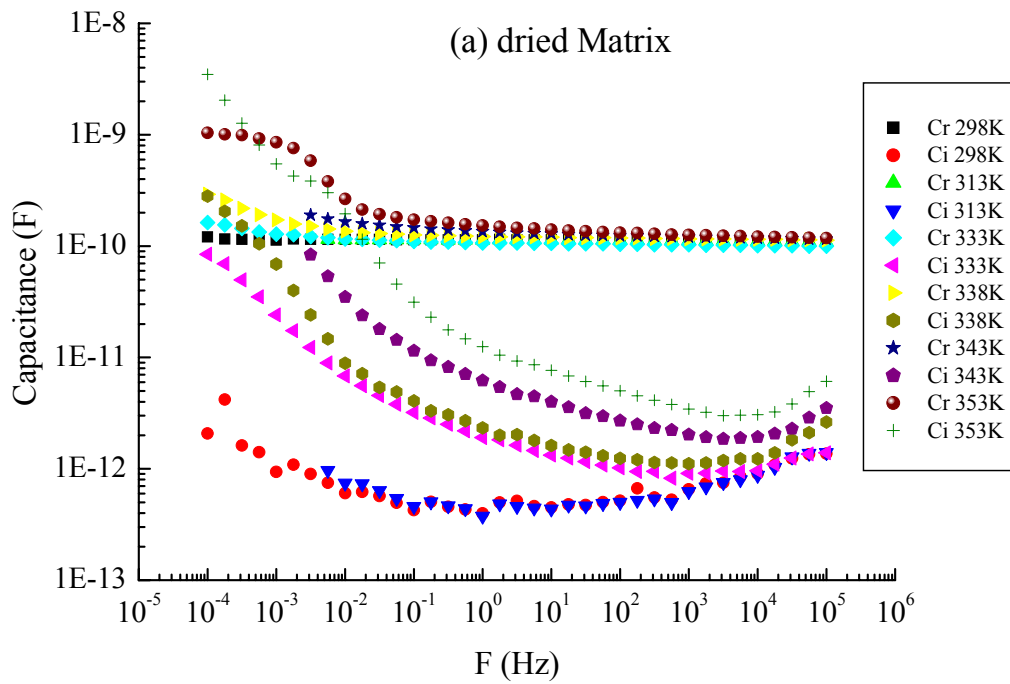
where B is a constant which comes from the integrating process.

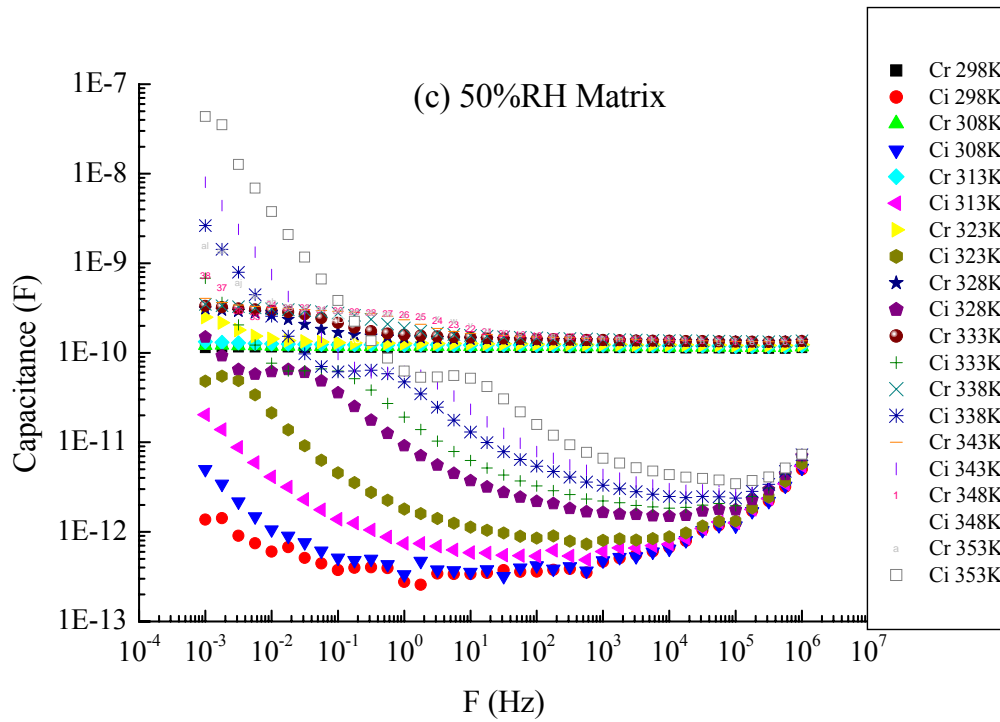
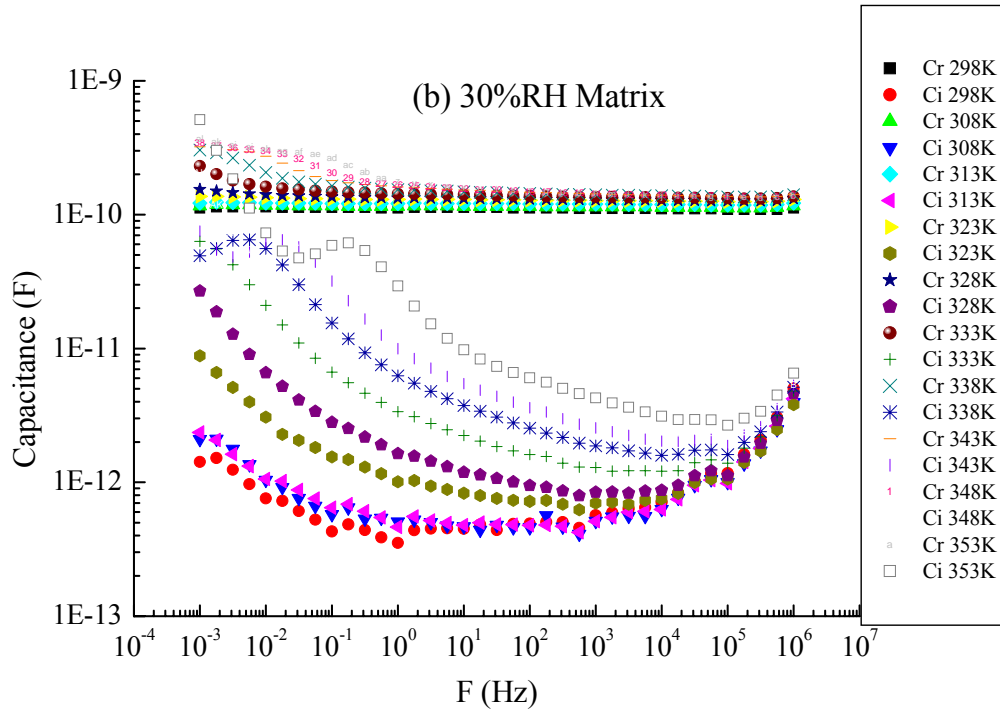
According to equation AII-8, it is noted, at small time, the water absorption in epoxy plate is direct ratio to the square root of time t .

Appendix III

The dielectric spectroscopy of epoxy materials

The dielectric spectroscopy results of epoxy materials are provided below as the reference.





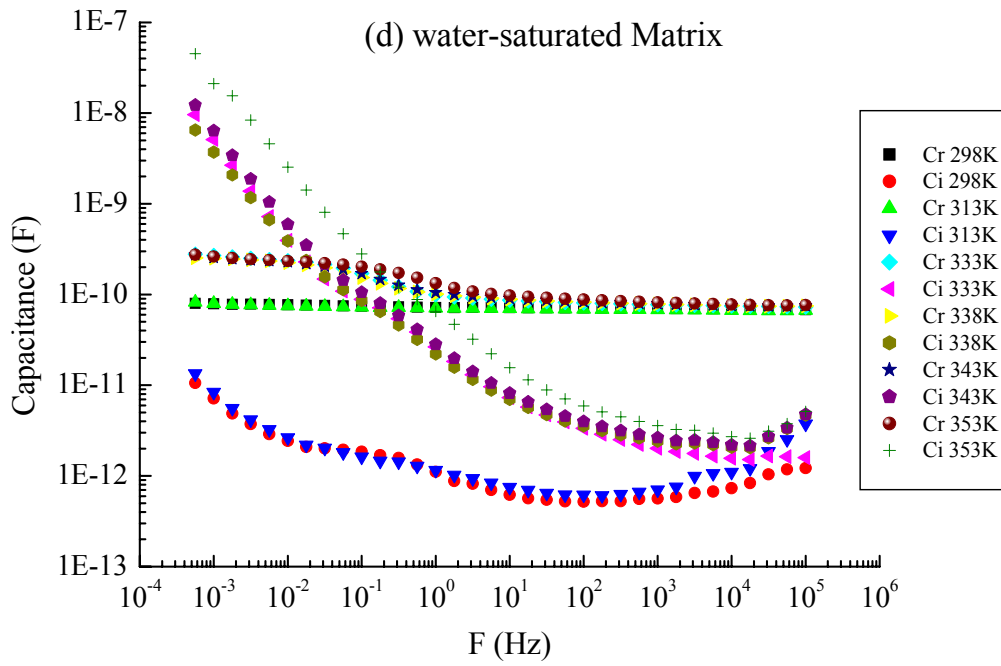
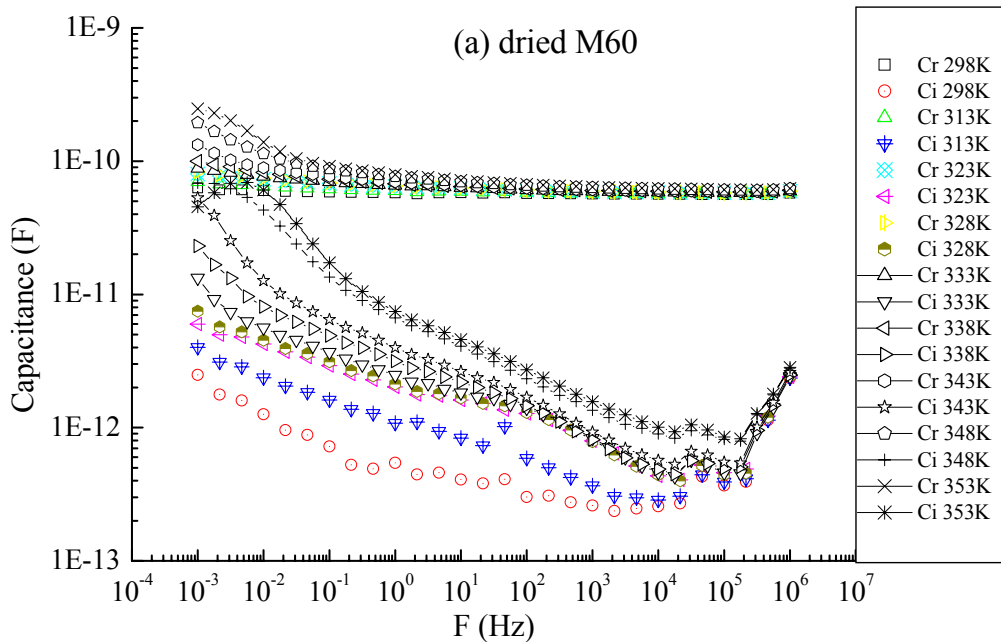
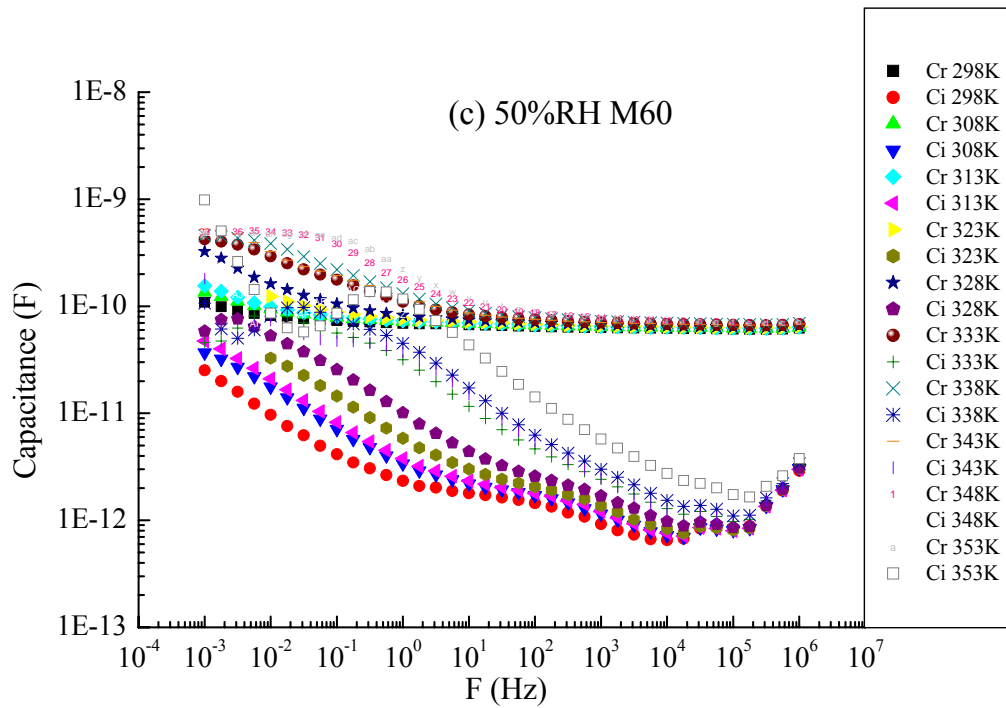
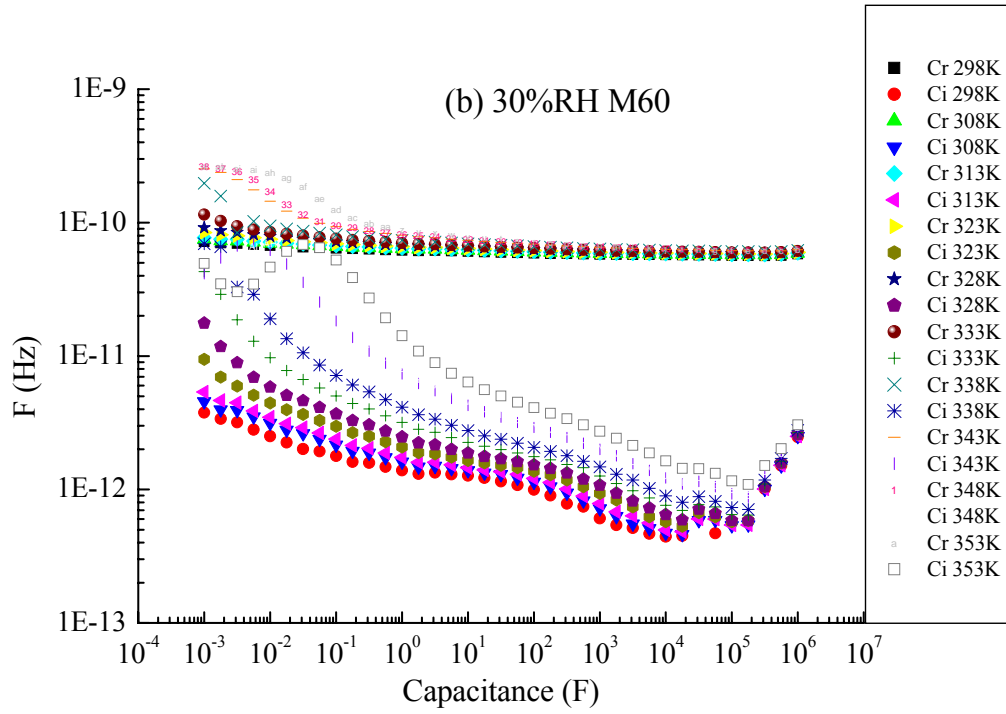


Figure AIII.1. The dielectric spectrum versus T of epoxy matrix at various relative humidities, (a) 0% RH, (b) 30% RH, (c) 50% RH and (d) 100% RH





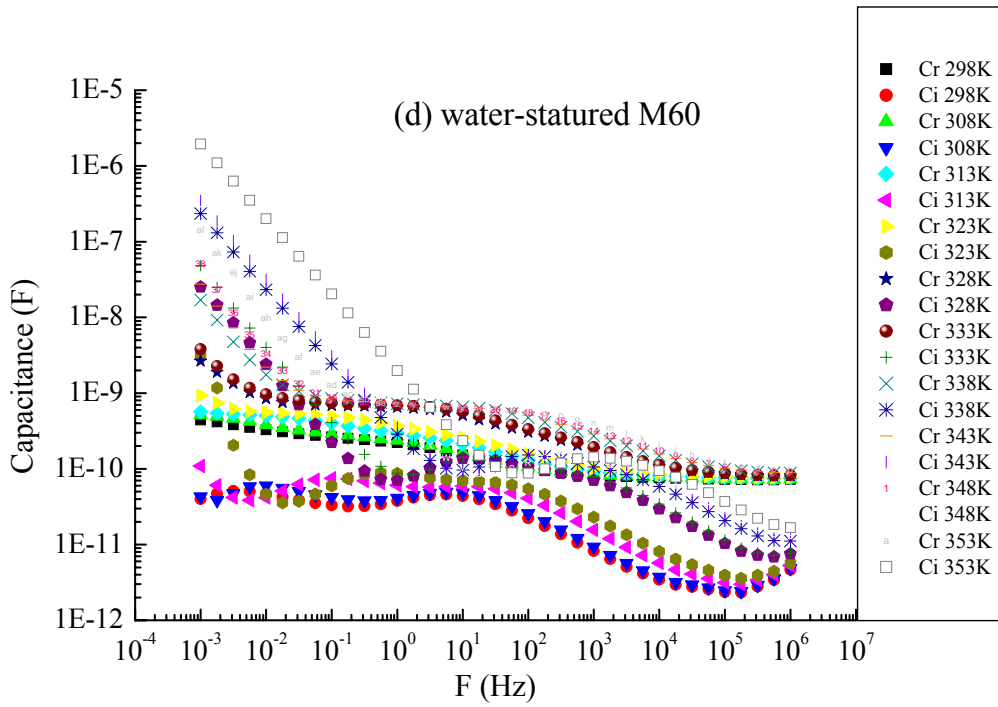
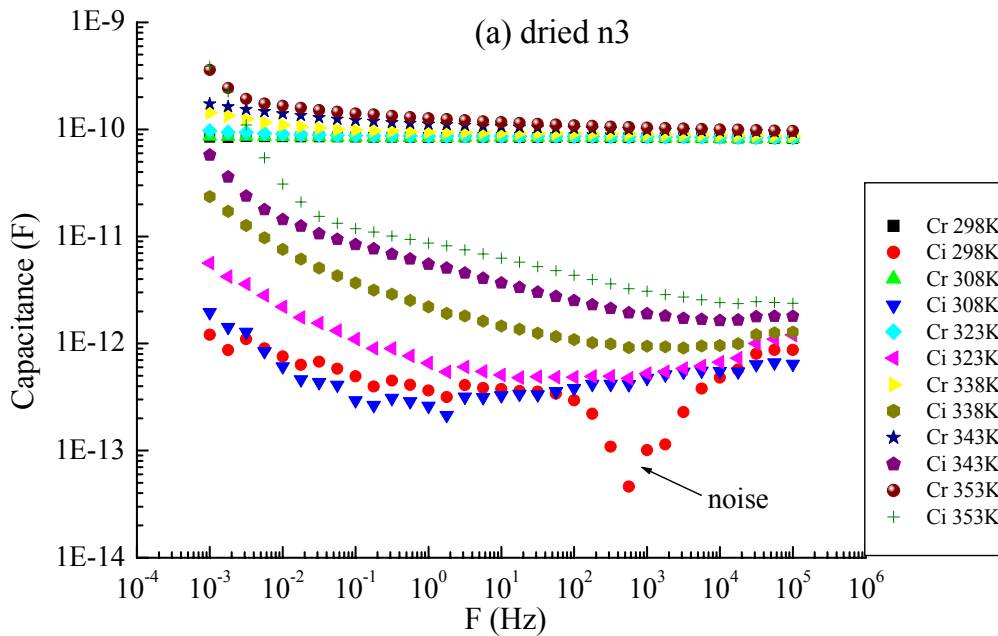
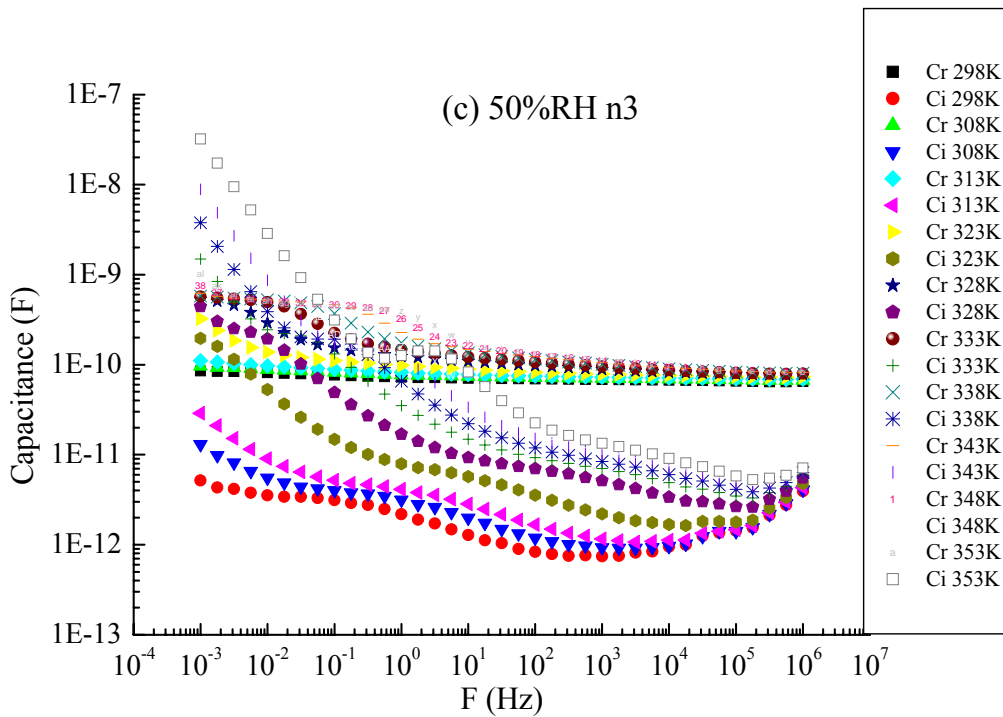
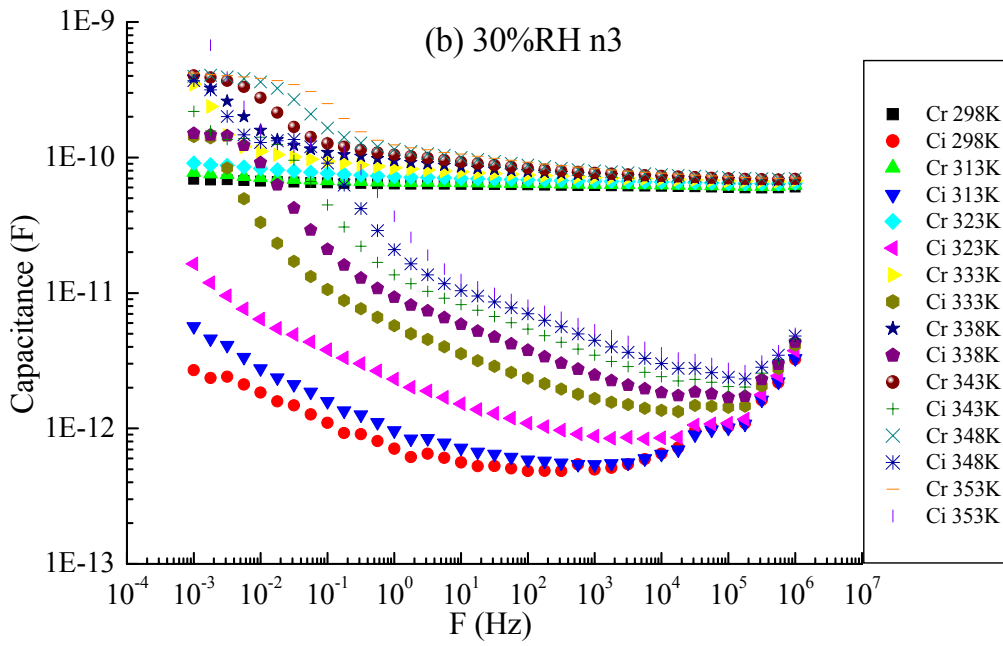


Figure AIII.2. The dielectric spectrum versus T of M60 at various relative humidities, (a) 0% RH, (b) 30% RH, (c) 50% RH and (d) 100% RH





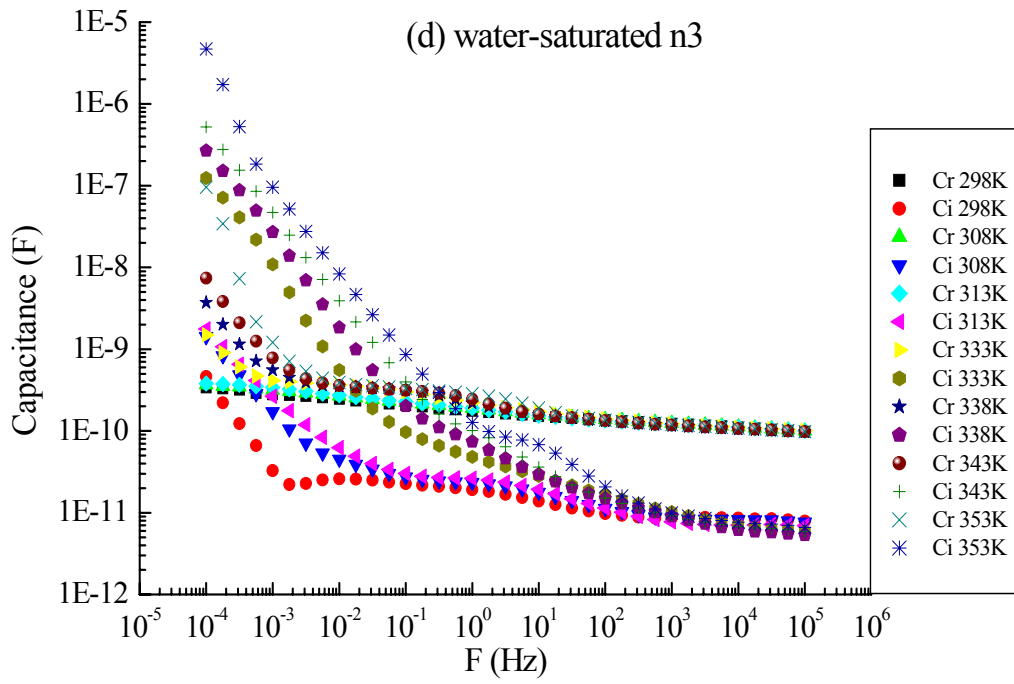
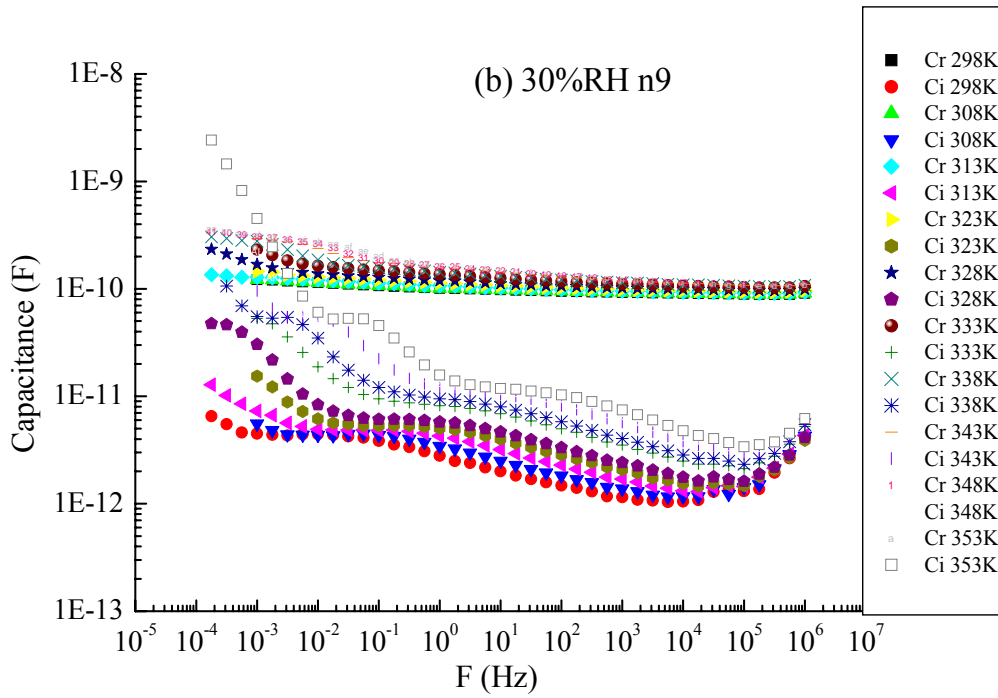
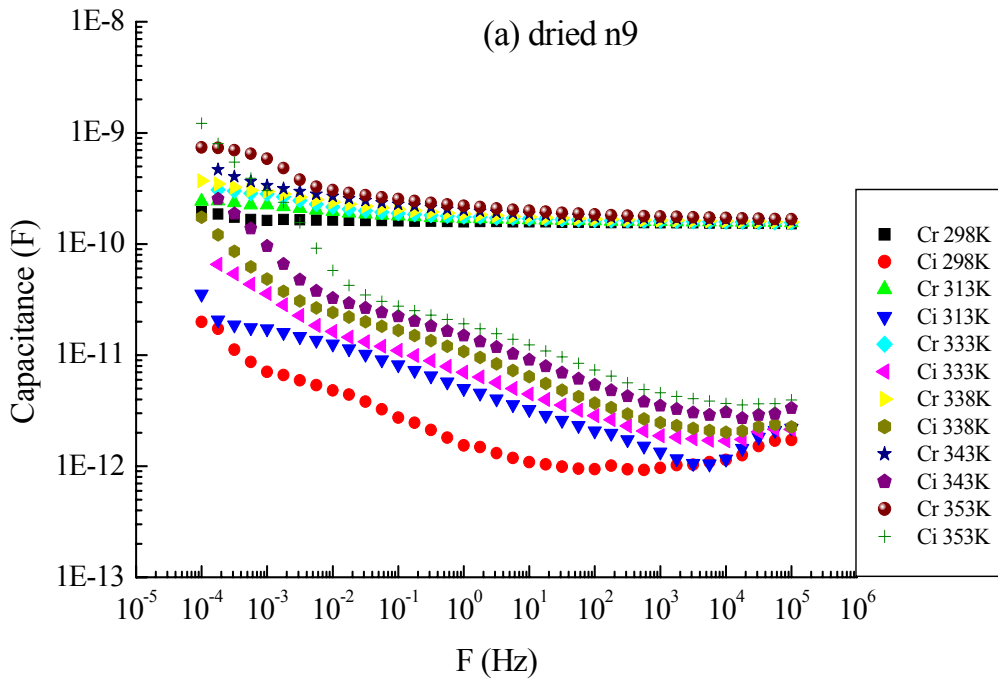


Figure AIII.3. The dielectric spectrum versus T of n3 at various relative humidities, (a) 0% RH, (b) 30% RH, (c) 50% RH and (d) 100% RH



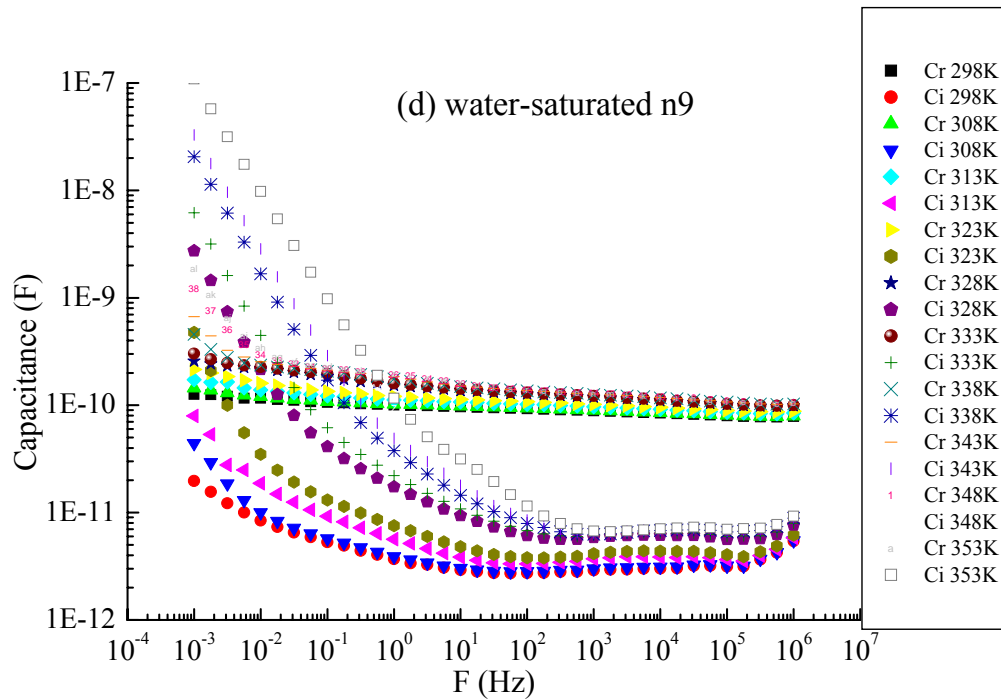
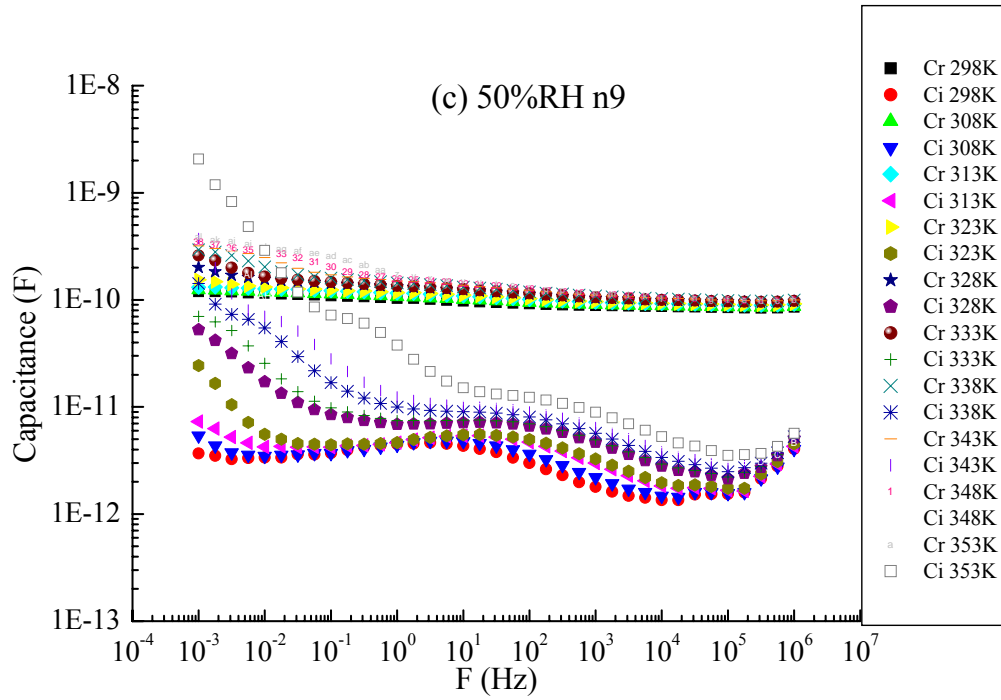


Figure AIII.4. The dielectric spectrum versus T of n9 at various relative humidities, (a) 0% RH, (b) 30% RH, (c) 50% RH and (d) 100% RH

Appendix IV

Electrode design

I. The three-electrode system for conduction current measurement

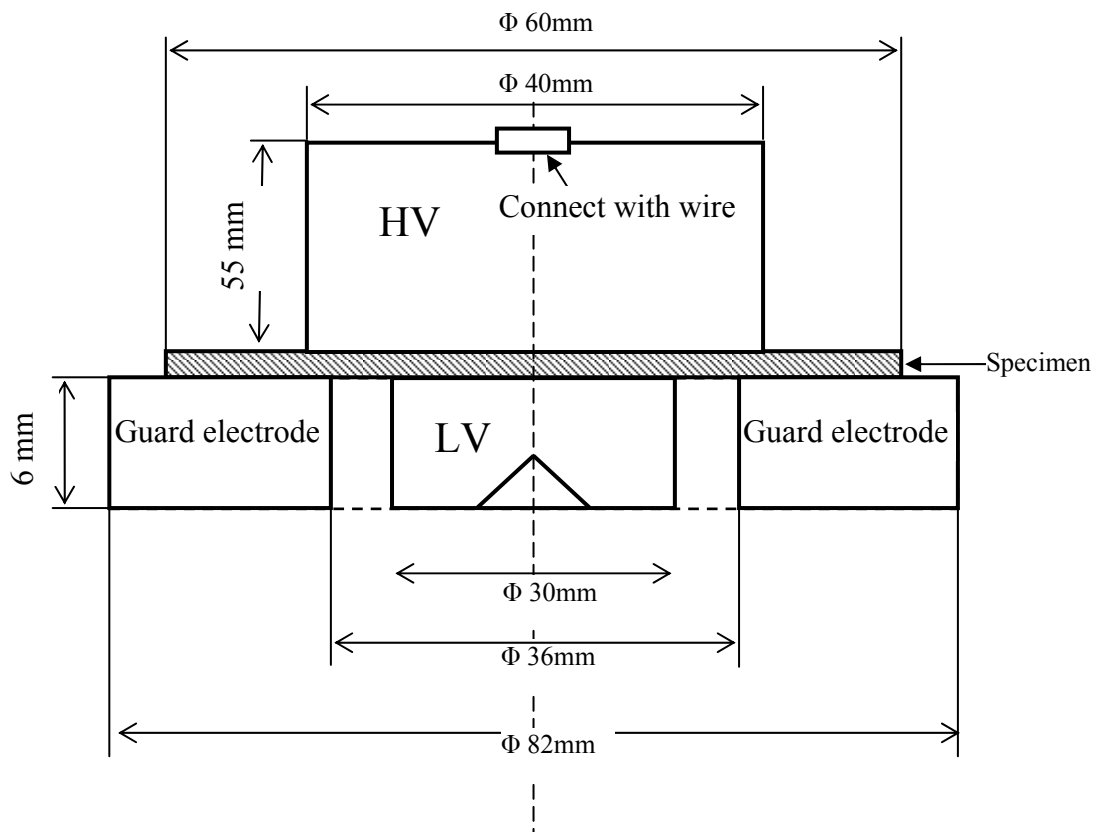


Figure AIV.1. The electrode system for conduction current measurements

The low voltage electrode is connected with a 10 M Ω protective resistor before Keithley 617 multifunction meter.

II. The electrode system for dielectric spectroscopy

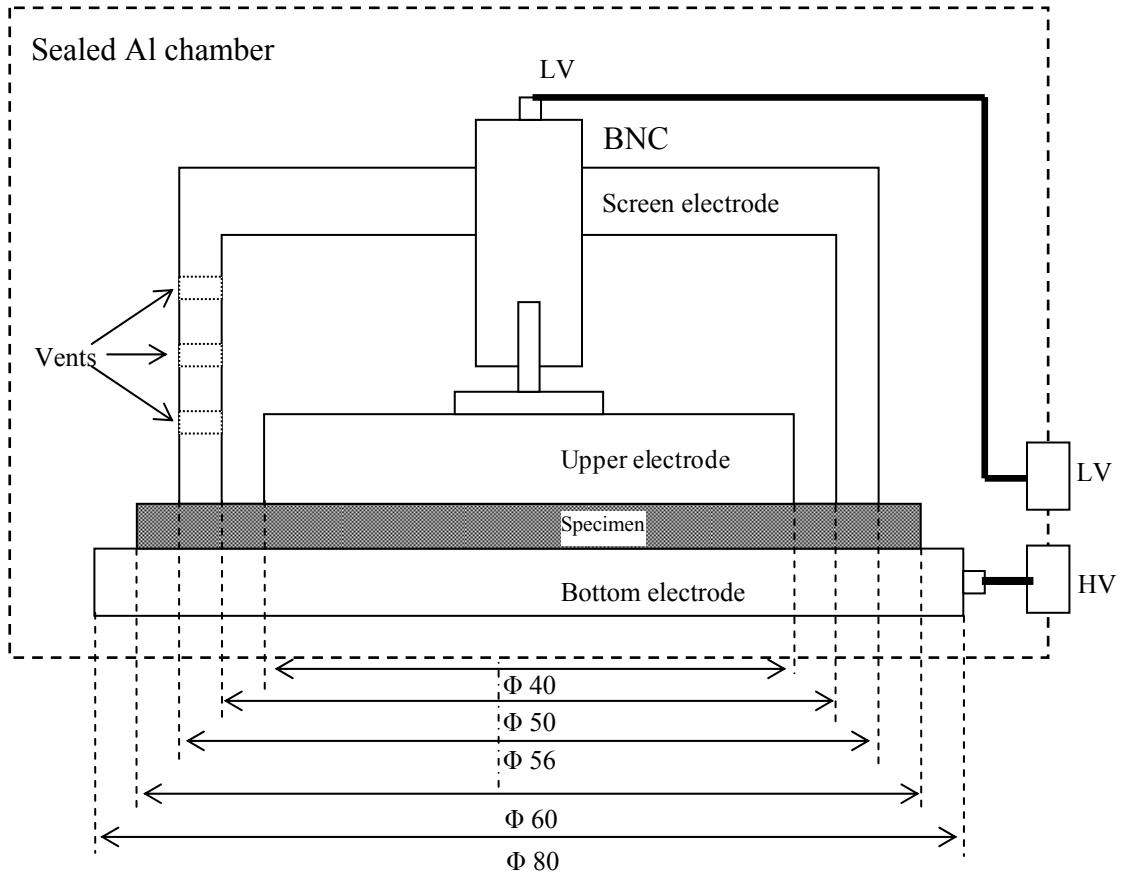


Figure AIV.2. The electrode system for dielectric spectroscopy measurements

The screen electrode has been evenly drilled 30 holes with the diameter of 1 mm for ventilation so that the relative humidity in the sealed chamber keeps same to that in the screen electrode.

Chapter 1 References

- [1] Encyclopaedia Britannica, “The Metal Ages: The chronology of the Metal Ages”.
- [2] Dissado L. A., Fothergill J. C., ‘Dielectrics and nanotechnology’, *IEEE Transactions on Dielectrics and Electrical Insulation*, Vol. 11, No. 5, pp 737–738, October 2004.
- [3] Hackam R., ‘Outdoor HV composite polymeric insulators’, *IEEE Trans. Dielectr. Electr. Insul.*, **6** 557–85, 1999.
- [4] Ma Dongling, Hugener Treese A, Siegel Richard W, Christerson Anna, Martensson Eva, Onneby Carina and Schadler Linda S, ‘Influence of nanocomposites surface modification on the electrical behaviour of polyethylene nanocomposites’, *Nanotechnology*, 16, pp 724–731, 2005.
- [5] Vaia Richard A., ‘A look inside nanotechnology’, *Amptiac*, Vol. 6, No. 1, special issue, 2001.
- [6] Frechette M. F., Trudeau M., Alamdari H. D., Boily S., ‘Introductory remarks on nanoDielectrics’, *CEIDP Annual Report*, pp. 92–99, 2001.
- [7] Ma Dongling, Siegel R. W., Hong J. I., Schadler L., Mårtensson E., Önnby C., ‘Influence of nanoparticle surfaces on the electrical breakdown strength of nanoparticle-filled low-density polyethylene’, *Journal of Material Research*, vol. 19, no. 3, 857–863, 2004.
- [8] Lewis T. J., ‘Interfaces are the Dominant Feature of Dielectrics at the Nanometric Level’, *IEEE Transactions on Dielectrics and Electrical Insulation*, Vol. 11, No. 5; October 2004.
- [9] Roy M., Nelson J. K., Schadler L. S., Zou C., Fothergill J.C., ‘The influence of physical and chemical linkage on the properties of nanocomposites’, *IEEE CEIDP*, USA, pp. 183–186, Oct 2005.
- [10] Zou C., Fothergill J. C., Fu. M. and Nelson J. K., ‘Improving the dielectric properties of polymers by incorporating nano-particles’, *10th INSUCON*, Birmingham, UK, pp.125–130, 24–26 May 2006.
- [11] Kinloch A. J., Ed. *Durability of structural adhesives*, Applied Science Publishers: England, 1983.
- [12] Kinloch A. J., Little M. S. G., Watts J. F., ‘The Role of the Interphase in the Environmental Failure of Adhesive Joints’, *Acta mater.* 48, pp. 4543–4553, 2000.
- [13] Zou C., Fothergill J. C., Rowe S. W., ‘The effect of hydration on the dielectric properties of epoxy nanocomposites’, *IEEE special issue: nanodielectric*, submitted.

Chapter 2 References

- [1] Paul C Painter, Michael M Coleman, *Fundamentals of Polymer Science: An introductory text*, 2nd Edition, Technomic Publishing Company, Inc., 1997.
- [2] Duncan Q. M. Craig, *Dielectric analysis of pharmaceutical systems*, Taylor & Francis, 1995.
- [3] Fothergill J. C., Dissado L. A., *Electrical Degradation and Breakdown in Polymers*, IET Publisher, 1992.
- [4] Leiwis T. J., 'Interfaces are the Dominant Feature of Dielectrics at the Nanometric Level', *IEEE Transactions on Dielectrics and Electrical Insulation*, Vol. 11, No. 5; October 2004.
- [5] Irwin P. C., Cao Y., Bansal L., Schadler L. S., 'Thermal and mechanical properties of polyimide nanocomposites', *Ann. Rep. Conf. on Electrical Insulation and Dielectric Phenomena IEEE (Albuquerque, NM)*, pp 120–3, 2003.
- [6] Henk P. O., Kortsen T. W., Kvarts T., 'Increasing the electrical discharge endurance of acid anhydride cured DGEBA epoxy resin by dispersion of nanoparticle silica', *High Perf. Polym.*, 11 281–96, 1999.
- [7] Nelson J. K., Hu Y., 'Nanocomposite dielectrics—properties and implications', *J. Phys. D: Appl. Phys.* 38, 213–222, 2005.
- [8] Michel F Frechette, Michel L Trudeau, Houshang D Alamdari and Sabin Boily, 'Introductory remarks on nanodielectrics', *IEEE Transactions on Dielectric and Electrical Insulation*, Vol. 11, No. 5, October 2004.
- [9] Zou C., Fothergill J. C., Fu. M. and Nelson J. K., 'Improving the dielectric properties of polymers by incorporating nano-particles', *10th INSUCON*, Birmingham, UK, pp.125–130, 24–26 May 2006.
- [10] Marinez J., Boulouz M., Mayoux C., Lacabanne C., 'Thermally stimulated creep for the study of ageing insulating polymers under electrical field', *IEEE International Symposium on Electrical Insulation*, Baltimore, MD USA, pp. 62–65, June 1992.
- [11] Lewis T. J., dielectric meeting in Autrans, August 2005.
- [12] Jonscher A. K., *Dielectric relaxation in solids*, Chelsea Dielectric Press, London, 1983.
- [13] James Clerk Maxwell, 'A Dynamical Theory of the Electromagnetic Field', *Philosophical Transactions of the Royal Society of London*, 155, 459–512, 1865.
- [14] Schönhalz F. K. A., *Broadband Dielectric Spectroscopy*, Springer, 2003.
- [15] Debye P., *Polar Molecules*, Dover, New York, 1945.
- [16] Frohlich H., *Theory of Dielectrics*, Clarendon Press, Oxford, pp 70, 1949.
- [17] Oncley J. L., 'The Investigation of Proteins by Dielectric Measurements', *Chem. Rev.* 30 (3), pp. 433–450, 1942.
- [18] Schwan H. P., Maczuk J., 'Simple Technique to Control the Stray Field of Electrolytic Cells', *Rev. Scient. Instrum.* 31, 59, 1960.
- [19] Mandel M., 'Comments on impedance measurements of protein solutions', *Proc. Colloquium Protides of Biological Fluids.*, 13, 415, 1965.

- [20] Rosen D., Bignall R., Wisse J. D. M., van der Drift, 'Radio frequency measurement of the dielectric constant of conducting liquids with $\tan \delta$ up to 500', *A.C.M., Journal of Physics E: Scientific Instruments*, 2 (1), 22–28, 1969.
- [21] Debye P., *Polar molecules*, The Chemical Catalog Co. Dover Publications, London, 1929.
- [22] Debye P., *Polar molecules*, The Chemical Catalog Co. Dover Publications, London, 1945.
- [23] Frohlich H., *Theory of electric Polarisation*, Elsevier, Oxford University Press, London, 1958.
- [24] Williams G., Fournier J., 'The determination of apparent memory functions from dielectric relaxation data for amorphous polymers and glass-forming liquids: Theory and experiment', *J. Chem. Phys.*, 104 (14), 5690–5698, 1996.
- [25] Runt J. P., Fitzgerald J. J., *Dielectric Spectroscopy of Polymeric Materials*, American Chemical Society, Washington, DC, 1997.
- [26] Cole K. S., Cole R. H., 'Dispersion and adsorption in dielectrics', *J. Chem. Rev.* 9 341–52, 1941.
- [27] Davidson D. W., Cole R. H., 'Dielectric relaxation in Glycerol, Propylene Glycol, and n-Propanol', *J. Chem. Phys.* 19, 1484–1490, 1951.
- [28] Harviliak, Negami S., 'A complex plane analysis of dispersion in some polymer systems', *J. Polym. Sci. C* 14, 99, 1966.
- [29] Blythe A. R., *Electrical properties of polymers*, Cambridge: Cambridge University Press, 191 p, 1979.
- [30] Jonscher A. K., Hill R. M., *Physics of Thin Films*, 8, pp169–249, 1975.
- [31] Dissado L. A., Hill R. M., 'Non-Exponential decay in Dielectrics and Dynamics of Correlated Systems', *Nature*, 279, pp685–689, 1979.
- [32] Dissado L. A., Hill R. M., 'Anomalous Low -frequency Dispersion', *J. chemical Society*, Faraday Transactions. 2, Vol 80,291–319, 1984.
- [33] Dissado L. A., Hill R. M., 'Invariant behaviour for the response of simple fractal circuits'. *J. Physics :Condense Matter* 3, pp 9773–9790, 1991.
- [34] Dissado L. A., Hill R. M., 'Constant Phase Angle Response with Fractal Electrodes', *Solid State Ionics* 26, pp 295–297, 1988.
- [35] Dissado L. A., Hill R. M., 'Constant- Phase Angle and Power Law Regimes in the Frequency Response of a General Determinate Fractal Circuit', *The American Physical Society, Physical Review B*, Vol 37, No7, pp3434–3439, 1988.
- [36] Jonscher A. K., *Universal relaxation law*, Chelsea Dielectrics, London, 1995.
- [37] Truls Norby, 'Solid-state protonic conductors: principles, properties, progress and prospects', *Solid State Ionics*, 125, pp.1–11, 1999.
- [38] Giulio Alberti, Mario Casciola, 'Solid state protonic conductors, present main applications and future prospects', *Solid State Ionics* 145, pp. 3–16, 2001.
- [39] Francesco Pizzitutti, Fabio Bruni, 'Electrode and interfacial polarization in broadband dielectric spectroscopy measurements', *Review of Science Instruments*, Vol 72, No. 5, 2001.
- [40] Hill R. M., Dissado L. A., 'The temperature dependence of relaxation processes', *J. Phys. C: Solid State Physics* 15, 5171, 1982.

- [41] Fothergill J. C., Dissado L. A. (eds.): *Space Charge in Solid Dielectrics*, The Dielectrics Society, ISBN: 0 9533538 0 X, 1998.
- [42] Mizutani T., Semi H., Kaneko K., 'Space charge behaviour in low-density polyethylene', *IEEE Transactions on Dielectrics and Electrical Insulation*, Vol: 7, No.: 4, pp 503–508, Aug 2000.
- [43] Lewis T. J., 'Charge Transporte in Polymers', *IEEE Proc. Electr. Insul. And Diel.*, pp. 533–561, 1976.
- [44] Mizutani T., 'Space Charge Measurement Techniques and Space Charge in Polyethylene', *IEEE Trans. DEI*, 1, 923–933, 1994.
- [45] Steven Boggs, 'A rational consideration of space charge', *DEIS*, Vol. 20, No. 4, July/August 2004.
- [46] Montanari G. C., Mazzanti G., Palmieri F., Perego G., Serra S., 'Dependence of space-charge trapping threshold on temperature in polymeric DC cables,' in *Proc.2001 IEEE Int. Conf. Solid Dielect.*, pp. 81–84, 2001.
- [47] Montanari G. C., 'Relation between space charge and polymeric insulation ageing: cause and effect', *IEEE Proc.-Sci. Meas. Technol.*, Vol. 150, No. 2, March 2003.
- [48] Head J. G., White N. M., Gale P. S., 'Modification of the dielectric properties of polymeric materials', *Fifth International Conference on Dielectric Materials, Measurements and Applications*, Volume , Issue, 27-30, pp. 61 – 64, Canterbury, UK, 1988.
- [49] McLachlan D. S., Blaszkiewicz M., Newnham R. E., 'Electrical Resistivity of Composites', *J. Am. Ceram. Soc.*, 73, [8], pp. 2187–2203, 1990.
- [50] Kokan J. R., Gerhardt R. A., Ruh R., McLachlan D. S., 'Dielectric Spectroscopy of insulator/Conductor Composites'; pp. 341–46 in *Materials Research Society Symposium Proceedings*, Vol. 500, *Electrically Based Microstructural Characterization II*. Edited by R. A. Gerhardt, M. A. Alim, and S. R. Taylor. Materials Research Society, Pittsburgh, PA, 1998.
- [51] Zallen R., *The Physics of Amorphous Solids*, Chapter 4, John Wiley and Sons, New York (1983).
- [52] Brouers F., 'Percolation threshold and conductivity in metal-insulator composite mean-field theories', *J. Phys. C: Solid State Phys.* 19, pp 7183–7193, 1986.
- [53] Bernasconi J., 'Conduction in anisotropic disorder systems: Effective-medium theory', *Physical Review B*: Vol 9, No. 10, 1974.
- [54] Bjorn Sanden, XLPE cable insulation subjected to HVDC stress: space charge, conduction and breakdown strength, *NTNU*, Trondheim, 1996.
- [55] Lewis T. J., 'Electrical Effect at Interfaces and Surfaces', *IEEE Transactions on Electrical Insulation.*, EI-21(3), pp.289–295. 1986.
- [56] H.J. Wintle, 'Charge Motion and Trapping in Insulators, Surface and Bulk Effects', *IEEE Transactions on Dielectrics and Electrical Insulation*, (The T. W. Dakin Lecture), Vol. 6 No. 1, pp1-10, February 1999,
- [57] Lampert M. A., *Current injection in solids*, Academic P, 1970.
- [58] Maruska H. P., Stevenson D. A., 'Mechanism of Light Production in Metal-Insulator-Semiconductor Diodes; GaN:Mg Violet Light-Emitting Diodes', *Solid-State Electronics*, Vol. 17, pp. 1171–1179, 1974.

Chapter 3 References

- [1] Roy M., Nelson J. K., Schadler L. S., Zou C., Fothergill J. C., 'The influence of physical and chemical linkage on the properties of nanocomposites', *CEIDP*, Oct 2005.
- [2] The scale of relative humidity of air certified against saturated salt solutions, *OIML R 121*, Edition 1996 (E).
- [3] Nyvlt J., Sohnel O., Solubility in inorganic two-component systems, *Elsevier*, 1981.
- [4] Katya I Ivanova, Richard A Pethrick, Stanley Affrossman, 'Hygrothermal aging of rubber modified and mineral filled dicyandiamide cured Diglycidyl ether of Bisphenol A epoxy resin. I. Diffusion behaviour', *Journal of Applied Polymer Science*, Vol. 82, 3468–3476, 2001.
- [5] Robert Comrie, Stanley Affrossman, David Hayward, Richard A. Pethrick, 'Nondestructive Examination of Epoxy Adhesive-bonded Structures Exposed to a Humid Environment: A Comparison of Low- and High-frequency Dielectric Measurements', *Taylor & Francis*, Volume 78, Number 11, pp 967–985, November 2002.
- [6] Runt James P. (James Patrick), *Dielectric spectroscopy of polymeric materials: fundamentals and applications*, American Chemical Society, 1997.
- [7] Vitkup D., Ringe D., Petsko G. A., Karplus M., 'Solvent mobility and the protein 'glass' transition'. *Nature Structural Biology* 7: 34–38, 2001.
- [8] Moy P., Karasz, F. E., in 'water in Polymers'; Rowland S.P., Ed., *ACS Symposium Series 127*, American Chemical Society: Washington, D.C., 1980.
- [9] Runt James P, 'Dielectric spectroscopy of polymeric materials: fundamentals and applications', *American Chemical Society*, 1997.
- [10] Friedrich Kremer, *Broadband dielectric spectroscopy*, Springer, 2003.
- [11] Péter Hedvig, *Dielectric spectroscopy of polymers*, Wiley, 1977.
- [12] Duncan Q. M. Craig, *Dielectric analysis of pharmaceutical systems*, Taylor & Francis, 1995.
- [13] 1255 H.F, Frequency Response Analyser, *Operating Manual, Solarton Instruments*, Issue 2a, Part No 12550006, 1987.
- [14] Pugh J., *Dielectric Spectrometer- User Guide*, Private issue provided with the system measurements.
- [15] Jonscher A. K., *Dielectric relaxation in solids*, Chelsea Dielectrics Press, London, 1983.
- [16] Graham Williams, Dale K. Thomas, 'Phenomenological and Molecular Theories of Dielectric and Electrical Relaxation of Materials', *Novocontrol Application Note*, Dielectrics 3
- [17] Takada T., Sakai T., 'Measurement of electric fields at a dielectric/electrode interface using an acoustic transducer technique', *IEEE Tans. Electr. Insul.*, EI-18 (6) 619–628, 1983.
- [18] Takada T., Maeno T., Kushibe H., 'An electric stress-pulse technique for the measurement of charges in a plastic plate irradiated by electron beam', *IEEE Trans. Electr. Insul.*, 22 (4) 497–501, 1987.

- [19] Maeno T., Futami T., Kushibe H., Takada T., Cooke C. M., 'Measurement of spatial charge distribution in thick dielectrics using the pulsed electroacoustic method', *IEEE Trans. on EI*, Vol. 23, pp. 433 – 439, 1988.
- [20] Maeno T., Futami T., Kushibe H., Takada T., 'Measurement and simulation of the spital charge distribution in electron-beam irradiated polymers', *J. Appl. Phys.*, 65 1147–1151, 1989.
- [21] Fothergill J. C., Dissado L. A., *Space charge in solid dielectrics*, Dielectrics Society, 1998.
- [22] John M Alison, 'A high field pulsed electro-acoustic apparatus for space charge and external circuit current measurement within solid insulators', *Meas. Sci. Technol.* 9, pp1737–1750, 1998.
- [23] John M Alison, 'The pulsed electro-acoustic method for the measurement of the dynamic space charge profile within insulators', *Space charge in solid dielectrics*, presented at the dielectric society meeting, 7–9 April 1997.

Chapter 4 References

- [1] Ramakrishna H. V., Rai S. K., 'Effect on the mechanical properties and water absorption of granite powder composites on toughening epoxy with unsaturated polyester and unsaturated polyester with epoxy resin', *Journal of Reinforced Plastics and Composites*, Vol. 25, No. 1, 2006.
- [2] Gledhill R. A., Kinloch A. J., 'Environmental failure of structural adhesive joints', *J. Adhesion*, Vol. 6, pp 315–330, 1974.
- [3] Kinloch A. J., Ed. 'Durability of structural adhesives', *Applied Science Publishers*: England, 1983.
- [4] Kinloch A. J., Little M. S. G., Watts J. F., 'The Role of the Interphase in the Environmental Failure of Adhesive Joints', *Acta mater.*, 48, pp 4543–4553, 2000.
- [5] Sternstein S. S., Zhu A. J., 'Reinforcement mechanism of nanofilled polymer melts as elucidated by nonlinear viscoelastic behaviour', *Macromolecules*, 35, pp 7262–73, 2002.
- [6] Zou C., Fothergill J. C., Fu M., Nelson J. K., 'Improving the dielectric properties of polymers by incorporating nano-particles', *Proc. 10th INSUCON International Electrical Insulation Conference*, Birmingham, pp.125–130, 24–26 May 2006.
- [7] Nelson J. K., Hu Y., 'Nanocomposite dielectrics—properties and implications', *J. Phys. D: Appl. Phys.*, 38, 213–222, 2005.
- [8] Li Liang, Zhang Shuyong, Chen Yuehui, Liu Mojun, Ding Yifu, Luo Xiaowen, Pu Zong, Zhou Weifang and Li Shanjun, 'Water Transportation in Epoxy Resin', *Chem. Mater.*, 17, 839–845, 2005.
- [9] Buchman A., Bryant R. G., 'Molded Carbon–Carbon Composites Based on Microcomposite Technology', *Applied Composite Materials* 6: 309–326, 1999.
- [10] The scale of relative humidity of air certified against saturated salt solutions, *OIML R 121*, Edition 1996 (E).
- [11] Wilkinson David S., *Mass Transport in Solids and Fluids*, Cambridge University Press, 2000.
- [12] Cussler E. L., *Diffusion: Mass Transfer in Fluid Systems*, 2nd Edition, Cambridge University Press, 1997.
- [13] Luo Shijian, Leisen Johanes, Wong C. P., 'Study on Mobility of Water and Polymer Chain in epoxy and Its Influence on Adhesion', *Journal of Applied Polymer Science*, Vol. 85, 1–8, 2002.
- [14] Fukao K., Miyamoto Y., 'Glass transitions and dynamics in thin polymer films: Dielectric relaxation of thin films of polystyrene', *Physical Review E*, Vol. 61, No. 2, February 2000.
- [15] Martin Y. M. Chiang, Marta Fernandez-Garcia, 'Relation of swelling and T_g Depression to the apparent free volume of a particle-filled, epoxy-based adhesive', *Journal of applied polymer science*, Vol. 87, 1436–1444, 2003.
- [16] Wintle H. J., in *Engineering Dielectrics* Vol. IIA, ed. Bartnikas R. and Eichhorn R. M., *ASTM Philadelphia USA*, Ch.3, 1983.
- [17] Fleming R. J., Pawlowski T., Ammala A., Casey P. S., Lawrence K. A., 'Electrical conductivity and space charge in LDPE containing TiO₂ nanocomposites', *IEEE Transactions on Dielectric and Electrical Insulation*, Vol. 12, No. 4, August 2005.

- [18] Lewis T. J., 'The work function of irregular metal surface', *Proc. Phys. Soc. (London)*, B67, pp 187–200, 1954.
- [19] Lewis T. J., 'Electrical Effect at Interfaces and Surfaces', *IEEE Transactions on Electrical Insulation*, EI-21(3), pp.289–295. 1986
- [20] Roy M., Nelson J. K., MacCrone R. K., Schadler L. S., Reed C. W., Keefe R. and Zenger W., 'Polymer Nanocomposite Dielectrics – The Role of the Interface', *IEEE Transactions on Dielectrics and Electrical Insulation*, Vol. 12, No. 6; December 2005.
- [21] Zou C., Fu M., Fothergill J. C., Rowe S. W., 'Influence of absorbed water on the dielectric properties and glass-transition temperature of silica-filled epoxy nanocomposites', *IEEE CEIDP 2006*, USA, 2006.
- [22] Dissado L. A., Hill R. M., 'Quasi-D.C. Conduction', *IEE DMMA. Conference Publication*, No. 239, p. 34–37, 1984.
- [23] Jonscher A. K., 'Dielectric relaxation in solids', *Chelsea Dielectric Press*, ISBN:0950871109., 1983.
- [24] Hill R. M., Dissado L. A., Nigmatullin R. R., 'Invariant behaviour classes for the response of simple fractal circuits', *J. Phys. Condens. Matter*, 3, pp9773–9790, 1991.
- [25] Hill R. M. and Dissado L. A., 'The temperature dependence of relaxation processes', *J. Phys. C: Solid State Phys.*, 15, 5171–5193, 1982.
- [26] Maxwell I. D., Pethrick R. A., 'Dielectric studies of water in epoxy resins', *Journal of Applied Polymer Science*, 28, 2363, 1983.
- [27] Tsonos C., Apekis L. and Pissis P., 'Water sorption and dielectric relaxation spectroscopy studies in hydrated Nafion® (-SO₃K) membranes', *Journal of Materials Science*, Volume 35, Number 23, pp. 5957-5965 December, 2000.
- [28] Moy P., Karasz F. E., 'Epoxy-water interactions', *Polym. Eng. Sci*, 20, 315–319, 1980.
- [29] Cooke R., Kuntz I. D., 'Properties of water in biological-systems', *Annu. Rev. Biophys. Bioeng.*, 3:95–126, 1974.
- [30] Jelinski L. W., Dunmais J. J., Cholli A. L., Ellis T. S., Karasz F. E., 'Nature of the Water-Epoxy Interaction', *Macromolecules*, 18, 1091–1095, 1985.
- [31] Pethig R., 'Dielectric and electronic properties of biological materials', *Wiley*, 1979.
- [32] Roy M., Nelson J. K., Schadler L. S., Zou C., Fothergill J. C., 'The Influence of Physical and Chemical Linkage on the Properties of Nanocomposites', *IEEE CEIDP*, USA, pp.183–186, 2005.
- [33] Dissado L. A., Laurent C., Montanari G. C., Morshuis P. H. F., 'Demonstrating a threshold for trapped space charge accumulation in solid dielectrics under dc field', *IEEE Trans DEI*, vol. 12(3), p 612–620, June, 2005.
- [34] Montanari G. C., Fabiani D., Palmieri F., Kaempfer D., Thomann R., Mulhaupt R., 'Modification of Electrical Properties and Performance of EVA and PP Insulation through Nanostructure by Organophilic Silicates', *IEEE Transactions on Dielectrics and Electrical Insulation*, Vol. 11, No. 5, October 2004.

Chapter 5 References

- [1] Leiwis T. J., 'Interfaces are the Dominant Feature of Dielectrics at the Nanometric Level', *IEEE Transactions on Dielectrics and Electrical Insulation*, Vol. 11, No. 5; October 2004.
- [2] Baraton M. I., Chancel F., Merhari L., 'In-situ determination of grafting on nanosized ceramic powders by FI-IR spectrometry', *Nanostruct. Mater.*, **9**:319–322, 1997.
- [3] Leiwis T. J., 'Interfaces: nanometric dielectrics', *J. Phys. D: Appl. Phys.*, **38** 202–212, 2005.
- [4] Baraton M. I., 'Chemical phenomena at the surface of nanoparticles, Functional gradient materials and surface layers prepared by fine particles technology', M-I. Baraton and I. Uvarova (eds.), *NATO-ASI Series*, Kluwer Academic Publishers, Dordrecht, 2001.
- [5] Roy M., Nelson J. K., MacCrone R. K., Schadler L. S., Reed C. W., Keefe R., Zenger W., 'Polymer nanocomposite dielectrics – the role of the interface', *IEEE Trans, Dielectr. Electr. Insul.*, Vol. 12, pp. 629–643, 2005.
- [6] Szymanski H. A., *Theory and Practice of Infrared Spectroscopy*, Plenum Press, New York, 1963.
- [7] Leidheiser H., Funke W., 'Water Disbondment and Wet Adhesion of Organic Coatings on Metals: A Review and Interpretation', *Journal of the Oil Color Chemistry Association*, Vol. 70, No. 5, pp. 121–132, 1987.
- [8] Funke W., Haagen H., 'Empirical or Scientific Approach to Evaluate the Corrosion Protective Performance of Organic Coatings', *Ind. Eng. Chem. Prod. Res. Dev.*, 17 (1), 50, 1978.
- [9] Nguyen T., Byrd W. E., Bentz D. P., 'Quantifying Water at the Organic Film/Hydroxylated Substrate Interface', *Journal of Adhesion*, 48, 169–194. 1995.
- [10] Linnossier I., Gaillard, F., Romand, M., Nguyen, T., 'A Spectroscopic Technique for Studies of Water Transport Along the Interface and Hydrolytic Stability of Polymer/Substrate Systems', *Journal of Adhesion*, 70, pp 221–239, 1999.
- [11] Bowden F. P., Throssell W. R., 'Adsorption of Water Vapour on Solid Surfaces', *Nature*, 167, 601, 1957.
- [12] Takahashi K. M., Sullivan T. M., 'AC impedance measurement of environmental water in adhesive interfaces', *J. Appl. Phys.*, 66, 3192, 1989.
- [13] Takahashi K. M., 'AC impedance measurements of moisture in interfaces between epoxy and oxidized silicon', *J. Appl. Phys.*, 67, 3419, 1990.
- [14] Wu W. L., Orts W. J., Majkrzak J., Hunston D. L., 'Water Adsorption at Polyimide/Silicon Water Interface', *Polymer Science and Engineering*, 35 (12), pp 1000–1004, 1995.
- [15] McCrum N. G., Read B. E., Williams G., 'Anelastic and Dielectric Effects in Polymeric Solids', *Wiley*, New York, 1967.
- [16] Nguyen T., Byrd W. E., Bentz D. P., Lin C., 'In situ measurement of water at the organic coating/substrate interface', *Prog. in Organic Coatings*, 27, 181–193, 1996.

Chapter 6 References

- [1] Toshikatsu Tanaka, 'Interpretation of Several Key Phenomena Peculiar to Nano Dielectrics in Terms of a Multi-Core Model', *IEEE CEIDP*, USA, 2006.
- [2] Lo Shiyin, 'Anomalous State of Ice', *Modern Physics Letters B*, Vol. 10, No. 19, pp. 909-919, 1996.
- [3] McCrum N. G., Read B. E., Williams G., *Anelastic and Dielectric Effects in Polymeric Solids*, Wiley, New York, 1967.
- [4] Bowden F. P., Throssell W. R., 'Adsorption of Water Vapour on Solid Surfaces', *Nature*, 167, 601, 1957.
- [5] Lewis T. J., 'Interfaces are the Dominant Feature of Dielectrics at the Nanometric Level', *IEEE Transactions on Dielectrics and Electrical Insulation*, Vol. 11, No. 5, October 2004.
- [6] Fothergill J. C., 'Ageing, Space Charge and Nanodielectrics: Ten Things We Don't Know About Dielectrics', E O Forster Memorial Lecture, *IEEE ICSD*, Winchester, UK, July 2007.
- [7] Jing X., Zhao W., Lan L., 'The effect of particle size on electric conducting percolation threshold in polymer/conducting particle composites', *Journal of Materials Science Letters*, Volume 19, Number 5, pp 377-379, March, 2000.
- [8] Rowe S. W., 'Electrical Ageing of Composites: An Industrial Perspective', *IEEE ICSD*, Winchester, UK, July 2007.

Appendix II Reference

[1] Cussler E. L., *Diffusion: Mass Transfer in Fluid Systems*, 2nd Edition, Cambridge University Press, 1997.

List of Publications

Zou C, Fothergill J C, Rowe S W, ‘The effect of hydration on the dielectric properties of epoxy nanocomposites’, *IEEE special issue: nanodielectric*, submitted.

Zou C, Fu M, Fothergill J C and Rowe S W, ‘The Influence of Water on Dielectric Behaviour of Silica-filled Epoxy Nano-composites and Percolation Phenomenon’, *IEEE CEIDP*, Canada, Oct 2007, to be published.

Zou C, Fothergill J C, Rowe S W ‘A “Water Shell” Model for the Dielectric Properties of Hydrated Silica-filled Epoxy Nano-composites’, *IEEE ICSD*, Winchester, UK, July 2007.

Fu M, Chen G, Dissado L A, Fothergill J C and **Zou C**, ‘The Effect of Gamma Irradiation on Space Charge Behaviour and Dielectric Spectroscopy of Low-density Polyethylene’, *IEEE ICSD*, Winchester, UK, July 2007.

Zou C, Fu M, Fothergill J C, ‘The influence of water on the dielectric properties of nano-silica epoxy composites’ (Poster), *Nanoelectronics-Materials and Technology*, Institute of Physics, London, UK, Feb 2007.

Zou C, Fu M, Fothergill J C and Rowe S W, ‘Influence of absorbed water on the dielectric properties and glass-transition temperature of silica-filled epoxy nanocomposites’, *IEEE CEIDP*, Kansas City, MO, USA, pp.321–324, Oct 2006.

Zou C, Fothergill J C, Fu M and Nelson J K, ‘Improving the dielectric properties of polymers by incorporating nano-particles’ (Presentation), *10th INSUCON*, Birmingham, UK, pp.125–130, 24–26 May 2006.

Roy M, Nelson J K, Schadler L S, **Zou C**, Fothergill J C, ‘The Influence of Physical and Chemical Linkage on the Properties of Nanocomposites’, *IEEE CEIDP*, USA, pp.183–186, 2005.